Quantum Technologies for Enhanced Sensing and Light Absorption

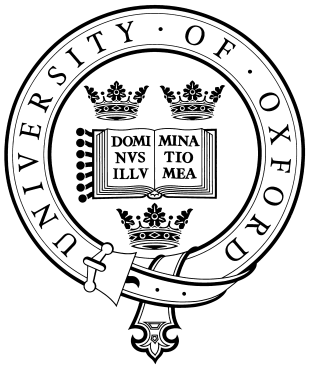

Kieran Higgins
Lincoln College
University of Oxford

A thesis submitted for the degree of
Doctor of Philosophy

2014

Abstract

The counterintuitive properties of quantum mechanics have the potential to produce revolutionary new technology. The applications of these devices are both vital and diverse: the efficient generation of energy from light, sensing and measuring with exquisite precision, and information processing with unparalleled speed. In this thesis, I use the theory of open quantum systems to investigate quantum technologies for enhanced sensing and light absorption. In the first research chapter, we develop a new method for describing qubit dynamics in the Rabi model. We obtain a new expression for the ac Stark shift, which enables practical and precise qubit thermometry of an oscillator. In the second research chapter, we demonstrate that it is possible to invert the phenomenon of Dicke Superradiance using nanostructures and quantum control. This creates the possibility of a new class of quantum light absorption technologies with a super-linear scaling in the absorption rate. In the final research chapter, we investigate another means of enhancing light absorption. We show that phonon assisted transitions to ratchet states in rings allow absorbed excitions to be protected from reemission.

Acknowledgements

To my supervisors Dr Erik Gauger, Dr Brendon Lovett and Professor Simon Benjamin for making my time at Oxford both happy and productive.

To Erik for providing excellent supervision in the skies over Scotland, the shipping lanes of the English Channel and the Glass House Mountains of Australia.

To EPSRC, Oxford Materials, the Institute of Physics, the Tottenham Grammar School Foundation and Hornsey Parochial Charities for making this work possible.

To my family and friends, for everything.

Publications

This thesis is based, in part, on the following publications.

1. Kieran D. B. Higgins, Brendon W. Lovett, and Erik M. Gauger, Quantum thermometry using the ac Stark shift within the Rabi model. *Phys. Rev. B*, 88, 155409, (2013).

2. K. D. B. Higgins, S. C. Benjamin, T. M. Stace, G. J. Milburn B. W. Lovett and E. M. Gauger, Superabsorption of light via quantum engineering. *Nature Communications* 5, 4705, (2014).

3. Kieran D. B. Higgins, Brendon W. Lovett, and Erik M. Gauger, Ratchet states for enhanced light absorption (in preparation).

Contents

List of Figures

CHAPTER 1

Introduction

1.1 Motivation and Outline

The previous century of technological advancement has come from our ability to manipulate matter on an ever smaller scale. This is not only true of electronics, on which we are ever more dependent, but also of new materials such as carbon nanotubes and graphene. This journey downward has now taken us beyond what can be explained by classical physics alone. To continue on this path, we must learn to engineer and control matter in the realm of quantum mechanics, with its counter intuitive properties of coherence, superposition and entanglement.

Quantum mechanics offers challenges, but also huge opportunity for exploiting effects made possible by these properties. Quantum computation is the most well known of these technologies; it offers the power to tackle problems that are intractable with our current computing paradigm. Quantum computing has been a goal of the research community for several decades. This testifies to the difficultly of maintaining and coordinating the large number of 'qubits' or quantum bits needed to be technologically relevant. Although the goal is closer than ever, there is growing interest in other quantum technologies, which have far more modest requirements, but have the potential to revolutionise other areas of technology. Quantum communication technologies made possible by entanglement offer the timely possibility of provably secure communications. Quantum enhanced sensors can detect and measure single molecules, with huge applications across physics, chemistry, biology and medicine. Measuring extremely small magnetic and electric fields allows material surfaces to be mapped in unprecedented detail. Enhanced light absorption has the potential to improve a wide range of technologies from solar cells to cameras and scientific instruments. These sensors also help explore the separation between quantum and classical

physics, one of the most important unanswered questions in science and has serious philosophical implications.

We are only just becoming able to engineer on the nano-scale, but nature has long done so. The objectives are shared: improved sensors, more efficient use of energy and faster processing of information. 'Quantum biology' was until recently considered an oxymoron: the preservation and exploitation of coherent quantum states was thought to be solely the domain of painstaking low temperature and low noise physics experiments. The underlying physics of how quantum coherent energy transfer is possible in a comparatively hot and chaotic environment is still debated. Complex interactions between the system and its environment must allow its fragile coherence to be maintained. This question is key to the emergent field of quantum biology where distinctly quantum properties like superposition and entanglement are posited to explain mysterious and powerful properties of organisms such as the avian compass, the operation of ion channels, olfaction and most controversially consciousness itself.

1.2 Quantum Sensor Technologies

In this section I shall outline the proposed and realised applications of sensors enhanced by quantum effects, with a particular focus on nanoelectromechanical systems, which are the subject of the first research chapter. Sensing and measurement are at the heart of any scientific endeavour, therefore any increase in the precision of measurements has a wide impact. *Quantum sensing* or *quantum metrology* has already produced commercially available technology . Nitrogen vacancy centres in diamond attached to atomic force microscope tips can produce exquisitely sensitive measurements of electromagnetic fields [68, 217]. This enables both better understanding of the structure of materials and molecules, but also the potential to study dynamic effects in biology such as the signalling of neuronal networks. Atomic clocks [140] and interferometers [221] enable time and distance measurements sensitive enough to probe the predictions of relativity in unprecedented detail. They may be the key to finally observing the gravitational waves predicated by Einstein. Such devices could also make practical inertial sensors possible, allowing accurate navigation independent of external systems like satellite networks.

Nanoelectromechanical systems are a union between nanoelectronic devices such as single electron transistors, quantum dots, superconducting circuits and mechanical structures such as nanometer scale beams or cantilevers crafted from semiconductors [48, 14]. These devices could revolutionise sensor technology, offering mass sensitivity

at the level of single molecules [181], which allows them to function as detectors for chemistry [35] and biology [31]. It has even been suggested they could be used to diagnose cancer [115, 210]. The ability of NEMS to store and manipulate quantum states has lead to them being proposed as a potential quantum computing architecture [49].

In addition to these direct applications NEMS can be used to explore fundamental physics. They can be used to probe the transition between quantum and classical. The collapse of the wavefunction is thought to be what creates this dichotomy, but its method and meaning, though much discussed, remain one of the greatest open questions in physics [4]. Nanomechanical resonators can be manufactured at scale where their behaviour is quantum mechanical yet they remain macroscopic objects. Quantum mechanics dictates that the energy separation between the fundamental modes of the resonator (oscillator) is discrete, therefore each excited state or 'phonon', is a quantum state and superpositions of them are possible. This means that an object comprising 10^{10} or more atoms can be put into a superposition state. Experiments have even been proposed that would, in theory, be sensitive enough to differentiate between different wavefunction collapse models [167, 212], such as Penrose's gravitational collapse model [196] and potentially rule out macrorealism [152]. Results from such experiments could profoundly change our understanding of physics and our philosophical interpretation of the universe we inhabit.

1.2.1 Experiments

In this section I focus on the nanomechanical systems relevant to the first research chapter. Experimental progress is being made toward attaining these goals. The current state-of-the-art experiments comprise a Cooper-Pair-Box (CPB) coupled to a nanomechanical resonator (NR), which was originally proposed in 2002 [9]. A CPB is a device comprising a superconducting metal island into which Cooper pairs (bound electron pairs [54]) can tunnel. The tunnelling is controlled via a gate voltage and the magnetic flux through the tunnel junction. The gate voltage is chosen such that there is a maximum of one Cooper pair in the box. In this way the CPB functions as a qubit, with basis states of the presence and absence or a Cooper pair. The quantum state of the CPB can be coherently controlled and read out using a microwave frequency AC voltage [183, 255]. The CPB is well described by the Hamiltonian [163]:

$$\hat{H}_{CPB} = \frac{1}{2}(E_C\sigma_z - E_J\sigma_x), \tag{1.1}$$

where E_C is the electrostatic energy difference between the two charge states and E_J is the capacitance of the tunnel junction, σ_z and σ_x are Pauli spin operators that count or transfer the charge state respectively. The nanomechanical resonator is a typically a 10-100 nm long beam or cantilever fabricated from semiconductors using lithographic techniques [50]. The basic operating principle of resonator sensors is that when mass is added to the resonator its resonant frequency shifts. The sensitivity of the resonator depends on its frequency, the higher the frequency and bigger the shift, the more sensitive the system is. The resonant frequency of such a system is high (MHz - GHz) and its mass minute (10^{-16}), offering exquisite sensitivity. The other important property of the resonator is its quality factor Q. This describes the rate at which the resonator dissipates energy $Q = \omega\tau_d$, where ω is the frequency of the resonator and τ_d is the energy decay constant. The quality factors of nanomechanical resonators are unparalleled ($10^3 - 10^4$) [176] and this is essential to their ability maintain quantum coherence. Although a NR is tiny, it is still a three dimensional object. However, typically only the lowest flexural mode interacts with the CPB, so it can be modelled as a single bosonic mode or quantum harmonic oscillator:

$$\hat{H}_{NR} = \omega_{NR}(a^\dagger a + \frac{1}{2}), \tag{1.2}$$

where ω_{NR} is the angular frequency of the oscillator, $a^\dagger$ and a represent its creation and annihilation operators, and the $\frac{1}{2}$ accounts for the zero point energy. The CPB and the resonator are coupled strongly, but in a controllable way, via electrostatic forces [9]. The resonator is usually made from a piezoelectric material, which deforms depending on the electric field. This allows the coupling between electronic and mechanical degrees of freedom. In the absence of dissipation, this interaction can be described by [126]:

$$\hat{H}_{\mathcal{I}} = (ga^\dagger + g^* a\ )\sigma_z. \tag{1.3}$$

There are of course huge experimental difficulties in fabricating and controlling NRs in a way that preserves their quantum coherence, but they have been successfully realised [147]. Temperature is a particular problem; an object of that size can still decohere very rapidly, even when cooled cryogenically. A good bench mark for the ability to exhibit quantum behaviour in such a system is:

$$\hbar\omega_{NR} \gtrsim k_b T, \tag{1.4}$$

where k_b is the Boltzmann constant and T is the temperature in Kelvin. By using a very high frequency resonator (6 GHz), the quantum ground state and single phonon control of the resonator has been achieved using such a set-up.

1.3 Light Absorption

The safe and efficient generation of energy is one of the most pressing problems facing humanity. The disastrous consequences of our continued use of fossil fuels are well known, but population growth and demand for energy show no signs of abatement. It is imperative therefore to develop alternative sources of energy [160]. Sunlight is a plentiful and widely available source of energy. It provides the initial energy input to the food chains, which support nearly all known living organisms. Nuclear fusion offers the potential to generate huge amounts of energy with low environmental impact [173]. However, commercial fusion remains elusive [270]. The low setup cost and distributed nature of solar power make it particularly attractive for developing countries as well in small stand-alone devices such as sensors and wearable technology. In this section we will give some background on photovoltaics focusing on the potential enhancements offered by quantum nanotechnologies. We shall focus on light harvesting applications, but the discussion is equally relevant to other light absorption technologies such as sensors.

Photovoltaic (PV) devices convert light into electrical current. This effect was first observed by Edmund Bequerel in 1839 using platinum electrodes suspended in acid. However it wasn't until the 1950's when semi-conductor electronics were developed that it began to be considered a viable source of power. There are three key elements to the photovoltaic process. First, the absorption of photons and the generation of excitons (electron hole pairs). Second the transport and separation of the electrons from the holes. Finally the electrons are passed through an external load in a circuit, the work done against this load produces power. Doped silicon, forming a p-n junction is the most widely material for creating solar cells, because it provides both a suitable bandgap for carrier generation as well as an intrinsic electric field, for carrier separation.

The efficiency of a solar cell is the proportion of the incident light energy it successfully converts into electrical energy. In order to try to enhance the efficiency of PV devices, we should understand the fundamental limits on their performance. The ultimate limit on the efficiency of a conventional solar cell is the thermodynamic Carnot efficiency [268]:

$$\eta = \left(1 - \frac{T_A}{T_S}\right) \approx 95\% \tag{1.5}$$

where T_S is the temperature of the sun 5800 K and T_A is the ambient temperature on earth $300K$. However, this limit is attainable only in the limit where no current

is extracted from the system. Of course, energy extraction is the very purpose of any practical device. Therefore, a slightly more realistic upper bound is found by calculating the efficiency at the point where maximum work can be extracted, which for an infinite stack of monochromatic absorbers covering the solar spectrum is found to be 86% [59]. The most practically relevant limit currently is the Shockley-Queisser Limit (SQL) [234], which gives a maximum efficiency of 31% under these conditions:

- There is a single bandgap for absorption.
- Only photons with energy above the bandgap are absorbed.
- All photon energy in excess of the bandgap is lost as heat.
- A single exciton is generated for every photon absorbed.
- The incident sunlight is unconcentrated.

The SQL is an elegant theory that accounts for the primary loss mechanisms in PV solar cells. It thus offers a benchmark for experimental implementations as well as inspiration for more exotic approaches. State-of-the-art single crystal silicon cells are approaching this efficiency limit of 26% [100]. Devices already exist that operate beyond the SQL, they do this by breaking the above assumptions. The most conceptually straightforward is to concentrate the incoming light. This can either be accomplished by marcoscopic optics such as lenses and mirrors, or via recently developed nanostructures [145]. Using this approach sun light can be concentrated up to over 400 times its original intensity [262], leading to efficiency gains of $5-10\%$ [111].

Another approach is to combine multiple bandgap materials into a single device. Monolithic stacks of varying bandgap p-n junctions are already used to similar effect, such devices currently hold the world record for efficiency 44% [100]. Integrating quantum dots into PV offer several potential advantages [139]. Their tuneable band gaps allow them to be optimised to the spectrum of the incident light. So called dye-sensitised solar cells, like natural light harvesters, separate out the role of absorbing photons to an antenna with tailored properties [190, 99, 107]. Although yet to compete for efficiency with crystalline Si solar cells, they can be made from much cheaper materials and form flexible thin-films [47]. The problem with such approaches is to maximise absorption from a thin layer, as well as provide carrier transfer and separation, which is no longer intrinsic like it is in silicon. However, here novel quantum

phenomena such as plasmons [108] and structures such as nanowires can help with this [156].

Quantum dots can also bypass the SQL restriction of only producing one exciton per photon. Multiple exciton generation, where excess photon energy is not lost but used to generate multiple carrier from a single photon. This turns a source of inefficiency into additional current [231]. They can also produce multiple absorption path solar cells, where several sub-bandgap photons produce a single exciton [120]. So called 'hot carrier' approaches aim to extract excitons before thermalisation has time to happen, leading to an increased voltage [213, 143, 79].

There are three main losses contributing to the SQL: spectral losses, thermalisation, and recombination. The previous examples have dealt with the two former processes. Although spectral losses (sub-bandgap photons) account for the larger part of the inefficiency in the SQL they are not a fundamental limitation. Similarly thermalisation losses are fundamentally the result of a missmatch between the bandgap of the absorber and the frequency of the incident light. Incoming sunlight can be filtered via prism like optics and directed toward cells optimised for absorption at their particular wavelength. The loss mechanism that has so far been unaddressed is recombination. Reemission is the time-reversed process of absorption that should be present in any system, a fact that links to the reversibility of Carnot cycle.

It was therefore extremely surprising when in 2003 Scully showed that, by exploiting quantum interference heat engines could operate beyond the Carnot efficiency [230]. In later work he applied this theory to a quantum photocell, which is able to absorb light without recombination [227] . This is possible by exploiting the reciprocal phenomenon of lasing without inversion [229, 165]. The essence of this effect is that a three level V system (one lower state, two higher) is subject to an incoherent optical field pumping the lower level upward, in addition a coherent microwave field drives the two closely spaced upper levels. Depending on the phase of the coherent field, optical photons excite superpositions of both the upper levels. However the two decay pathways interfere with each other creating an overall one way absorption of the optical photon.

Quantum nanostructure enabled light harvesters have the potential to produce a new generation of solar cells, which operate closer to the theoretical limit, whilst being composed of cheaper and more plentifully materials.

1.4 Quantum Biology

Despite early consideration of the idea that quantum mechanics might play a role in biology by Schrödinger, it was concluded that only 'trivial' quantum effects were involved [223]. The quantisation energy determines the chemical structures underpinning biology, but no theory or experiment supported the role of 'non-trivial' effects such as coherence and entanglement. The greater understanding of environment induced decoherence in the 1980's further cemented the idea that such effects would be impossible in biological systems, due their "hot and wet" nature. The decoherence rate was known to increase significantly with temperature [271, 248, 33], and with the strength and number of interactions (collisions) between a system and it's environment [90, 121]. Using these models vanishingly small coherence times were predicted for biological systems [241], which were later discredited [216]. This idea that quantum biology was impossible was indirectly reinforced by the great difficultly experimentalists faced in cooling and isolating systems to preserve their fragile coherence for quantum information experiments, such as ion traps [185]. So it would appear that biological environments are pessimal for quantum coherent behaviour.

However, this not a complete picture. Firstly, there is the tacit assumption that biological systems are at thermal equilibrium, but in fact they consume energy to maintain a state very far from equilibrium. They therefore have the potential to maintain different thermodynamic environments within themselves and some theoretical work suggests the creation of extremely low effective temperatures (mK) on certain molecular structures [169]. One would expect that by isolating individual structures from the rest of the cell, decoherence times could be greatly extended. Secondly, the structured nature of the cellular environment could help to suppress decoherence [172]. Strong interactions with elements of the environment can, paradoxically, lead to coherence preservation via quantum Zeno like effects [185, 1]. This greater understanding of the subtleties of decoherence has lent credence to previously ignored or rejected suggestions of a role for quantum mechanics in biology.

The sense of smell, or olfaction, was thought to be adequately explained by a lock and key type mechanism [30]. However, some examples can be found that would appear to contradict this, where molecules of near identical shape, but differing vibrational spectra can be distinguished [86]. This led to the revival of a proposed alternative mechanism, which used phonon assisted electron tunnelling to detect the vibrational spectra of molecules [246]. Quantum mechanics is essential to such a mechanism and the physics of it was shown to be theoretically sound [27]. However,

debate on this matter continues [117], particularly with regard to the mammalian sense of smell.

The ability of birds to navigate across long distances is another remarkable natural phenomenon that is not yet fully understood. The 'avian compass' in some birds, such as the homing pigeon, was long thought to comprise the magnetic material in their beaks [266, 233]. However, this has recently been called into question [244]. In other species such as the European robin, a more complex system is needed to explain the experimental evidence, whereby a photon creates a pair of free radicals in the bird's eye [211]. The spins of the free electrons in the pair experience different local fields as well as interacting with the Earth's magnetic field. This difference causes a quantum coherent oscillation of the system, between a singlet and triplet state, dependant on its orientation to the earth's magnetic field [93]. The oscillation creates a difference in the rate of production a chemical and hence its concentration, which the bird is able to sense.

Ion channels are nanometer scale structures, which selectively conduct ions across cell membranes with great speed and efficiency [119, 161]. Classical simulations do not reproduce the observed level of ion selectivity and quantum models have been proposed [254]. The speed with which the brain can process information has lead some to suggest that it is employs quantum information processing and even further that consciousness itself is quantum mechanical [110]. This should be regarded as pure speculation and appears worryingly like an attempt to tie together two loose ends in our understanding of nature. However, attempts to prove or disprove the idea should foster fascinating new science.

1.4.1 Photosynthesis

The safe and efficient generation of energy is one of the most pressing problems facing humanity. Photosynthetic structures in nature have undergone billions of years of evolution to perfect them for this very purpose. Light entering such a structure creates an exciton (electron-hole pair), which needs to be transferred to a reaction centre before its energy can be chemically distributed to elsewhere in the organism. There is now compelling experimental evidence that this electronic energy transfer (EET) cannot be explained by classical physics alone and must make use of purely quantum mechanical effects. This process is called quantum coherent energy transfer. An explanation of the highly efficient way that plants harvest sunlight could lead to new technologies for artificial energy generation.

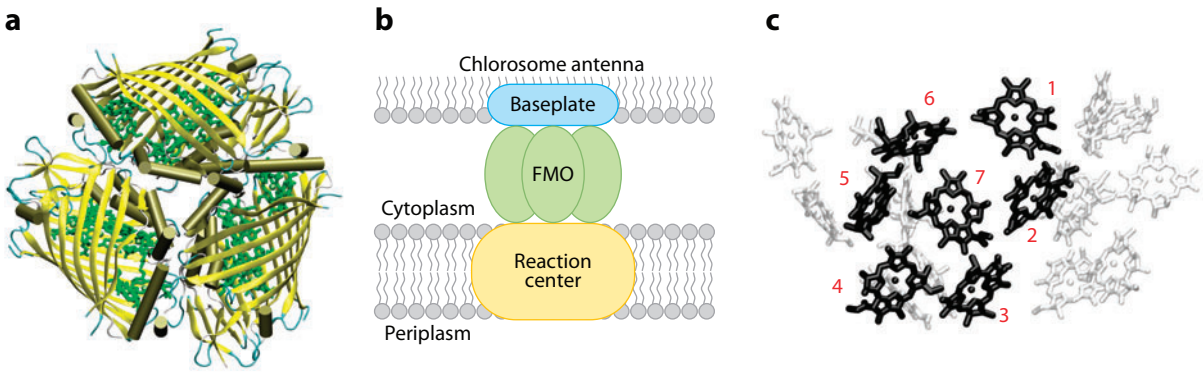

Figure 1.1: a) A view of the FMO trimer, with protein manifold. b)Position of the FMO in green sulphur bacterium. c) A view of pigments inside single FMO monomer. Picture credit [42]

At this time coherent energy transfer in photosynthesis is the only quantum biological effect to have significant and precise experimental evidence to support it. Photosynthesis is the means by which plants and bacteria generate energy from light. The light used is photosynthesis is in the visible range 400-700 nm for most chlorophyll containing organisms, unsurprisingly this is centred around the peak of the solar spectrum [16].

As one would expect there is great diversity of photosynthetic structures in nature, but they have common features. The initial absorption of photons occurs in an antenna complex, comprised of pigments, such as chlorophyll, and protein chains. The absorption creates an excited state in the system. This exciton is then transferred either directly or across other pigments to the reaction centre where charge separation and subsequent chemistry occur. In conditions of low to medium light intensity the quantum efficiency of photosynthesis is near unity [16]. It is this feature that has lead to decades of theoretical and experimental research into energy transfer in photosynthesis. The Fenna-Matthews-Olson complex (Fig.1.1), named after Fenna and Matthews who characterised it and Olson who discovered it, has been the focus of much of this work [189, 80]. It appears in green sulphur bacteria and is responsible for conducting excitons from the antenna complex to the reaction centre [15]. It is the simplest known pigment-protein complex found in nature and the first to be characterised by X-ray spectroscopy. The fact that it is soluble in water, lent it itself well to experiments and its simple structure yet complex dynamics make it ideal for theoretical studies. The FMO contains a trimer of identical subunits, each of which contains bacteriochlorophyll (BChl) molecules (pigments) wrapped in a protein manifold. There were originally thought to be 7 BChl a in each subunit, however the

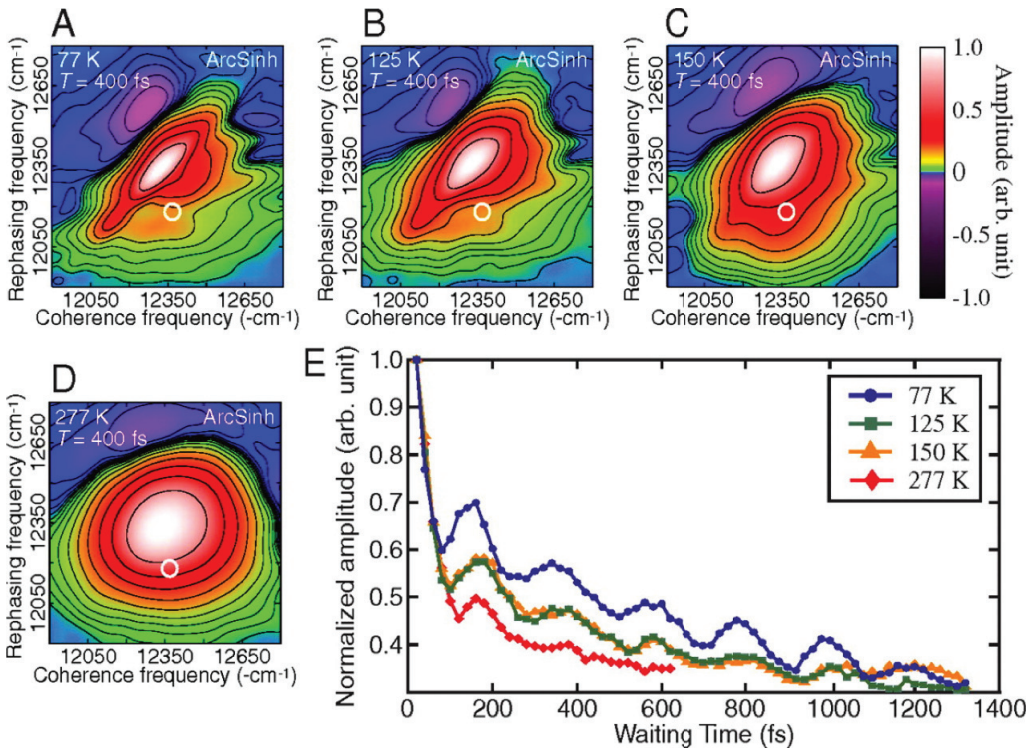

Figure 1.2: Example experimental data from [193]. A-D) Show 2D Fourier electron spectroscopy data with increasing temperature, where the white circle indicates the local of an off diagonal peak 'cross peak'. E) Shows the coherent oscillations of the site population with time at different temperatures.

most recent data suggests the existence of an 8th [245]. However, almost all work has focused on the 7 BChl system and continues to do so [114]. The excitonic properties of the complex had been explored via pump-probe experiments [87] and theoretical work [5]. From this it was known that the transfer between the BChl molecules occurred on sub-picosecond timescales. However, it was thought that this transfer occurred in a incoherent fashion i.e. the exciton classically hopped from one molecule to the next until it reached the reaction centre [250].

1.4.2 Evidence of Quantum Effects in Photosynthesis

The coherent movement of excitations through the FMO complex was first demonstrated in a seminal paper by Graham Fleming's group in 2007 [77]. They employed 2D Fourier transform spectroscopy to reveal the electronic coupling strengths and how coherences of the system evolve in time [215, 123, 26, 46, 219]. The technique uses a sequence of three pulses. The first creates a superposition of ground and excited states (a coherence) which evolves for a time τ. Then a second pulse creates an

excited state population, which evolves for time T. Finally, the third pulse creates a coherence with opposite phase to the first, rephasing occurs and a signal pulse is emitted. In Fourier space the 'input' coherence frequency is correlated with an 'output' rephasing frequency. The correlation between the two depends on the dynamics that occurred during T, for instance if the BChl's were uncoupled, the output frequency would be the same as the input plus some noise. In the FMO off diagonal peaks are observed, which indicate energy transfer has occurred (Fig.1.3A). By varying T the time evolution of the transfer can be captured and coherent oscillations in the peaks 'quantum beats' can be seen (Fig.1.3E). The beats result from interference of the frequency of the component two exciton states [41]. This demonstrates the quantum coherent nature of the transfer and the coherence was found to persist for 660 fs: far longer than expected.

The original experiment was conducted at cryogenic temperature (77 K), a follow up showed that coherences were still present at physiological temperature (300K) and were long enough (300 fs) to affect energy transfer efficiency [193]. Quantum coherence has also been observed in other organisms, such as plants [34], purple bacteria [150] and marine algae [52]. It should be noted that the experiments thus far conducted do not prove that quantum coherence is responsible for the high efficiency of EET. However, only theoretical models using that concept have been able to explain it adequately. Similarly, these experiments only prove coherent transport occurs when excited by coherent light. Sunlight is of course incoherent, but there has been theoretical work suggesting this should not make a difference to the results [164, 131].

1.5 Theoretical Background

1.5.1 Quantum Information

1.5.1.1 Pure states

One of the most remarkable features of quantum mechanics is that external observation of a system affects its physical behaviour. This is the idea encapsulated in the world's most famous thought experiment: Schrödinger's cat [222]. The realisation that 'Information is physical' [185] and the consequent union of classical information theory and quantum mechanics created the field of quantum information. The fundamental unit of information, the bit, can have two possible values 0 or 1. Any piece of information can be expressed in this form and it can have any physical manifestation, such as high and low voltages in an electrical circuit. If the physical object is

governed by quantum mechanics, for instance the spin of an electron, then quantum mechanical principle of superposition generalises the bit into a 'qubit'. Superposition allows the physical system to inhabit both states simultaneously [166]. The overall state of a qubit is thus described by a vector in terms the two basis states (using Dirac's bra-ket notation) [65]:

$$|\psi\rangle = \alpha\,|0\rangle + \beta\,|1\rangle \tag{1.6}$$

where $|0\rangle$ and $|1\rangle$ are the basis states and α and β are arbitrary complex numbers whose squares sum to unity. A measurement of the state of qubit will find it to be in one of the basis states with probability $|\alpha|^2$ or $|\beta|^2$ respectively. The coherent quantum state represented by $|\psi\rangle$ has collapsed into one of the two possible results. This is critical because although a quantum system is not deterministic, it must give a definite result to measurements, in order to reconcile it with the classical world we perceive.

1.5.1.2 Mixed states

This mathematical description of a quantum state is fine for 'pure' states, however in many physical scenarios the state is 'mixed'. This means that the state can be a range of different pure states with different probabilities. For instance imagine an experiment, which aims to creates a particular pure state but for practical reasons its efficiency is limited. With some (hopefully large) probability it will create the desired state, but sometimes it will fail and create another state. The output of such an experiment is a mixed state. To describe such states we use the density matrix formalism [256, 18]:

$$\hat{\rho} = \sum_n p_n\,|\psi_n\rangle\,\langle\psi_n|, \tag{1.7}$$

where each $|\psi_n\rangle$ is a pure state and p_n is the probability of ρ being in that particular state.

The density matrix formalism is particularly useful for describing systems interacting with a wider environment and the resultant decoherence. Decoherence of a quantum system is the decay of the coherent superposition between its states. Figuratively speaking the 'quantumness' of the system is lost, and all that remains are results with some classical probability. In this way it explains the behaviour observed in macroscopic world despite the seemingly paradoxical and contradictory laws of quantum mechanics [220]. A measurement can fully decohere a system instantly, but the effect can also occur incrementally via interactions with the environment [136].

Generally the larger a system is the greater the strength of its interaction with the environment and the faster it decoheres, hence we do not observe superpositions of everyday objects. Decoherence is the bane of any potential quantum technology, because the superposition is often the very resource they seek to exploit. This has been particularly evident in the struggle to build a quantum computer [66].

1.5.1.3 Operators

The manipulation of the state in Quantum Mechanics is done via operators, which for a qubit take the form of 2×2 matrices:

$$\sigma_x = \begin{pmatrix} 0 & 1 \\ 1 & 0 \end{pmatrix}, \sigma_y = \begin{pmatrix} 0 & i \\ -i & 0 \end{pmatrix}, \sigma_z = \begin{pmatrix} 1 & 0 \\ 0 & -1 \end{pmatrix}. \tag{1.8}$$

Originally defined by Pauli to describe a spin $\frac{1}{2}$ particle in a magnetic field, they work generally to describe manipulations of the state of a quantum two level system. It is also useful to define direct transitions between the basis states:

$$\sigma_+ = \begin{pmatrix} 0 & 0 \\ 1 & 0 \end{pmatrix}, \sigma_- = \begin{pmatrix} 0 & 1 \\ 0 & 0 \end{pmatrix}. \tag{1.9}$$

1.5.2 Open Quantum Systems

Early quantum mechanics focused on 'closed' systems; single atoms or field modes completely isolated from their environment. This was sufficient to reveal a huge wealth of new physics, from the precise spectra for atoms to the EPR paradox [75] and non-locality [12]. However, in reality the isolated system is only ever an approximation. The time evolution of a closed system is given by the Schrödinger equation [203]:

$$i\hbar \frac{d}{dt} |\psi(t)\rangle = \hat{H} |\psi(t)\rangle, \tag{1.10}$$

where $\hat{H}$ is the Hamiltonian of the system and we have now explicitly given the states time dependance, known as the 'Schrödinger picture' [203]. This evolution is referred to as unitary dynamics and is reversible in time. However, all systems, both quantum and classical, interact with their environment in a significant way. The environment of a quantum system, also referred to as the 'bath' or 'reservoir', can be composed of neighbouring particles or fields. The total Hamiltonian of a generic open system is:

$$\hat{H}_{\mathcal{SE}} = \hat{H}_{\mathcal{S}} + \hat{H}_{\mathcal{E}} + \hat{H}_{\mathcal{I}}, \tag{1.11}$$

where the subscripts denote operators acting on the respective Hilbert spaces $\mathcal{S}$ system, $\mathcal{E}$ environment and combined $\mathcal{SE}$ and $\hat{H}_{\mathcal{I}}$ is the Hamilton of the interaction

between the system and bath. Its presence induces both dissipation (movement toward energetic equilibrium) and dephasing, collectively referred to as decoherence [135, 91]. The environment has a large (possibly infinite) number of degrees of freedom, compared to the system of interest. Thus equations governing the overall system and bath would be hugely complex. However, we are by definition uninterested in the precise behaviour of the environment, we only want to be able to accurately describe its effect on the system of interest. The density matrix formalism allows us to do this elegantly, by tracing out the environmental degrees of freedom:

$$\hat{\rho}_{\mathcal{S}}(t) = \mathrm{Tr}_{\mathcal{E}}[\hat{\rho}_{\mathcal{SE}}(t)], \tag{1.12}$$

where the $\hat{\rho}_{\mathcal{S}}(t)$ is 'reduced density matrix' of the system, $\hat{\rho}_{\mathcal{SE}}(t)$ is the total system and environment density matrix. To understand the dynamics of open quantum systems we want to find the time evolution of the $\rho_{\mathcal{S}}$. This evolution is given by a 'Quantum Master Equation'. The evolution will generally be non-unitary as the interaction with the environment causes the system to journey toward a mixed state in a non-reversible manner. Master equations are a critical tool for studying open quantum systems and there are various species of them, which are best explained through an outline of their derivation.

1.5.2.1 Master Equations

Starting from the Von Neumann equation, which is the equivalent of the Schrödinger equation in density matrix notation [25]:

$$\frac{d}{dt}\hat{\rho}(t) = -\frac{i}{\hbar}[\hat{H}_I(t), \hat{\rho}(t)], \tag{1.13}$$

where $\hat{H}_I(t)$ is the Hamiltonian in the 'interaction picture' and $\hbar$ is the reduced Planck constant. The interaction picture is a transformation which treats $\hat{H}_I$ as a perturbation to the uncoupled system and environment ($\hat{H}_{\mathcal{S}}$ and $\hat{H}_{\mathcal{E}}$) [267]. The interaction picture corrisponds to the following unitary transformation:

$$\widetilde{H}(t) = e^{-i(H_S+H_{\mathcal{E}})t} H e^{-i(H_S+H_{\mathcal{E}})t} \tag{1.14}$$

The interaction Hamiltonian is time-dependent in the interaction picture. From here on we shall adopt the standard convention of setting $\hbar = 1$. First we formally integrate (1.13) and insert the result back into the original equation, then we trace over the environmental degrees of freedom:

$$\frac{d}{dt}\tilde{\rho}_S(t) = -\int_0^t dt' \mathrm{Tr}_{\mathcal{E}}[\tilde{H}_I(t), [\tilde{H}_I(t'), \tilde{\rho}_{\mathcal{SE}}(t')]]. \tag{1.15}$$

The master equation at this point is exact, but implicit, due to the presence of $\tilde{\rho}_{\mathcal{SE}}(t')$ in the commutator, to make it explicit we make a series of approximations. The first is known as the 'Born Approximation': the density matrix of the total system is approximated by a product of the system density matrix and a time independent bath density matrix:

$$\frac{d}{dt}\tilde{\rho}_S(t) = -\int_0^t dt' \mathrm{Tr}_{\mathcal{E}}[\tilde{H}_I(t), [\tilde{H}_I(t'), \tilde{\rho}_{\mathcal{S}}(t') \otimes \tilde{\rho}_{\mathcal{E}}]]. \tag{1.16}$$

This assumes that the coupling between the system and the environment is weak and that the environment is large such that the interaction does not significantly affect the state of the environment [25]. However, the system may still excite the bath and it can become entangled with it, but only on a far shorter timescale than that of the system dynamics [25]. This is because the approximation is only an assertion that the effect of total system on the reduced system dynamics can be well approximated by this product [267]. Equation (1.16) still contains reference to two points in time t and t', to simplify it further we want to make it time-local i.e. only dependent on t. To achieve this we make the 'Markov Approximation', physically this is the assumption that the bath has no 'memory' i.e. its interaction with the system depends only on its current state. Any internal correlations within the bath die away much faster than the timescale of significant changes to the system reduced density matrix [25]. To this end we make the system density matrix $\tilde{\rho}_{\mathcal{S}}(t')$ only dependent on the current time $\tilde{\rho}_{\mathcal{S}}(t)$:

$$\frac{d}{dt}\tilde{\rho}_S(t) = -\int_0^t dt' \mathrm{Tr}_{\mathcal{E}}[\tilde{H}_I(t), [\tilde{H}_I(t'), \tilde{\rho}_{\mathcal{S}}(t) \otimes \tilde{\rho}_{\mathcal{E}}]]. \tag{1.17}$$

This equation is called the Redfield equation [207], although the preceding step is sometimes referred to as the Markov approximation [38], it is not yet complete because it still refers to specific start time ($t = 0$). To complete the Markov approximation we make the change of variables $t = t - t'$ and let the limit run to infinity:

$$\frac{d}{dt}\tilde{\rho}_S(t) = -\int_0^\infty dt' \mathrm{Tr}_{\mathcal{E}}[\tilde{H}_I(t), [\tilde{H}_I(t-t'), \tilde{\rho}_{\mathcal{S}}(t) \otimes \tilde{\rho}_{\mathcal{E}}]]. \tag{1.18}$$

This is known as the 'Born-Markov Master Equation' and has had extensive use in applications of open quantum systems theory. The approximations it uses are particularly applicable to quantum optics [258], where relatively weak coupling to

large environment is common such as a single atom or photon interacting with a EM field. We will work through this example in Section 1.5.4. The Born-Markov Master Equation is not yet guaranteed to give physical results, for instance the density matrix may not preserve its trace. In order to obtain a guaranteed physical master equation a further approximation must be made. Alternately refereed to as the secular or rotating wave approximation (RWA), this corresponds to an averaging out of fast rotating terms, relative the intrinsic timescale of the system dynamics. In order to introduce this approximation we must study the form of the the interaction Hamilton, before inserting it into the equation above. A general interaction in the Schrödinger picture can be decomposed into pairs of operators acting on the system and on the bath:

$$H_I = \sum_\alpha A_\alpha \otimes B_\alpha \,, \tag{1.19}$$

Before moving into the interaction picture, we first project the interaction Hamiltonian onto the the system eigenbasis:

$$A_\alpha(\omega) = \sum_{\epsilon' - \epsilon = \omega} \Pi(\epsilon)\, A_\alpha\, \Pi(\epsilon') \,, \tag{1.20}$$

where $\Pi(\epsilon)$ is the projector on to the state $|\epsilon\rangle$. Since the projectors have rotated the system part of the interaction Hamiltonian into the system eigenbasis, it's operators are eigenoperators:

$$[H_S, A_\alpha(\omega)] = \omega A_\alpha(\omega) \,, \tag{1.21}$$

$$[H_S, A_\alpha^\dagger(\omega)] = -\omega A_\alpha^\dagger(\omega) \,. \tag{1.22}$$

After this projection moving to the interaction picture is simple (1.14):

$$\widetilde{A}_\alpha(t) = e^{i(H_S+H_\mathcal{E})t} A_\alpha(\omega) e^{-i(H_S+H_\mathcal{E})t} = e^{i\omega t} A_\alpha(\omega) \,, \tag{1.23}$$

$$\widetilde{A}_\alpha^\dagger(t) = e^{i(H_S+H_\mathcal{E})t} A_\alpha^\dagger(\omega) e^{-i(H_S+H_\mathcal{E})t} = e^{-i\omega t} A_\alpha^\dagger(\omega) \,, \tag{1.24}$$

where the $H_\mathcal{E}$ part of the operator is ignored, because it has no effect on the system Hilbert space. The operators $A_\alpha(\omega)$ have the property:

$$A_\alpha(\omega) = A_\alpha^\dagger(-\omega) \,. \tag{1.25}$$

If these operators are summed over all the energy differences the completeness relation means that:

$$\sum_\omega A_\alpha(\omega) = \sum_\omega A_\alpha^\dagger(\omega) = A_\alpha \,. \tag{1.26}$$

Transforming the bath operators yields:

$$\widetilde{B}_\alpha(t) = e^{iH_\mathcal{E}t} B_\alpha(\omega) e^{-iH_\mathcal{E}t}\,, \tag{1.27}$$

$$\widetilde{B}^\dagger_\alpha(t) = e^{iH_\mathcal{E}t} B^\dagger_\alpha(\omega) e^{-iH_\mathcal{E}t}\,. \tag{1.28}$$

We can now write the interaction Hamiltonian, in the interaction picture, in a convenient form:

$$\widetilde{H}_I(t) = \sum_{\alpha,\omega} e^{i\omega t} A_\alpha(\omega) \otimes B_\alpha(t)\,. \tag{1.29}$$

We are now ready to insert our interaction picture Hamiltonian into the master equation (1.18). First we expand out the commutator to yield:

$$\frac{d}{dt}\widetilde{\rho}_S(t) = \int_0^\infty \mathrm{Tr}_\mathcal{E}[\widetilde{H}_I(t-t')\rho_S(t)\otimes\rho_\mathcal{E}\widetilde{H}_I(t) - \widetilde{H}_I(t)\widetilde{H}_I(t-t')\rho_S(t)\otimes\rho_\mathcal{E}] + \text{h.c.}\,. \tag{1.30}$$

Then we insert (1.29) into (1.30):

$$\frac{d}{dt}\widetilde{\rho}_S(t) = \sum_{\omega,\omega'}\sum_{\alpha,\beta} e^{i(\omega-\omega')t}\Gamma_{\alpha,\beta}(\omega)\left(\hat{A}_\beta(\omega)\rho_S(t)\hat{A}^\dagger_\alpha(\omega') - \hat{A}^\dagger_\alpha(\omega')\hat{A}_\beta(\omega)\rho_S(t)\right) + \text{h.c.}\,. \tag{1.31}$$

When justifying the Markov approximation we stated that correlations in the bath must decay on a time scale much faster than the intrinsic system timescale. Let us call that timescale τ_s, this timescale will be given by the average value of $\tau \approx \langle(\omega-\omega')\rangle^{-1}$. The other relevant timescale is the relaxation timescale τ_R, this is timescale of the systems relaxation to equilibrium. If τ_S is large relative to τ_R, terms the fast rotating terms $\omega - \omega'$, will average out their effect to zero over time it takes to significantly alter ρ_S. Thus only the terms where $\omega = \omega'$ need to be retained:

$$\frac{d}{dt}\widetilde{\rho}_S(t) = \sum_{\omega}\sum_{\alpha,\beta} \Gamma_{\alpha,\beta}(\omega)\left(\hat{A}_\beta(\omega)\rho_S(t)\hat{A}^\dagger_\alpha(\omega) - \hat{A}^\dagger_\alpha(\omega)\hat{A}_\beta(\omega)\rho_S(t)\right) + \text{h.c.}\,. \tag{1.32}$$

We now turn our attention to the spectral correlation tensor defined by:

$$\Gamma_{\alpha,\beta}(\omega) = \int_0^\infty dt' e^{i\omega t'} \mathrm{Tr}_\mathcal{E}[B^\dagger_\alpha(t) B_\beta(t-t')\rho_E]\,. \tag{1.33}$$

The reservoir correlation function is defined $C_{\alpha,\beta}(t-t')$ by :

$$C_{\alpha,\beta}(t-t') = \mathrm{Tr}_\mathcal{E}[B^\dagger_\alpha(t) B_\beta(t-t')\rho_E] = \langle B^\dagger_\alpha(t) B_\beta(t-t')\rangle\,. \tag{1.34}$$

As part of the Born approximation we have already assumed that the bath's density matrix doesn't evolve in time. Therefore, its correlation function is also time independent:

$$C_{\alpha,\beta}(t') = \langle B^\dagger_\alpha(t') B_\beta(0)\rangle\,, \tag{1.35}$$

which of course implies that the transition rates (1.33). This is only true in Born-Markov case, non-Markovian processes can have time dependent rates. It is instructive to decompose the transition rates (1.33) in the following way:

$$\Gamma_{\alpha,\beta}(\omega) = \frac{1}{2}\gamma_{\alpha,\beta}(\omega) + iS_{\alpha,\beta}(\omega)\,, \tag{1.36}$$

where $S_{\alpha,\beta}(\omega)$ is the coefficient of the Lamb shift and $\gamma_{\alpha,\beta}(\omega)$ is given by:

$$\gamma_{\alpha,\beta}(\omega) = \Gamma_{\alpha,\beta}(\omega) + \Gamma_{\alpha,\beta}(\omega)^* = \int_{-\infty}^{\infty} dt' e^{i\omega t'} \left\langle B_\alpha(t') B_\beta(0) \right\rangle \,, \tag{1.37}$$

Combining these results allows us to write the master equation in the extremely compact form:

$$\frac{d}{dt}\widetilde{\rho}_S(t) = -i[H_{LS}, \rho_S(t)] + D(\widetilde{\rho}_s(t))\,. \tag{1.38}$$

The Lamb shift term H_{LS} commutes with the Hamiltonian and can be accounted for by simply shifting the energies of the system.

$$H_{LS} = \sum_{\omega} \sum_{\alpha,\beta} S_{\alpha,\beta}(\omega) A^\dagger_\alpha(\omega) A_\beta(\omega)\,. \tag{1.39}$$

The Lamb shift is usually considered negligible [38], but it can have interesting consequences, as we show in 3.4.1.1 it can describe field induced interactions between atoms. The second term in (1.38) $D(\widetilde{\rho}_s(t))$ is called the dissipator and describes the non-unitary evolution of the system:

$$D(\widetilde{\rho}_s(t)) = \sum_{\omega} \sum_{\alpha,\beta} \gamma_{\alpha,\beta}(\omega)(A_\beta(\omega)\rho_S A^\dagger_\alpha(\omega) - \frac{1}{2}\{A^\dagger_\alpha(\omega)A_\beta(\omega), \rho_S\})\,. \tag{1.40}$$

The dissipator has a clear physical interpretation, the operators $A_\beta(\omega)$ describe transitions between the system's eigenstates. These transitions are mediated by the environment. Each transition has a specific frequency at which it samples the environment and the structure of the environment as well as the strength of coupling determines the rate a which these transitions occur. By diagonalising the matrix $\gamma_{\alpha,\beta}(\omega)$ (1.40) and returning to the Schrödinger picture the master equation (1.38) can be cast into Lindblad form [25]:

$$\mathcal{L}\rho_S = -i[H, \rho_S] + \sum_k \gamma_k \left(L_k \rho_S L_k^\dagger + \frac{1}{2} L_k^\dagger L_k \rho_S + \frac{1}{2} \rho_S L_k^\dagger L_k \right) \,, \tag{1.41}$$

where k is the index of the Lindblad operators and γ_k is the requisite transition rate.

1.5.2.2 Non-Markovian Dynamics

Unfortunately the exotic effects in biology and nanotechnology that we are interested are, in general, not manifest in this convenient regime. For example the interaction of a superconducting qubit with its environment (typically charged defects in the surrounding material) at low temperature [179, 158] and quantum dots interacting with phonons are known to exhibit non-Markovian behaviour [20]. This is typically identified by the characteristic non-exponential decay of density matrix elements [159, 146]. Biological systems are known to have coupling strengths comparable to energy scale of the system, making the weak coupling condition questionable [232]. There is also evidence that two way interaction with the environment can be integral to EET; beats in the decay of site populations and a more efficient transfer relative to a Markovian model occurs [127, 206].

There are a raft of non-Markovian techniques designed to approach these problems. However, this is a regime of great mathematical and physical complexity, where few intuitive or satisfying solutions exist, even for toy models. Equations of the form of (1.16) can in some cases be solved using Laplace transforms, though this is contingent on the form of the correlation function [171]. For example Brandes has derived equations of motion valid in the strong coupling limit by preforming a polaron transform [162, 257], and subsequent Laplace transformation [22]. The Nakajima-Zwanzig projection operator technique [182, 272] can be applied, but it also produces time non-local equations that are analytically unwieldy, so it is more often employed as a basis for approximations and numerical methods. A similar approach, but one which yields time local equations is the 'time-convolutionless projection operator technique' [39, 214]. This methods is peturbative, but the parameter being expanded depends on the system, and is not obvious, so careful consideration of its validity must be made [24]. Futhermore Non-Markovian Quantum Jumps (NMQJ) [198] and Non-Markovian Quantum State Diffusion (NMQSD) [63], are generally restricted to numerical techniques and further approximations respectively. Finally the technique of pseudomodes can be applied when the environment has a specific spectral density [92]. This technique is linked to recent efforts to understand a non-Markovian bath in terms of a memory part and dissipative part [172, 62], which has the potential restore a physically intuitive understanding of the dynamics and to unify the diverse and complex methods discussed here.

1.5.2.3 Types of Environment

Although we are not concerned with the specific dynamics of the environment, it must of course be an accurate representation of what we are trying to model. This appears to be a huge problem: how can one find an appropriate $\hat{H}_{\mathcal{E}}$ to reflect anything from a semiconductor substrate to the interior of a cell? Fortunately the entire spectrum of physical environments can be mapped on to one of two models: the spin bath and the oscillator bath. The spin bath is composed of an infinite number of two level systems and deals with localised effects and strong coupling, which are dominant in the solid state at low temperature [179]. The oscillator bath is an infinite number of bosonic modes (photon, phonons etc.) and applies best to delocalised environments [151, 263]. Perhaps surprisingly, it is universal in the weak coupling limit [81, 32] and is therefore the most commonly used form.

The physical structure of the environment (given by the spectral density) dramatically affects its behaviour. For instance an oscillator bath with flat spectral density induces very different system dynamics to one with a few dominant modes (a structured bath). This may determine whether or not the system exhibits non-Marokivan behaviour and the rate at which it decoheres [172, 95].

1.5.2.4 Modelling of Transport in Biomolecules

These extraordinary experimental results spurred theoretical efforts to explain how quantum coherence could persist in such a structures and whether it is responsible for their extremely high transfer efficiency. Photosynthetic structures such as the FMO complex are difficult to model for several reasons. Firstly, they lie in an intermediate coupling regime where the system's coupling to its environment is of comparable strength to the system's parameters when isolated. This makes it difficult to apply perturbative approaches to the system. Secondly, the dynamics are not well captured by any of the typical simplifications, such as the Born-Markov approximation.

To describe the system, the interaction between pigments or 'sites', we employ the Frenkel exciton model, which is suited to strongly coupled systems with delocalised excitations [171]:

$$\hat{H}_{\mathcal{S}} = \sum_{n=0}^{N} \epsilon_n \left|n\right\rangle \left\langle n\right| + \sum_{m<n} \Delta_{nm}(\left|n\right\rangle \left\langle m\right| + \left|m\right\rangle \left\langle n\right|), \tag{1.42}$$

where the first term describes a series of N sites with energy splitting ϵ_n and the second describes the coupling or tunnelling between sites n and m with rate Δ_{nm}.

This system interacts with a bosonic bath:

$$\hat{H}_{\mathcal{E}} = \sum_{j=-\infty}^{\infty} \omega_j (a_j^\dagger a_j), \tag{1.43}$$

$$\hat{H}_{\mathcal{I}} = \sum_{j,n} g_{jn} (a_j^\dagger + a_j) \left|n\right\rangle \left\langle n\right|, \tag{1.44}$$

where ω_j is frequency of given bosonic mode, $a_j^\dagger$ and a_j are its creation and anihilation operators respectively and g_{jn} is the coupling strength between a given mode and site. This is an extended spin boson type model [151]. Förster theory has long been applied to such systems across physics chemistry and biology [85]. It is valid in the limit of strong system-bath coupling and low tunnelling ($g > \Delta$) and describes and incoherent hopping process between sites due to point like dipole interactions. In the opposite limit, the case of weak coupling ($g < \Delta$), the standard open quantum systems techniques of Lindbald [25] and Redfield [207] master equations (ME) can be used. However, perturbative approaches from either extreme breakdown in the intermediate regime [128]. Non-Markovian effects have been identified in experimental data [208], studied theoretically [209, 242] and found to be potentially important to the transfer efficiency [232].

Master Equations, employing the polaron transform to extend their validity into the strong coupling regime, have been used to produce both numerical [132] and interesting analytical results [184] for a dimer system. Similarly, extensions of the Redfield equations have been created with a greater area of applicability [36], but these methods remain perturbative.

Non-perturbative models also face problems. The Haken-Reineker-Strobl approach [109, 37] models the environment as classical white noise, which induces dephasing of the system interactions. It correctly predicts long lived coherences but not the relaxation process and results in an even distribution of population across the sites. However, there has been a recent attempt to fix the model [259].

Numerical simulations in principle offer arbitrary precision results for particular parameters, but are restricted by the available computational power due to the large number of degrees of freedom involved in such systems. Hierarchal master equations have been particularly successful. Originally developed by Tanimura and Kubo [240, 239], they were recently applied to the FMO [129, 130]. These methods have been able to accurately reproduce the observed coherent oscillations in the FMO. But they do not reveal the physics of the underlying processes. Other approximate

simulations have been devised to reduce the computational cost. An interesting example is [232], in which higher order correlations in the bath are removed resulting in a non-Markovian, non-perturbative master equation, but the results only roughly match those of [129]. The density matrix renormalisation group (DMRG), which analytically maps system-bath structures into a linear chain, has also been suggested as a method for efficiently simulating EET in biomolecules [200].

Accounting for the observed efficiency has also been problematic. It was originally suggested that delocalisation of the exciton into a wave led to the exploration of all the paths and the selection of the most efficient [77]. How such selection occurred was not clear, this lead some to high profile claims that the structure was somehow employing the quantum computing algorithm 'Grover's search' [104] to find the optimal path [77]. A more realistic proposal based on quantum walks [177] was also shown to be wrong, as it did not offer speed up in the conditions under which photosynthetic EET operates [122].

Just as there is an intermediate regime of two coupling strengths in photosynthetic EET there is also an intermediate regime of two timescales: the timescale of the transfer process between sites (J^{-1}) and the timescale of the dephasing processes induced by the system bath interaction (τ_d) [127]. If ($\tau_{rn} \ll J^{-1}$) the exciton will have dephased before each transfer, making it equivalent to a classical hop. If ($\tau_{rn} \gg J^{-1}$) the excitation will spread out across the sites coherently until collapsed. Fully coherent transport is not optimal, and there is a consensus that the middle ground of 'noise assisted' transport is superior [44].

The spectral density of the pigment protein complex is also thought to play a role in the transport properties. Experiments have shown a complex environment involving strong coupling to discrete modes in the FM0 [265, 205]. Similar peaked spectral densities have been used in theoretical work [5], where they have been shown to be important to the transfer efficiency [45, 43].

In conclusion, coherent EET in photosynthesis occurs due to a delicate interplay between coherent and incoherent dynamics. Although much work has been done on the field, many of the fundamental mechanisms remain unclear. For instance what is the enabling feature for systems exhibiting this high transport efficiency: coherent fluctuations of the site energy induced by the protein manifold, a non-markovian interaction with a structured bath, orientation of the pigments and proteins? Numerical methods have been effective in modelling the overall dynamics observed and hinting at what aspects may be responsible. However, the individual processes and

building blocks of such structures will need to be understood if we are to realise the ultimate goal of the exploiting these properties in artificial systems.

1.5.3 Quantum Optics

The latter two research chapters deal with how light absorption might be enhanced, by using quantum technologies. We shall therefore now cover the history and methodology of treating light as a quantum field. The results from this will be the basic Hamiltonians that we use later to model our candidate absorption technologies.

1.5.3.1 History

The classical theory of light culminated in 1865 when James Clerk Maxwell unified the myriad empirical laws of electricity and magnetism into a single coherent set [170]. This contraction of theories revealed that light propagates as an electromagnetic wave. The original 20 equations were then brought into their modern form by eccentric English electrical engineer Oliver Heaviside [116]. The quantum theory of light began in 1901 with Max Planck reluctantly postulating the quantisation of the harmonic oscillator, which allowed him to explain the widely observed spectrum of blackbody radiation [199]. Einstein was the first to propose that light quanta or photons were 'real' (as opposed to mathematical trick) and were essential to the photoelectric effect [73]. In the 1920's Paul Dirac developed a full theory of light as a quantum field using what became the canonical quantisation procedure [64].

1.5.3.2 Maxwell's Equations & Classical Light

In this section we first show that a classical treatment of light starting from Maxwell's equations can be cast in a form that allows a direct correspondence between quantum and classical. Of course, classical degrees of freedom are generally continuous in contrast to quantum ones, which are principly discrete. However, considering light confined in a volume of free space imposes boundary conditions, which discretise the modes of classical light by only allowing certain frequencies to be present. This leads to a formal equivalence between to individual light modes and simple harmonic oscillators. Arriving at this result allows the field to be quantised in straight forward way, by transforming the mode amplitudes to quantum operators.

Maxwell's equations, in vector calculus form, are:

$$\boldsymbol{\nabla} \times \boldsymbol{E} = -\frac{\delta \boldsymbol{B}}{\delta t}\,, \tag{1.45}$$

$$\mu_0^{-1} \boldsymbol{\nabla} \times \boldsymbol{B} = \epsilon_0 \frac{\delta \boldsymbol{E}}{\delta t} + \boldsymbol{J}\,, \tag{1.46}$$

$$\epsilon_0 \boldsymbol{\nabla} \cdot \boldsymbol{E} = \sigma\,, \tag{1.47}$$

$$\boldsymbol{\nabla} \cdot \boldsymbol{B} = 0\,. \tag{1.48}$$

where ϵ_0 and μ_0 are the permittivity and permeability of free space respectively. For the quantisation procedure it more convenient to express $\boldsymbol{E}$ and $\boldsymbol{B}$ in terms of a scalar potential $\boldsymbol{\nabla}\phi$ and vector potential $\boldsymbol{A}$. Defining the potentials such that they satisfy Equations (1.45, 1.48) yield:

$$\boldsymbol{E} = -\boldsymbol{\nabla}\phi - \frac{\delta \boldsymbol{A}}{\delta t}\,, \tag{1.49}$$

$$\boldsymbol{B} = \boldsymbol{\nabla} \times \boldsymbol{A}\,. \tag{1.50}$$

The solutions to the remaining two Maxwell equations are gauge invariant. We are therefore free to choose the Coulomb gauge where:

$$\boldsymbol{\nabla} \cdot \boldsymbol{A} = 0\,, \tag{1.51}$$

$$\boldsymbol{\nabla}\phi = 0\,. \tag{1.52}$$

Further assuming that the field is in free space ($\sigma = 0, \boldsymbol{J} = 0$), Equations (1.49, 1.50) simplify to:

$$\boldsymbol{E} = -\frac{1}{c}\frac{\delta \boldsymbol{A}}{\delta t}\,, \tag{1.53}$$

$$\boldsymbol{B} = \boldsymbol{\nabla} \times \boldsymbol{A}\,, \tag{1.54}$$

and Equations (1.46, 1.47) yield:

$$-\boldsymbol{\nabla}^2 \boldsymbol{A} + \frac{1}{c^2}\frac{\delta^2 \boldsymbol{A}}{\delta t^2} = 0\,, \tag{1.55}$$

which has the familiar form of a wave equation. This equation is linear and separable, we therefore express our potential as a Fourier series of traveling waves:

$$\boldsymbol{A} = \frac{1}{\sqrt{V}} \sum_{\boldsymbol{k},\lambda} A_{\boldsymbol{k},\lambda} \boldsymbol{\epsilon}_{\boldsymbol{k},\lambda} e^{i\boldsymbol{k}\cdot\boldsymbol{r} - i\omega t} + A^*_{\boldsymbol{k},\lambda} \boldsymbol{\epsilon}^*_{\boldsymbol{k},\lambda} e^{-i\boldsymbol{k}\cdot\boldsymbol{r} + i\omega t}\,. \tag{1.56}$$

Each wave has a polarisation, which describes its motion in the plane perpendicular to $\boldsymbol{k}$. This polarisation is defined by $\boldsymbol{\epsilon}_{\boldsymbol{k},\lambda}$, where an index λ denoting the two basis

vectors in this plane ($\boldsymbol{\epsilon}_{\boldsymbol{k},\lambda} \cdot \boldsymbol{k} = 0$). The following properties of the polarisation will be useful in later calculations and stem directly from the orthogonality requirements:

$$\boldsymbol{\epsilon}_{\boldsymbol{k},\lambda} \cdot \boldsymbol{\epsilon}_{\boldsymbol{k'},\lambda'} = \delta_{\lambda,\lambda'} \,, \tag{1.57}$$

$$\sum_{\lambda=1,2} \boldsymbol{\epsilon}^i_{\boldsymbol{k},\lambda} \boldsymbol{\epsilon}^j_{\boldsymbol{k},\lambda} = \delta_{i,j} - \frac{k^i k^j}{|k|^2} \,, \tag{1.58}$$

where $i, j = x, y, z$. We now consider a cubic box of free space with volume V and length L. The box imposes periodic boundary conditions on the the waves, giving the following allowed values of for the components of the wavevector $\boldsymbol{k}$:

$$\boldsymbol{k}_x = \frac{2\pi n_x}{L}, \;\; \boldsymbol{k}_y = \frac{2\pi n_y}{L}, \;\; \boldsymbol{k}_z = \frac{2\pi n_z}{L} \,, \tag{1.59}$$

where $n_v \in \mathbb{Z}$. Since the different components all independently satisfy (1.55) it is easy to that:

$$\omega_k = c|k| \,, \tag{1.60}$$

where ω_k is the angular frequency of the wave with wavevector k, and c is the speed of light. By combining Eqns. (1.53, 1.54, 1.56) we can express the electromagnetic field in the box as:

$$\boldsymbol{E}(\boldsymbol{r}, t) = i \sum_{\boldsymbol{k},\lambda} \omega_k (A_{\boldsymbol{k},\lambda} \boldsymbol{\epsilon}_{\boldsymbol{k},\lambda} e^{i\boldsymbol{k}\cdot\boldsymbol{r} - i\omega t} + A^*_{\boldsymbol{k},\lambda} \boldsymbol{\epsilon}^*_{\boldsymbol{k},\lambda} e^{-i\boldsymbol{k}\cdot\boldsymbol{r} + i\omega t}) \,, \tag{1.61}$$

$$\boldsymbol{B}(\boldsymbol{r}, t) = i \sum_{\boldsymbol{k},\lambda} \boldsymbol{k} \times (A_{\boldsymbol{k},\lambda} \boldsymbol{\epsilon}_{\boldsymbol{k},\lambda} e^{i\boldsymbol{k}\cdot\boldsymbol{r} - i\omega t} + A^*_{\boldsymbol{k},\lambda} \boldsymbol{\epsilon}^*_{\boldsymbol{k},\lambda} e^{-i\boldsymbol{k}\cdot\boldsymbol{r} + i\omega t}) \,. \tag{1.62}$$

To make plain the formal analogy between our confined field and a set of harmonic oscillators it's helpful to study the total energy of the system. The energy of the electromagnetic field in a volume is given by [154]:

$$U = \frac{1}{8\pi} \int_V \left(\epsilon_0 \boldsymbol{E}^2 + \mu_0^{-1} \boldsymbol{B}^2 \right) dV \,. \tag{1.63}$$

By using our expressions for the electromagnetic field, in conjunction with the following property stemming from the orthogonality of the plane waves [226, 154] in the box:

$$\int_V d\boldsymbol{r} e^{i\boldsymbol{k}\cdot\boldsymbol{r}} e^{-i\boldsymbol{k'}\cdot\boldsymbol{r}} = V \delta_{\boldsymbol{k},\boldsymbol{k'}} \tag{1.64}$$

and noticing that $\boldsymbol{A_{k,\lambda}} = \boldsymbol{A^*_{-k,\lambda}}$:

$$\int_V d\boldsymbol{r} \epsilon_0 |\boldsymbol{E}|^2 = \int_V d\boldsymbol{r} \mu_0^{-1} |\boldsymbol{B}|^2 = 2\epsilon_0 V \sum_{\boldsymbol{k},\lambda} \frac{\omega_k^2}{c^2} (A_{\boldsymbol{k},\lambda} A^*_{\boldsymbol{k},\lambda} + A^*_{\boldsymbol{k},\lambda} A_{\boldsymbol{k},\lambda}) \,, \tag{1.65}$$

which by normalising the Fourier components appropriately ($A_{\boldsymbol{k},\lambda} = \sqrt{\frac{2\pi\hbar}{2\epsilon_0 V\omega_k}}\alpha_{\boldsymbol{k},\lambda}$) yields the total energy:

$$U = \frac{1}{2}\sum_{\boldsymbol{k},\lambda}\omega_k(\alpha^*_{\boldsymbol{k},\lambda}\alpha_{\boldsymbol{k},\lambda} + \alpha_{\boldsymbol{k},\lambda}\alpha^*_{\boldsymbol{k},\lambda})\,, \tag{1.66}$$

$$U = \sum_{\boldsymbol{k},\lambda}\hbar\omega_k n_{\boldsymbol{k},\boldsymbol{\lambda}}\,, \tag{1.67}$$

where $n_{\boldsymbol{k},\lambda} = \alpha^*_{\boldsymbol{k},\lambda}\alpha_{\boldsymbol{k},\lambda}$ counts the number of excitons in a particular mode.

1.5.3.3 Canonical Quantisation

We have demonstrated that a light field in a volume of free space is formally analogous to a set of harmonic oscillators. The harmonic oscillator is one of the very few systems for which the Schrödinger equation can be solved exactly. Quantisation of the harmonic oscillator is the canonical example of the correspondence principle: fields become operators and the total energy is given by the Hamiltonian. For now let us consider a single mode and drop the $\boldsymbol{k}$ and λ indices. Defining the quantum versions of the Fourier components α and α^*

$$\alpha^* \to a^\dagger\,, \tag{1.68}$$

$$\alpha \to a\,. \tag{1.69}$$

Since photons are bosons a and $a^\dagger$, obey bosonic commutation relations:

$$[a^\dagger, a] = 1\,, \tag{1.70}$$

and are normalised such that:

$$a\,|n\rangle = \sqrt{n}\,|n-1\rangle\ ,\ \ a^\dagger\,|n\rangle = \sqrt{n+1}\,|n+1\rangle\ , \tag{1.71}$$

where a and $a^\dagger$ are the creation and annihilation operators respectively. They create and destroy quanta of energy in the mode, in the case of the EM field this corresponds to the creation and annihilation of photons. Rewriting our equation for the energy of classical light modes (1.66) using these quantum operators yields:

$$\hat{H} = \frac{1}{2}\hbar\omega\left(a^\dagger a + aa^\dagger\right)\,, \tag{1.72}$$

$$\hat{H} = \hbar\omega\left(a^\dagger a + \frac{1}{2}\right)\,. \tag{1.73}$$

The commutation relation has introduced a zero point energy to the equation. In contrast to the classical harmonic oscillator the lowest energy state is not zero, but

half a quantum $\hbar\omega$. This is necessary to satisfy the uncertainty relation for the ground state: its position and momentum would otherwise be absolutely defined. However, for our purposes this term can safely be dropped, because we shall be dealing with interacting systems, for which only energy differences are important. The Hilbert space defined by (1.73) is called a Fock space as is generated by the eignstates of the number operator $\hat{n} = a^\dagger a$:

$$\hat{n}\left|n\right\rangle = n\left|n\right\rangle \quad n = 0, 1, 2, 3... \infty\,. \tag{1.74}$$

1.5.3.4 Generalisation to many modes

Returning to our general field composed many of normal modes:

$$\hat{H} = \sum_{\boldsymbol{k},\lambda} \hbar\omega_k \hat{n}_{\boldsymbol{k},\boldsymbol{\lambda}}\,, \tag{1.75}$$

The orthogonality of the modes means each has independent operators $a^\dagger_{\boldsymbol{k},\lambda}$ and $a_{\boldsymbol{k},\lambda}$, e.g.:

$$\hat{n}_{\boldsymbol{k},\lambda}\left|n\right\rangle_{\boldsymbol{k},\lambda} = n_{\boldsymbol{k},\lambda}\left|n\right\rangle_{\boldsymbol{k},\lambda}\,. \tag{1.76}$$

Each with there own Fock space. The total Hilbert space is composed of tensor products of the individual Fock spaces:

$$\left|\{n_{\boldsymbol{k},\lambda}\}\right\rangle = \left|n^1_{\boldsymbol{k},\lambda}\right\rangle \otimes \left|n^2_{\boldsymbol{k},\lambda}\right\rangle \otimes \left|n^3_{\boldsymbol{k},\lambda}\right\rangle ... \tag{1.77}$$

We can now write the equations for the quantised EM field by straightforward replacement of our classical field modes (1.53, 1.54) by quantum operators:

$$\boldsymbol{E}(\boldsymbol{r},t) = i\sum_{\boldsymbol{k},\lambda}\sqrt{\frac{2\pi\hbar\omega_k}{V}}(\hat{a}_{\boldsymbol{k},\lambda}\boldsymbol{\epsilon}_{\boldsymbol{k},\lambda}e^{i\boldsymbol{k}\cdot\boldsymbol{r}-i\omega t} + \hat{a}^\dagger_{\boldsymbol{k},\lambda}\boldsymbol{\epsilon}^*_{\boldsymbol{k},\lambda}e^{-i\boldsymbol{k}\cdot\boldsymbol{r}+i\omega t})\,, \tag{1.78}$$

$$\boldsymbol{B}(\boldsymbol{r},t) = i\sum_{\boldsymbol{k},\lambda}\frac{1}{k}\sqrt{\frac{2\pi\hbar\omega_k}{V}}\,(\boldsymbol{k}\times\boldsymbol{\epsilon}_{\boldsymbol{k},\boldsymbol{\lambda}})\,\hat{a}_{\boldsymbol{k},\lambda}e^{i\boldsymbol{k}\cdot\boldsymbol{r}-i\omega t} + (\boldsymbol{k}\times\boldsymbol{\epsilon}^*_{\boldsymbol{k},\boldsymbol{\lambda}})\hat{a}^\dagger_{\boldsymbol{k},\lambda}e^{-i\boldsymbol{k}\cdot\boldsymbol{r}+i\omega t}\,., \tag{1.79}$$

1.5.4 The Quantum Optical Master Equation

To provide a practical example linking together the theory of quantum optics and open quantum systems we shall now derive the canonical quantum optical master equation. The quantum optical master equation describes the interaction between an 'atom' or two level system and an electromagnetic field:

$$H = H_S + H_{\mathcal{E}} + H_I \,. \tag{1.80}$$

The atom is a two level system with a ground state $|g\rangle$ and an excited state $|e\rangle$ separated by a energy $\hbar\omega_A$:

$$H_S = \frac{\omega_A}{2}(|e\rangle\langle e| - |g\rangle\langle g|) = \frac{\omega_A}{2}\sigma_Z \,. \tag{1.81}$$

The EM field has the following form, which we derived in the previous section:

$$H_{\mathcal{E}} = \sum_{\boldsymbol{k},\lambda} \omega_{\boldsymbol{k}} \hat{a}^\dagger_{\boldsymbol{k},\lambda} \hat{a}_{\boldsymbol{k},\lambda} \,. \tag{1.82}$$

The interaction between the two is given by:

$$\hat{H}_I = -\hat{\boldsymbol{D}} \cdot \hat{\boldsymbol{E}} \,, \tag{1.83}$$

$$\hat{H}_I = (\hat{\sigma}_- \, \boldsymbol{d} + \hat{\sigma}_+ \boldsymbol{d}^*) \cdot \hat{\boldsymbol{E}} \,, \tag{1.84}$$

where $\hat{\sigma}_+ = |e\rangle\langle g|$ and $\hat{\sigma}_- = |g\rangle\langle e|$ describe the excitation and de-excitation of the atom respectively, and $\boldsymbol{d}$ is the atomic dipole vector. The electric field operator is given by:

$$\hat{\boldsymbol{E}} = i \sum_{\boldsymbol{k},\lambda} \sqrt{\frac{2\pi\omega_k}{V}} \boldsymbol{\epsilon}_{\boldsymbol{k},\lambda} \left(\hat{a}_{\boldsymbol{k},\lambda} - \hat{a}^\dagger_{\boldsymbol{k},\lambda} \right) \,, \tag{1.85}$$

We want to find the dynamics of the atom, when coupled to the field. We therefore need to calculate the dissipator (1.40) for the system. Following the procedure in Section (1.5.2.1), we first project the system and bath operators in (1.82) on to the system eigenbasis and then apply the unitary operator (1.14). For the field operator:

$$\hat{\boldsymbol{E}}(t) = -i \sum_{\boldsymbol{k},\lambda} \sqrt{\frac{2\pi\omega_k}{V}} \boldsymbol{\epsilon}_{\boldsymbol{k},\lambda} \left(\hat{a}_{\boldsymbol{k},\lambda} e^{-i\omega_k t} - \hat{a}^\dagger_{\boldsymbol{k},\lambda} e^{i\omega_k t} \right) . \tag{1.86}$$

This is the same as the result we derived in the previous section (1.78), but ignoring the spatial variable $\boldsymbol{r}$, because we define our atom to be at the origin. For the the dipole operator we have:

$$A(t) = \sum_{\omega} A(\omega) = A(\omega_A) + A(-\omega_A) \,, \tag{1.87}$$

$$A(t) = e^{i\omega_A t} \hat{\sigma}_+ + e^{-i\omega_A t} \hat{\sigma}_- \,. \tag{1.88}$$

Combing (1.86) and (1.87) gives us the interaction Hamiltonian in the interaction picture:

$$\widetilde{H}_I = (\hat{\sigma}_- \, \boldsymbol{d} + \hat{\sigma}_+ \boldsymbol{d}^*) \sum_{\boldsymbol{k},\lambda} \sqrt{\frac{2\pi\omega_k}{V}} \boldsymbol{\epsilon}_{\boldsymbol{k},\lambda} \left(\hat{a}_{\boldsymbol{k},\lambda} e^{-i\omega_k t} - \hat{a}^\dagger_{\boldsymbol{k},\lambda} e^{i\omega_k t} \right) . \tag{1.89}$$

The rotating wave approximation could be made at the level of the interaction Hamiltonian, by retaining only the terms $\hat{\sigma}_- a^\dagger$ and $\hat{\sigma}_+ a$. However, this leads to an incorrect Lamb shift term.

The system operator $A(t)$ describe the excitation and de-excitation of the atom. Similarly, the bath operators $E(t)$ describe the creation and annihilation of photons in the bath. We now have the operator $A(t)$, which causes transitions between the system's eigenstates, next we need to calculate the rates at which these transitions occur. As we saw in Section (1.5.2.1) the rates are derived from the spectral correlation tensor (1.33):

$$\Gamma_{\alpha,\beta}(\omega) = \int_0^\infty dt' e^{i\omega t'} \mathrm{Tr}_{\mathcal{E}}[E^\dagger_\alpha(t) E_\beta(t-t') \rho_E] \, . \tag{1.90}$$

Substituting (1.86) into this expression and collating the exponents yields:

$$\begin{aligned} \Gamma_{\alpha,\beta}(\omega) = \frac{2\pi}{V} \sum_{\boldsymbol{k},\boldsymbol{k'}} \sum_{\lambda,\lambda'} \sqrt{\omega_k \omega_{k'}} (\boldsymbol{\epsilon}^\alpha_{\boldsymbol{k},\lambda} \cdot \boldsymbol{\epsilon}^\beta_{\boldsymbol{k'},\lambda'}) \int_0^\infty dt' \big(& \langle \hat{a}_{\boldsymbol{k},\lambda} \hat{a}^\dagger_{\boldsymbol{k'},\lambda'} \rangle_{\mathcal{E}} e^{+i(\omega_{k'}-\omega_k)t - i(\omega_{k'}-\omega_k)t'} \\ & + \langle \hat{a}^\dagger_{\boldsymbol{k},\lambda} \hat{a}_{\boldsymbol{k'},\lambda'} \rangle_{\mathcal{E}} e^{-i(\omega_{k'}-\omega_k)t + i(\omega_{k'}+\omega_k)t'} \\ & - \langle \hat{a}^\dagger_{\boldsymbol{k},\lambda} \hat{a}_{\boldsymbol{k'},\lambda'} \rangle_{\mathcal{E}} e^{-i(\omega_{k'}+\omega_k)t + i(\omega_{k'}+\omega_k)t'} \\ & - \langle \hat{a}^\dagger_{\boldsymbol{k},\lambda} \hat{a}_{\boldsymbol{k'},\lambda'} \rangle_{\mathcal{E}} e^{+i(\omega_{k'}+\omega_k)t - i(\omega_{k'}-\omega_k)t'} \big) \, . \end{aligned} \tag{1.91}$$

To proceed we must give $\rho_{\mathcal{E}}$ a specific form. In the derivation of the master equation we have assumed the the environment is large and that its state in unchanged by its interaction with the system. A logical and common choice is to assume that the environment is at thermal equilibrium. This means that population in its density matrix is distributed as it is in the canonical ensemble:

$$\rho_{\mathcal{E}} = \frac{e^{-H_{\mathcal{E}}/k_B T}}{Tr_{\mathcal{E}}[e^{-H_{\mathcal{E}}/k_B T}]} \, , \tag{1.92}$$

where k_B is the Boltzmann constant and where T is the temperature. This corresponds to a diagonal matrix with level populations determined by Boltzmann factors. It follows that:

$$\langle \hat{a}_{\boldsymbol{k},\lambda} \hat{a}_{\boldsymbol{k'},\lambda'} \rangle_{\mathcal{E}} = 0 \, , \tag{1.93}$$

$$\langle \hat{a}^\dagger_{\boldsymbol{k},\lambda} \hat{a}^\dagger_{\boldsymbol{k'},\lambda'} \rangle_{\mathcal{E}} = 0 \, , \tag{1.94}$$

$$\langle \hat{a}_{\boldsymbol{k},\lambda} \hat{a}^\dagger_{\boldsymbol{k'},\lambda'} \rangle_{\mathcal{E}} = \delta_{\boldsymbol{k}\boldsymbol{k'}} \delta_{\hat{\lambda}\hat{\lambda}'} \left(1 + n(\omega_k)\right) \, , \tag{1.95}$$

$$\langle \hat{a}^\dagger_{\boldsymbol{k},\lambda} \hat{a}_{\boldsymbol{k'},\lambda'} \rangle_{\mathcal{E}} = \delta_{\boldsymbol{k}\boldsymbol{k'}} \delta_{\hat{\lambda}\hat{\lambda}'} \, n(\omega_k) \, , \tag{1.96}$$

where $n(\omega_k)$ is the bosonic occupation number of the mode with frequency ω_k:

$$n(\omega_k) = \frac{1}{e^{\omega_k/k_B T} - 1}\,. \tag{1.97}$$

To simplify the summations over wave vectors $\boldsymbol{k}$ and $\boldsymbol{k'}$ we move to the continuum limit:

$$\frac{1}{V}\sum_{\boldsymbol{k}} \to \frac{1}{(2\pi)^3 c^3}\int_0^\infty d\omega_k\, \kappa(\omega_k)\omega_k^2 \int d\Omega\,, \tag{1.98}$$

where $\kappa(\omega)$ is the spectral density given by the density of states weighted by the coupling strength, $\kappa(\omega) = \sum_k |g_k|^2 \delta(\omega - \omega_k) \equiv \chi(\omega)|g(\omega)|^2$. In this case we'll assume that the spectral density is flat. The solid angle integration is carried out with the help of polarisation completeness property (1.58)

$$\int d\Omega \left(\delta_{\alpha,\beta} - \frac{k^\alpha k^\beta}{|k|^2}\right) = \frac{8\pi}{3}\delta_{\alpha,\beta}\,, \tag{1.99}$$

which follows from k^α and k^α being the Cartesian components of the wave vector. Collecting these results greatly simplifies the spectral correlation tensor (1.90):

$$\Gamma_{\alpha,\beta}(\omega) = \frac{2}{3\pi\hbar c^3}\delta_{\alpha,\beta}\int_0^\infty d\omega_k\, \omega_k^3 \Bigg[(n(\omega_k)+1)\int_0^\infty dt' e^{-i(\omega_k-\omega)t'} \tag{1.100}$$

$$+ n(\omega_k)\int_0^\infty dt' e^{+i(\omega_k+\omega)t'}\Bigg]\,. \tag{1.101}$$

We can simiplify further by using the following identity:

$$\int_0^\infty dt' e^{-i\epsilon t'} = \pi\delta(\epsilon) - iP\frac{1}{\epsilon}\,, \tag{1.102}$$

where P is the Cauchy Principle value. This breaks apart the dissipator and Lamb Shift terms, as we've seen previously (1.36):

$$\Gamma_{\alpha,\beta}(\omega) = \delta_{\alpha,\beta}\left(\frac{1}{2}\gamma(\omega) + iS(\omega)\right)\,. \tag{1.103}$$

This splits the master equation into two parts. The real part forms the dissipator and produces non-unitary system dynamics. The imaginary part contributes extra unitary evolution known as the Lamb shift [149], by analogy with atom physics. For clarity we will deal with each of these parts in a separate section before recombining them.

1.5.4.1 Lamb and ac Stark Shift

We now turn to the imaginary part $S(\omega)$ of the spectral correlation tensor, which will be responsible for shift the energy of the eignestates in the Hamiltonian, thus detuning the transition frequencies. This is given by (1.39):

$$S(\omega) = \frac{2}{3\pi\hbar c^3} P \int_0^\infty d\omega_k \, \omega_k^3 \left(\frac{1 + n(\omega_k)}{\omega - \omega_k} + \frac{n(\omega_k)}{\omega_k + \omega} \right). \tag{1.104}$$

Inserting this into the expression for the Lamb shift:

$$H_{LS} = \sum_{\omega \in \pm\omega_A} S(\omega) A^\dagger(\omega) A(\omega) \tag{1.105}$$

Expanding out the summation yields:

$$H_{LS} = \left(S(\omega_A) - S(-\omega_A) \right) \left(\hat{\sigma}_+ \hat{\sigma}_- - \hat{\sigma}_- \hat{\sigma}_+ \right), \tag{1.106}$$

$$H_{LS} = \frac{1}{2} \left(S(\omega_A) - S(-\omega_A) \right) \hat{\sigma}_z \,. \tag{1.107}$$

The total shift Δ_T is given by:

$$\Delta_T = S(\omega_A) - S(-\omega_A) \,, \tag{1.108}$$

$$\Delta_T = \frac{2|d|^2}{3\pi\hbar c^3} P \int_0^\infty d\omega_k \, \omega_k^3 \,, \left(\frac{1}{\omega - \omega_k} + \frac{1}{\omega_k + \omega} \right) (1 + 2n(\omega_k)) \,. \tag{1.109}$$

This can be separated into a temperature dependent and temperature independent part, known as the Lamb shift (Δ_L) and ac Stark shift (Δ_S) respectively:

$$\Delta_T = \Delta_L + 2\Delta_S \,, \tag{1.110}$$

$$\Delta_L(\omega_A) = \frac{2|d|^2}{3\pi\hbar c^3} P \int_0^\infty d\omega_k \, \omega_k^3 \left(\frac{1}{\omega_A - \omega_k} + \frac{1}{\omega_k + \omega_A} \right), \tag{1.111}$$

$$\Delta_S(\omega_A) = \frac{2|d|^2}{3\pi\hbar c^3} P \int_0^\infty d\omega_k \, \omega_k^3 \left(\frac{1}{\omega_A - \omega_k} + \frac{1}{\omega_k + \omega_A} \right) n(\omega_k) \,. \tag{1.112}$$

Had we made the rotating wave approximation at the Hamiltonian level, rather than the later as the secular approximation, the $(\omega_k + \omega_A)^{-1}$ terms would be missing [6].

1.5.4.2 Dissipation

Now considering the real part of equation (1.103):

$$\Re(\Gamma_{\alpha,\beta}(\omega)) = \frac{2}{3\hbar c^3} \delta_{\alpha,\beta} \int_0^\infty d\omega_k \, \omega_k^3 \Big[(n(\omega_k)+1)\delta(\omega_k - \omega) + n(\omega_k)\delta(-\omega_k - \omega) \Big] \,. \tag{1.113}$$

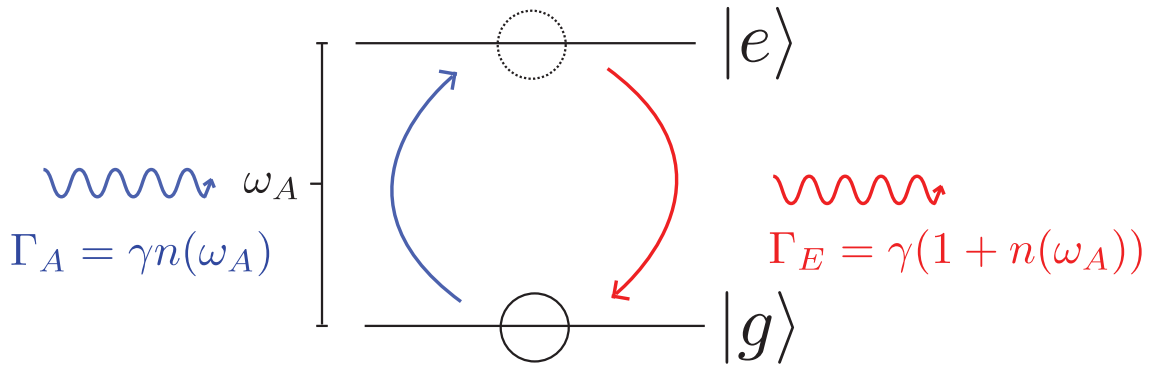

Figure 1.3: Dynamics of the Quantum optical master equation. The two level system emits light at rate Γ_E and absorbs it a Γ_A, transitioning between its ground and excited state as it does so. The free atom decay rate is the combination of constants $\gamma = \frac{4\omega^3|d|^2}{3\hbar c^3}$.

The second term cancels out, because the integral only runs over positive values of ω_k leaving:

$$\Re(\Gamma_{\alpha,\beta}(\omega)) = \frac{2\omega_k^3}{3\pi\hbar c^3}(n(\omega)+1)\delta_{\alpha,\beta}\,. \tag{1.114}$$

Therefore using the definition (1.103) yields:

$$\gamma(\omega) = \frac{4\omega^3}{3\pi\hbar c^3}(n(\omega)+1)\,. \tag{1.115}$$

Substituting this into the generic dissipator (1.40) yields:

$$D(\widetilde{\rho}_s(t)) = \sum_{\omega\in\pm\omega_A} \frac{4\omega^3}{3\hbar c^3}(1+n(\omega))\left(A(\omega)\rho_S A^\dagger(\omega) - \frac{1}{2}\{A^\dagger(\omega)A(\omega),\rho_S\}\right)\,. \tag{1.116}$$

The delta function $\delta_{\alpha,\beta}$ has removed the α and β dependence from $\gamma(\omega)$, making the matrix diagonal, therefore the dissipator will already in Lindblad form. Substituting in (1.88) and using frequency selectivity of the $A(\omega)$ decomposition (1.87) we obtain:

$$\begin{aligned} D(\widetilde{\rho}_s(t)) =& \frac{4\omega^3|d|^2}{3c^3}(1+n(\omega_A))\left(\hat{\sigma}_-\widetilde{\rho}_s\hat{\sigma}_+ - \frac{1}{2}\{\hat{\sigma}_+\hat{\sigma}_-,\widetilde{\rho}_s\}\right) \\ &+ \frac{4\omega^3|d|^2}{3c^3}n(\omega_A)\left(\hat{\sigma}_+\widetilde{\rho}_s\hat{\sigma}_- - \frac{1}{2}\{\hat{\sigma}_-\hat{\sigma}_+,\widetilde{\rho}_s\}\right)\,, \end{aligned} \tag{1.117}$$

where we made use of the $n(-\omega) = -(1+n(\omega))$ property of Bose-Einstein distribution. This is now the canonical quantum optical master equation in Lindblad form, with The Lindblad operators are

$$L_+ = \sqrt{\frac{4\omega^3|d|^2}{3c^3}(1+n(\omega_A))}\hat{\sigma}_-\,, \qquad L_- = \sqrt{\frac{4\omega^3|d|^2}{3c^3}n(\omega_A)}\hat{\sigma}_+\,. \tag{1.118}$$

Returning to the Schrödinger picture we obtain:

$$\dot{\rho}_s(t) = -i[H_S + H_{LS}] + D(\rho_s(t))\,. \tag{1.119}$$

Substituting in (1.117) and (1.106) gives:

$$\begin{aligned}\dot{\rho}_s(t) = -i\omega'_A[\hat{\sigma}_Z, \rho_s(t)] + \gamma(1 + n(\omega_A))\left(\hat{\sigma}_-\rho_s\hat{\sigma}_+ - \frac{1}{2}\{\hat{\sigma}_+\hat{\sigma}_-, \rho_s\}\right) \\ + \gamma n(\omega_A)\left(\hat{\sigma}_+\rho_s\hat{\sigma}_- - \frac{1}{2}\{\hat{\sigma}_-\hat{\sigma}_+, \rho_s\}\right)\end{aligned} \tag{1.120}$$

where $\omega'_A = \left(\frac{\hbar\omega_A}{2} + \Delta_T\right)$ and where we have defined the free atom decay rate as:

$$\gamma = \frac{4\,\omega_A^3|d|^2}{3\hbar c^3}\,. \tag{1.121}$$

The dissipator (1.117) describes quantum jumps from the atom's ground state to the excited state and visa versa. These occur while absorbing $\hbar\omega_A$ of energy from the field or emitting $\hbar\omega_A$ into the field. These transitions are depicted in Fig. 1.3. The rates at which these transitions occur are identical to the famous Einstein A and B coefficients and those derived by Wigner and Weisskopf [264]. The emission rate has an extra term $(1 + n(\omega_A))$ relative to absorption $n(\omega_A)$. This extra term accounts for spontaneous emission. In the vacuum field limit ($n(\omega_A) = 0$) no absorption should occur, but the excited state of the atom can still decay.

A number of approximations have gone into the derivation of (1.120). It is therefore worth considering the validity of these in the regime of quantum optics. Most of these appeal to the idea of timescales, which being sufficiently different from one another allow terms to be neglected or simplified. The Born-Markov approximation required that bath correlation timescale $\tau_B \approx \omega^{-1}$ be greater than the relaxation time scale, which we have now found to be γ (1.121). This amounts to a requirement of weak coupling, which is well met for optical systems. For the RWA to be valid we require $\tau_S \approx \langle\omega' - \omega\rangle^{-1}$. In the case of the single atom this constitues to the same condition. However, in more complex multi-site systems care must be taken to make sure this is appropriate for all transitions. The RWA allows individual Lindblad operators to be assigned to a given transition between eigenstates, so it may not be valid when collective mechanisms are important.

CHAPTER 2

The Rabi model

2.1 Synopsis

In this chapter we discuss the Rabi model: a quantum two level system coupled to a harmonic oscillator, which is a ubiquitous physical system. New experiments in circuit QED and nano-electromechanical systems (NEMS) achieve unprecedented coupling strength at large detuning between qubit and oscillator, thus requiring a theoretical treatment beyond the Jaynes Cummings model. Here we present a new method for describing the qubit dynamics in this regime, based on an oscillator correlation function expansion of a non-Markovian master equation in the polaron frame. Our technique yields a new numerical method as well as a succinct approximate expression for the qubit dynamics. These expressions are valid in the experimentally interesting regime of strong coupling at low temperature. We obtain a new expression for the ac Stark shift and show that this enables practical and precise qubit thermometry of an oscillator.

2.2 Introduction

The qubit-oscillator model has gone by many names in many fields, owing its tenacity to the breadth of its applicability: It is the simplest non-trivial model of the interaction between light and matter. At its inception it was used to describe the interaction of an atom with a magnetic field [202], and referred to thereafter as the Rabi model. In the subsequent decades it has been extensively studied in quantum optics [235] and cavity QED [204]. Physical chemists have used a 'vibration-dimer' model to study the spectra of molecules [89]. Applying the rotating wave approximation (RWA) to the Rabi model yields the Jaynes Cummings model (JCM) [133], which is valid when the detuning between the qubit transition frequency Ω and the resonator frequency ω is

negligible ($\Omega \approx \omega$) and the coupling between the qubit and oscillator is weak ($g < \omega$) [142]. This is an excellent approximation in the case of cavity QED where typical coupling strengths are of order $g/\omega \approx 10^{-6}$. The JCM can be extended to incorporate tunnelling, and has provided an adequate description of experiments for decades, but a new era of experiments are pushing beyond its boundaries in terms of both coupling and detuning. Circuit QED experiments couple superconducting qubits to LC and waveguide resonators, allowing coupling strengths up to $g/\omega \approx 10^{-1}$, recently enabling demonstrations of the breakdown of the JCM [186, 84]. Superconducting qubits coupled to nanomechanical resonators (NR) generally have more modest coupling strengths [147, 188], but combined with large detuning they could also operate outside the validity of the JCM [125].

The Hamiltonian for the Rabi model can be decomposed into three parts:

$$\hat{H} = \hat{H}_Q + \hat{H}_O + \hat{H}_I. \tag{2.1}$$

The qubit, atom or two level system is described by:

$$\hat{H}_Q = \frac{\epsilon}{2}\sigma_z + \frac{\Delta}{2}\sigma_x, \tag{2.2}$$

where σ_z and σ_x are the Pauli spin operators. They describe a two level system with an energy splitting ϵ and a spontaneous tunnelling between the states at a rate Δ. In isolation such a system would undergo Rabi oscillations with a frequency $\Omega_r = \sqrt{\epsilon^2 + \Delta^2}$. The Hamiltonian of the oscillator is:

$$\hat{H}_O = \omega a^\dagger a, \tag{2.3}$$

where ω is the frequency of the oscillator and $a^\dagger$ and a are its creation and annihilation operators respectively. Note we have neglected the zero point energy. The Hamiltonian for the interaction between the two is:

$$\hat{H}_I = g(a + a^\dagger)\sigma_z, \tag{2.4}$$

where g is the coupling strength between the qubit and oscillator.

Recent experimental progress has sparked a renewed theoretical interest in extending solutions of (2.1) beyond the RWA. For instance, a change of basis prior to applying the RWA leads to a generalised RWA with validity extending beyond the very weak coupling limit [124]. However, this is limited to the case of $\epsilon = 0$. As an alternative approach, Van Vleck perturbation theory [253] has been used to investigate the dynamics in the ultra strong ($g/\omega > 1$) coupling regime [112, 113]. This approach

contains the splitting and tunnelling elements, but it is perturbative in the latter and fails to recover the JCM in the weak coupling limit. This approach is therefore more applicable to circuit QED, rather than the more modest couplings achieved in Cooper pair box (CPB) coupled to NR systems.

An analytic expression for the eigenspectrum of the full Rabi model was recently found by Braak [21], a surprising and significant result for such a long standing problem. In addition to solving the model Braak proved that it is non-integrable i.e. the time-dependence of important properties cannot be found in closed form. T Braak's work was followed by others who have reformulated it to provide a more direct derivation[40, 269], but the eigenenergies are still the solution to transcendental functions. There is therefore still a need for approximate results governing areas of particular experimental interest. There is therefore still a need for concise analytic forms for the dynamics in particular parameter regimes.

2.3 Method

In order to simplify the expression and extend the validity of the approximations that we will subsequently describe into the strong coupling regime, we first perform a 'polaron' transformation [257, 162]. This unitary Hamiltonian transformation ($H' = e^s H e^{-s}$) is equivalent to dressing qubit excitations with the vibrational modes to form quasi-particles called polarons. With $s = \alpha/2(a^\dagger - a)\sigma_z$ and $\alpha/2 = g/\omega$ we obtain

$$H' = \frac{\epsilon}{2}\sigma_z + \omega a^\dagger a + \frac{\Delta}{2}(D(\alpha)|0\rangle\langle 1| + D(-\alpha)|1\rangle\langle 0|)\,, \tag{2.5}$$

where $D(\xi) = \exp(\xi a^\dagger - \xi^* a)$ is the displacement operator. We have neglected a term proportional to the identity $g^2/\omega\ \mathbf{1}$, which does not influence the dynamics. The first two terms involve the qubit and oscillator individually and so can be removed by going to the interaction picture. We insert the resulting Hamiltonian into the von Neumann equation and then derive equations of motion for the qubit [23, 22]). First we move into the interaction picture:

$$\tilde{\rho}_{00}(t) = \rho_{00}, \quad \tilde{\rho}_{11}(t) = \rho_{11}, \tag{2.6}$$

$$\tilde{\rho}_{01}(t) = \rho_{01}e^{i\epsilon t}D_t, \quad \tilde{\rho}_{10}(t) = \rho_{10}e^{-i\epsilon t}D_t^\dagger, \tag{2.7}$$

where D_t and $D_t^\dagger$ are the time dependent versions of the displacement operators introduced by the polaron transform. In the interaction picture the polaron transformed interaction is given by:

$$\tilde{H}_I\,(t) = \frac{\Delta}{2}\left(\rho_{01}(t) + \rho_{10}(t)\right)\,. \tag{2.8}$$

Starting from the Von Neumann equation:

$$\frac{d}{dt}\tilde{\rho}(t) = -i\left[\tilde{H}_I(t), \tilde{\rho}(t)\right], \tag{2.9}$$

we have

$$\tilde{\rho}(t) = \rho_0 - i\int_0^t dt'[\tilde{H}_I(t'), \tilde{\rho}(t')]. \tag{2.10}$$

To study the dynamics we need the time dependent expectation values of the density matrix elements [23, 22]. These are given by:

$$\langle O\rangle_t = \mathrm{Tr}[\rho(t)O] = \mathrm{Tr}[\tilde{\rho}(t)\tilde{O}_t]. \tag{2.11}$$

Substituting in (2.10) we obtain:

$$\langle O\rangle_t - \langle O\rangle_0 = -i\int_0^t dt'\mathrm{Tr}[[\tilde{H}_I(t'), \tilde{\rho}(t')]\tilde{O}_t], \tag{2.12}$$

By xxploiting the cyclic property of traces we obtain:

$$\langle O\rangle_t - \langle O\rangle_0 = -i\int_0^t dt'\mathrm{Tr}[\tilde{\rho}(t')[\tilde{O}_t, \tilde{H}_I(t')]]. \tag{2.13}$$

Substituting O for the relevant operator eg. $\tilde{\rho}_{00}(t)$, evaluating the commutator, and tracing over the qubit degrees of freedom yields:

$$\langle\rho_{00}(t)\rangle - \langle\rho_{00}(0)\rangle = -i\tfrac{\Delta}{2}\int_0^t dt'(\langle\rho_{10}(t')\rangle - \langle\rho_{01}(t')\rangle), \tag{2.14}$$

$$\langle\rho_{11}(t)\rangle - \langle\rho_{11}(0)\rangle = \quad i\tfrac{\Delta}{2}\int_0^t dt'(\langle\rho_{10}(t')\rangle - \langle\rho_{01}(t')\rangle), \tag{2.15}$$

$$\langle\rho_{01}(t)\rangle - \langle\rho_{01}(0)\rangle = -i\tfrac{\Delta}{2}\int_0^t dt' e^{i\epsilon(t-t')}(\langle\rho_{00}(t')D_t D_{t'}^\dagger\rangle - \langle\rho_{11}(t')D_{t'}^\dagger D_t\rangle), \tag{2.16}$$

$$\langle\rho_{10}(t)\rangle - \langle\rho_{10}(0)\rangle = \quad i\tfrac{\Delta}{2}\int_0^t dt' e^{-i\epsilon(t-t')}(\langle\rho_{00}(t')D_{t'} D_t^\dagger\rangle - \langle\rho_{11}(t')D_t^\dagger D_{t'}\rangle). \tag{2.17}$$

At this point we make the Born approximation (assuming the density matrix of system and bath are factorable)

$$\langle\rho_{00}(t')D_t(\alpha)D_{t'}(\alpha)\rangle_{t'} \approx \langle\rho_{00}(t')\rangle\langle D_t(\alpha)D_{t'}(\alpha)\rangle. \tag{2.18}$$

T The bosonic correlation function is defined as $C(t-t')$:

$$C(t-t') = \langle D_t(\alpha)D_{t'}^\dagger(\alpha)\rangle = \mathrm{Tr}_B[\rho_B D_t(\alpha)D_{t'}^\dagger(\alpha)], \tag{2.19}$$

where the subscript B represents the bosonic degrees of freedom. We substitute this into (2.14) and by assuming there is no initial coherence in the system we obtain:

$$\tfrac{\mathrm{d}}{\mathrm{d}t}\rho_{00}(t) = \quad -i\frac{\Delta}{2}(\rho_{10}(t) - \rho_{01}(t))), \tag{2.20}$$

$$\tfrac{\mathrm{d}}{\mathrm{d}t}\rho_{11}(t) = \quad i\frac{\Delta}{2}(\rho_{10}(t) - \rho_{01}(t))), \tag{2.21}$$

where $\rho_{00}(t)$ and $\rho_{11}(t)$ are the time dependant population elements of the qubit's reduced density matrix. The coherences are given by:

$$\rho_{01}(t) = i\tfrac{\Delta}{2}\int_0^t \mathrm{d}t' e^{-i\epsilon\tau}\left[\rho_{00}(t')C^*(\tau) - \rho_{11}(t')C(\tau)\right], \tag{2.22}$$

$$\rho_{10}(t) = -i\tfrac{\Delta}{2}\int_0^t \mathrm{d}t' e^{i\epsilon\tau}\left[\rho_{00}(t')C(\tau) - \rho_{11}(t')C^*(\tau)\right], \tag{2.23}$$

where $\tau = t - t'$ and $C(\tau)$ and $C^*(\tau)$ are the correlation function of the oscillator and its complex conjugate respectively. In deriving these equations, we have employed the Born approximation, i.e. we have assumed that the vibrational mode and the qubit states can be factored at all times. Physically, this corresponds to an oscillator that thermalises on a timescale faster than that characteristic of the qubit dynamics. The equations of motion take the form of a system of integro-differential equations involving the bosonic correlation function and its complex conjugate. Laplace transforming the equations of motion yields a set of simultaneous equations that can be solved algebraically [23, 22]:

$$R_{00}(s) = \frac{s\rho_0 + \left(\frac{\Delta}{2}\right)^2\left[C'_+ + C''_-\right]}{s^2 + s\left(\frac{\Delta}{2}\right)^2\left[C'_- + C''_- + C'_+ + C''_+\right]} \tag{2.24}$$

$$R_{10}(s) = -i\frac{\Delta}{2}\left[(C'_- + C''_-)R_{00}(s) - \frac{1}{s}C''_-\right] \tag{2.25}$$

where s is our Laplace space variable, $R_{00}(s)$ and $R_{10}(s)$ are the Laplace transforms of $\rho_{00}(t)$ and $\rho_{10}(t)$, ρ_0 is the initial population of the ground state and $C'_\pm = C'(s \pm i\epsilon)$ and $C''_\pm$ are the Laplace transforms of the correlation function and its conjugate respectively. It is sufficient to solve these two equations alone because from their solutions the behaviour of the other density matrix elements can be trivially derived.

To obtain expressions for the dynamics of Eqns (2.24) and (2.25) in the time domain we need to find the Laplace transform of the bosonic correlation and its conjugate, solve and then take the inverse Laplace transform of the equations. The correlation function is defined as

$$C(\tau) = \langle D_t(\alpha)D^\dagger_{t'}(\alpha)\rangle = \mathrm{Tr}_B\left[\rho_B D_t(\alpha)D^\dagger_{t'}(\alpha)\right] \tag{2.26}$$

The bosonic correlation function (2.26) for an oscillator with a single mode in a thermal state is defined as:

$$C(t-t') = \mathrm{Tr}_B[\rho_B D_t(\alpha)D^\dagger_{t'}(\alpha)], \tag{2.27}$$

where:

$$\rho_B = \frac{\exp(-\beta\omega a^\dagger a)}{\mathrm{Tr}_B[\exp(-\beta\omega a^\dagger a)} = \frac{1}{Z}\exp(-\beta\omega a^\dagger a). \tag{2.28}$$

This can be evaluated in different ways, one of which is presented below. Starting from the time dependence of the displacement operator in the interaction picture we obtain:

$$D_t(\xi) = e^{iH_0 t} D(\xi) e^{-iH_0 t} = e^{i\omega a^\dagger a t} D(\xi) e^{-i\omega a^\dagger a t}, \tag{2.29}$$

or, alternatively, through the time dependence of creation and annihilation operators:

$$D_t(\xi) = e^{\xi a^\dagger e^{i\omega t} - \xi^* a e^{-i\omega t}} = D(\xi e^{i\omega t}). \tag{2.30}$$

In order to perform the trace Tr_B in the number state basis, we need to know the action of $e^{\xi a^\dagger a}$ and $D(\xi)$ on a number state $|n\rangle$. The first simply evaluates to $e^{\xi n}$ and the latter gives the so-called displaced number state $|\xi, n\rangle$. The displaced number state can be expanded in the number state basis

$$|\xi, n\rangle = \sum_{m=0}^{\infty} C_{nm} |m\rangle , \qquad C_{nm} = \langle m| D(\xi) |n\rangle , \tag{2.31}$$

with (see, e.g., Oliviera et al [58] or M. Crisp [57])

$$C_{nm} = \sqrt{\frac{n!}{m!}} e^{-\frac{1}{2}|\xi|^2} \xi^{m-n} L_n^{m-n}(|\xi|^2), \tag{2.32}$$

where $L_n^{m-n}(|\xi|^2)$ is an associated Laguerre polynomial. This is only valid for $m > n$, but for $m < n$ the displacement operator, or rather its Hermitian conjugate, can be made to act on $\langle m|$ instead of on $|n\rangle$. We use Eq. (2.30) for the displacement operator and the property $D(x)D(y) = \exp[(xy^* - yx^*)/2]D(x+y)$ to evaluate Eq. (2.28). This leads to a series of the following form

$$C(t-t') = \frac{1}{Z} e^{-|\alpha|^2[1-e^{-i\omega(t-t')}]} \sum_{n=0}^{\infty} e^{-\beta\omega n} L_n[2|\alpha|^2(1-\cos[\omega(t-t')])]. \tag{2.33}$$

By virtue of the property $\sum_{n=0}^{\infty} L_n(y) z^n = (1-z)^{-1} \exp[yz/(z-1)]$ and with $N = (e^{\beta\omega} - 1)^{-1}$ and $Z = (1 - e^{-\beta\omega})^{-1}$ we finally arrive at the result:

$$C(t-t') = e^{-i|\alpha|^2 \sin\omega(t-t')} e^{-2|\alpha|^2(1-\cos\omega(t-t'))(N+1/2)}. \tag{2.34}$$

Note that this expression agrees with Mahan's result for a single mode (Ref [162], section 4.3). Mahan derives this in a similar fashion but without using Eqs. (2.31, 2.32). Instead, he uses the 'Feynman disentanglement of operators' to arrive at an equivalent infinite series of Laguerre polynomials:

$$C(\tau) = e^{-|\alpha|^2((1-\cos(\omega\tau))\coth\frac{\beta\omega}{2} + i\sin(\omega\tau))}. \tag{2.35}$$

Unfortunately, it is not straightforward to Laplace transform this expression directly, so we employ the Jacobi-Anger series expansion:

$$e^{z\cos\theta} = \sum_{n=-\infty}^{\infty} I_n(z)e^{in\theta}, \tag{2.36}$$

where z is an arbitrary complex number and $I_n(z)$ is the modified Bessel function of order n and argument z. By exploiting an angle addition identity we can rewrite (2.35) as:

$$C(\tau) = e^{-|\alpha|^2\coth\left(\frac{\beta\omega}{2}\right)}e^{z\cos(\omega\tau+x)}, \tag{2.37}$$

where $x = i\beta\omega/2$ and $z = 2|\alpha|^2\sqrt{N(N+1)}$. Using Eqn (2.36) this gives:

$$C(\tau) = e^{-|\alpha|^2(2N+1)}\sum_{n=-\infty}^{\infty} I_n(z)e^{in(\omega\tau+x)}; \tag{2.38}$$

where $N = (e^{\beta\omega}-1)^{-1}$ is the average oscillator occupation number. In this form the correlation function can be Laplace transformed trivially. The physical interpretation of this series expansion is that the n^{th} term describes processes, which create ($n > 0$) or annihilate ($n < 0$) n phonons in the oscillator [162]. The $n = 0$ term describes interactions with no net change in phonon number, this is called the zero-phonon line. For experimentally relevant parameters (i.e. low temperatures and moderate to strong coupling), we would expect this $n = 0$ term to be the most significant[2].

Retaining only interactions that conserve the total phonon number in the oscillator complements the underlying Born Approximation, which assumes the oscillator remains in thermal equilibrium. Including only the dominant zeroth term in the series allows the equations (2.24) and (2.25) to be inverse Laplace transformed:

$$\rho_{00}(t) = \frac{\rho_0\epsilon^2 + \frac{1}{2}e^{-b}\Delta^2 I_0(z)\left((2\rho_0-1)\cos(t\Omega)+1\right)}{\Omega^2}, \tag{2.39}$$

$$\rho_{10}(t) = -\frac{e^{-b}\Delta\left(2\rho_0-1\right)I_0(z)(\epsilon\cos(t\Omega)+i\Omega\sin(t\Omega)-\epsilon)}{2\Omega^2}, \tag{2.40}$$

$$\Omega = \sqrt{\Delta^2 e^{-b}I_0(z)+\epsilon^2}, \tag{2.41}$$

where $b = |\alpha|^2(2N+1)$. From Eqn (2.41) we can see that the presence of the oscillator alters the tunnelling rate by a factor $I_0(z)e^{-b}$, essentially corresponding to a temperature dependent ac Stark shift on the qubit due to the presence of the single oscillator mode [126, 224]. In contrast to previous work our expression is not confined to the weak coupling or large detuning limit, rather our results are valid in the experimentally less restrictive regime of low temperature and strong coupling. Nonetheless, our expression still takes a surprisingly simple closed form.

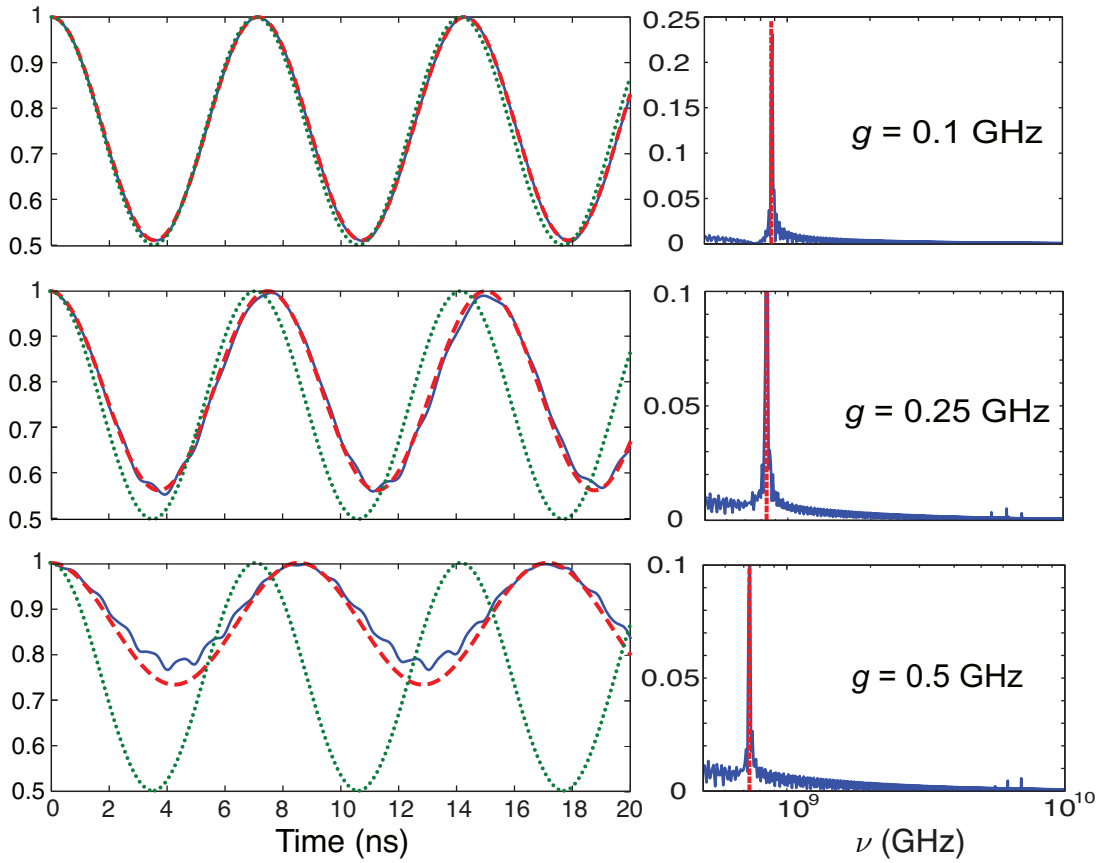

Figure 2.1: Comparison of the single term approximation (red) and a numerically exact approach (blue) for different coupling strengths. Uncoupled Rabi oscillations are also shown as a reference (green). Left: the population $\rho_{00}(t)$ in the time-domain. Right: the same data in the frequency domain. The full numerical solution was Fourier transformed using Matlab's FFT algorithm. Other parameters are $\omega = 1$ GHz, $\epsilon = \Delta = 100$ MHz and $T = 10$ mK.

2.4 Results

Figure 2.1 shows a comparison of the dynamics predicted using these expressions and a numerically exact approach. The latter are obtained by imposing a truncation of the oscillator Hilbert space at a point where the dynamics have converged and any higher modes have an extremely low occupation probability. Our zeroth order approximation proves to be unexpectedly powerful, giving accurate dynamics well into the strong coupling regime ($g/\omega = 0.25$) and even beyond this it still captures the dominant oscillatory behaviour, see Figure 2.1. Stronger coupling increases the numerical weight of higher frequency terms in the series, causing a modulation of the dynamics. The approximation starts to break down at ($g/\omega = 0.5$). The equations (2.39) and (2.40) are obviously unable to capture the higher frequency modulations to the dynamics or any potential long time phenomena like collapse and revival, but these are unlikely to be resolvable in near future experiments in any case. Nonetheless, it is worth pointing out that even in this strong coupling case the base frequency of the qubit dynamics is still adequately captured by our single term approximation.

Our methodology can be used to predict dynamics of nanomechanical resonators connected to either quantum dots or superconducting qubits. The criterion for the single term approximation to be valid is readily met by current experiments such as those presented in Refs. [147, 188] and their parameters yield near perfect agreement between numerical and analytic results. Most experiments operate in a regime where the qubit dynamics are not greatly perturbed by the presence of the oscillator, which has a much lower frequency ($\epsilon \approx \Delta \approx 10$ GHz, $\omega = 1$ GHz). In Figure 2.1, we chose $\epsilon \approx \Delta \approx 100$ MHz, because this better demonstrates the effect of the oscillator on the qubit. These parameters can be achieved experimentally using the same qubit design but with an oscillating voltage applied to the CPB bias gate [125]. However, we stress the accuracy of our method is not restricted to this regime.

Including extra terms in the series expansion (2.38) makes the time dependence of the qubit dynamics analytically unwieldy, because the rational function form of the series leads to a complex interdepence of the positions of the poles in (2.24). However, if the values of the parameters are known the series can truncated at ($\pm N_{\mathrm{MAX}}$) to give an efficient numerical method to obtain more accurate dynamics, extending the applicability of our approach beyond low temperatures and moderate to strong coupling. This is demonstrated in Fig. 2.2, where the dynamics are clearly dominated by two frequencies – an effect that could obviously never be captured by a single term approximation. There is a qualitative agreement between the many terms expansion

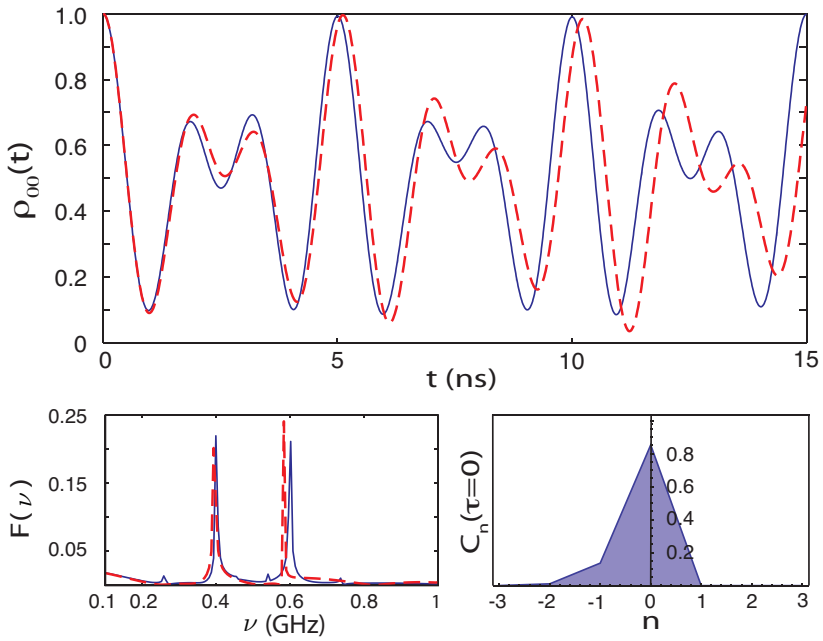

Figure 2.2: Main panel: comparison of dynamics calculated from truncating (2.38) at $N_{\mathrm{MAX}} = \pm 10$ (red) and a numerically exact approach (blue). Lower left: Fourier transform of the dynamics. Lower right: the numerical weight of the n^{th} term in the series expansion of (2.38), showing there are still only two dominant frequencies at $n = 0$ and $n = -1$. Parameters: $\omega = 0.5$ GHz, $g = 0.1$ GHz, $\epsilon = 0$, $\Delta = 0.5$ GHz, $T = 1$ mK.

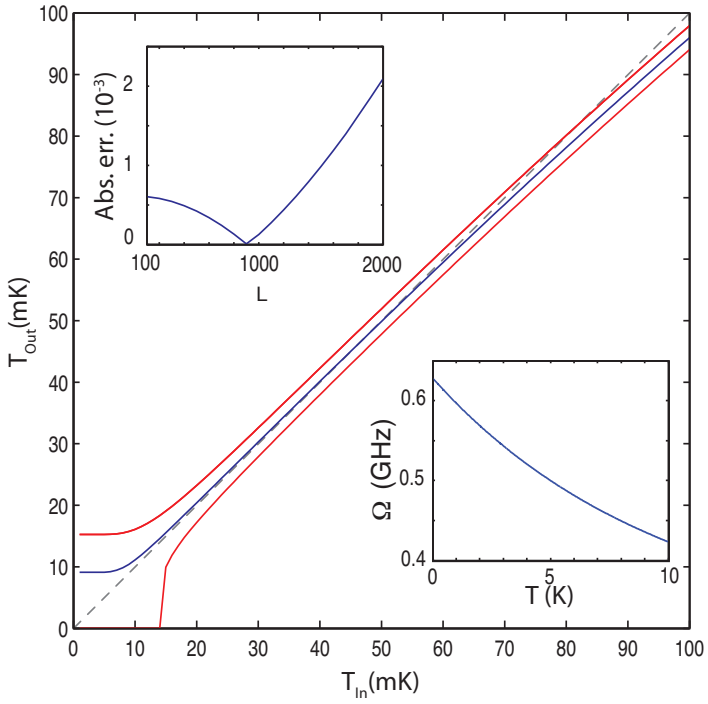

Figure 2.3: Demonstration of qubit thermometry: $T_{\rm in}$ is the temperature supplied to the numerical simulation of the system and $T_{\rm out}$ is the temperature that would be predicted by fitting oscillations with frequency (2.41) to it. The blue line is the data and red line shows the effect of a 10kHz error in the frequency measurement; the grey dashed line serves as a guide to the eye. The lower inset shows the variation of the qubit frequency Ω with temperature. The upper inset shows the dependence of the absolute error in the prediction against the signal length (see text). Other parameters are: $\omega = 1$ GHz, $g = 0.01$ GHz, $\epsilon = 0$, $\Delta = 100$ MHz.

and full numerical solution, particularly at short times. We would not expect a particularly good agreement in this case because the simulations are of the dynamics in the high tunnelling regime ($\Delta = 0.5$), and the polaron transform makes the master equation perturbative in this parameter. For large tunnelling the traditional numerical approach of oscillator Hilbert space truncation would be more suitable. However, for more moderate tunnelling the rapid convergence of the series is shown in the lower right panel of Fig. 2.2; $N_{\rm MAX} = 5 - 10$ is sufficient to calculate $\rho_{00}(t)$ and $\rho_{10}(t)$ with an accuracy only limited by the underlying Born Approximation. The asymmetry of the amplitudes of the terms in the series expansion of (2.38) is due to the exponential functions in the series.

2.5 Quantum Thermometry

We now discuss the application of our model system to the measurement of the temperature of an oscillator by observing the coupled qubit. We picture a situation in which the qubit oscillation frequency Ω is the measured quantity. The tunnelling, coupling strength and energy splitting are usually within the control of the experimentalist (or are at least known constants), and this yields the possibility of using the measured Ω to estimate the temperature. A related idea was recently used in the calibration of a seminal resonator experiment [188] to verify that the oscillator was in its ground state (a critical part of the work). In that case, the authors used a comparison of numerical results for different occupation numbers N with the measured population in the excited state of the qubit after a certain interaction time. A theoretical study of the same approach was preformed in [28], where the system was described by the JCM without a tunnelling term. They also recently extended their more abstract quantum estimation theory approach to other forms of coupling [29]. In contrast, we here propose a practical implementation that uses our simple analytic expressions for the qubit dynamics, which are valid beyond the weak coupling regime, to directly measure the temperature and hence N of the oscillator, simply by observing the effective qubit Rabi frequency Ω.

Figure 2.3 demonstrates this idea, showing that by measuring Ω and fitting it to our expression (2.41), we can obtain submilli-Kelvin precision in the experimentally relevant regime of 20-55 mK. At low temperatures the single term frequency plateaus, causing the accuracy to break down. In the higher temperature limit, we also see a deviation from the diagonal, this is to be expected, as we leave the regime where we safely assume the accuracy of the approximation. Naturally accuracy in this region could be improved by retaining higher order terms in (2.38), but this would become a more numeric than analytic approach. The upper inset shows the dependence of the accuracy of the prediction on the number of points (at a separation of 1ns) sampled from the dynamics. The accuracy increases initially as more points improve the fitted value of Ω, however after a certain length the accuracy is diminished by long term envelope effects in the dynamics not captured by the single term approximation. We note that the corresponding analysis in the frequency domain would not be equally affected by the long time envelope, however a large number of points in the FFT is then required in order to obtain the desired accuracy. The lower inset of Figure 2.3 shows the direct dependence of Ω on the temperature. The temperature range with steepest gradient and hence greatest frequency dependence on temperature varies

with the coupling strength; thus the device could be specifically designed to have a maximal sensitivity in the temperature range of the most interest.

2.6 Further Work

In this chapter we have developed a novel way to treat the bath correlation functions in a non-Markovian master equation. We applied this theory to the problem of quantum thermometry, but it could have other interesting applications. In particular using this formalism to study transport properties, since theses are evaluated at infinite time they can easily be calculated in Laplace space. This would mean the truncation of the series was unnecessary. For instance if we use the Rabi model to describe two to two level systems (sites) in the single exciton subspace. We can then use the model to study the efficiency of transport in the presence of the mode η:

$$\eta = 2\gamma_T \int_0^\infty \langle \mathrm{trap}|\rho(\mathrm{t})\,|\mathrm{trap}\rangle \ , \tag{2.42}$$

$$\eta = 2\gamma_T \langle \mathrm{trap}|\mathrm{R}(\mathrm{s}=0)\,|\mathrm{trap}\rangle \ , \tag{2.43}$$

where γ_T the rate of exciton extraction. Of course for efficiency to be meaningful we must introduce some loss into the system for example by recombination. The could be done by adding the following term to the master equation (2.10):

$$\mathcal{L}_{loss} = -\gamma_{loss}(\{|0\rangle\langle 0|, \rho(t)\} + \{|1\rangle\langle 1|\rho(t)\}) - \gamma_T\{|1\rangle\langle 1|\rho(t)\} \tag{2.44}$$

As we discussed in the Section 1.5.2.4, strong coupling to discrete environmental modes is thought to have an important role in EET. This model could potential elucidate the effect of such modes. Another extensions of the work could be generalising to multi-site and multi-mode systems. In the case of many modes additional analytic progress might be possible for specific spectral densities; offering dynamics as well as steady state properties.

2.7 Conclusion

In this chapter, we have developed and explored a new approach to the Rabi model, which yields succinct expressions for the qubit dynamics. In contrast to previous theoretical approaches, our expressions are valid in the stronger coupling regime that is rapidly gaining experimental relevance. We have further proposed an application of our model enabling precise temperature measurements of the oscillator mode. This

could be used either as part of the calibration of an oscillator experiment or as a tuned, standalone device.

CHAPTER 3

Superabsorption of Light

3.1 Synopsis

Light absorption underpins a huge range of technologies from cameras to scientific instruments and solar cells. Therefore, any enhancement of the process that can be offered by quantum mechanics would have diverse and important applications. In this research chapter, which is based on [118], we show that a collective enhancement effect know as 'superradiance' can be inverted to produce an non-linear scaling in the rate of light absorption. Structures that superradiate must also have enhanced absorption, but the former always dominates in natural systems. However, we demonstrate that this restriction can be overcome by combining several well-established quantum control techniques. In this chapter we explain the origin of superradiance and present analytical and numerical calculations to show that superabsorption can be achieved and sustained in certain simple nanostructures, by trapping the system in a highly excited state through transition rate engineering. We conclude by detailing the potential experimental implementations and technological applications.

3.2 Introduction

3.3 Superradiance

"For want of a better term, a gas which is radiating strongly because of coherence will be called superradiant." Dicke 1954 [60]

Almost 60 years ago Dicke introduced the term superradiance to describe a signature quantum effect: N atoms can collectively emit light at a rate proportional to N^2. Superradiance occurs when N individual atoms interact with the surrounding

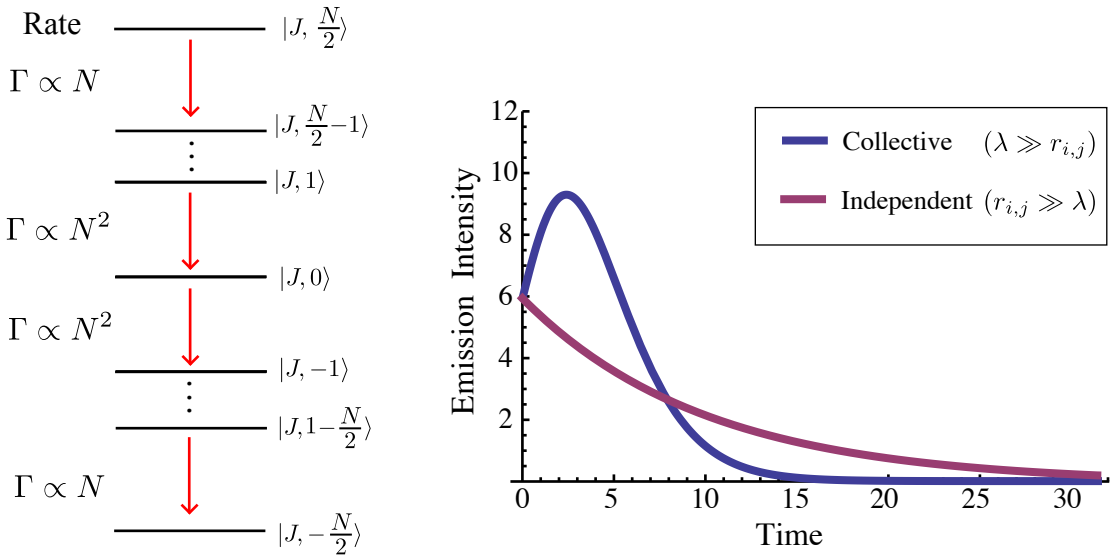

Figure 3.1: The Dicke ladder & Superradiance. **Left)** The ladder of Dicke states and their transition rates. The red arrows denote the cascade downward for a system initialised in the fully excited state. **Right)** The plot shows the rate of photon emission in time, for a group of initially excited atoms. In the collective case they emit light as a superradiant pulse. When the atoms are well separated (the independent case) they decay exponentially.

electromagnetic field [60], whose wavelength is much larger that the separation between the atoms. Following an initial excitation of all atoms, dipole-allowed decay down a series of symmetrical 'Dicke ladder' states leads to an enhanced light-matter coupling that, when the system reaches the state half way down the ladder, depends on the square of the atomic transition dipole [60, 103, 22]. Thus when N dipoles add coherently, light can be emitted at an enhanced rate proportional to N^2. Even for moderate N this represents a significant increase over the prediction of classical physics. The Dicke ladder and the resulting superradiant pulse of light emission are depicted in Fig. 3.1

Although originally studied in context of atomic gases, superradiance can also occur in any system with a discrete dipole-allowed transition, including semiconductor quantum dots [218], crystal defects, and molecules [260]. The effect has found applications ranging from probing exciton delocalisation in biological systems [178], to developing a new class of laser [19], and may even lead to observable effects in astrophysics [252].

The Hamiltonian of an ensemble of N identical atoms is ($\hbar = 1$):

$$\hat{H}_S = \frac{\omega_A}{2} \sum_{i=1}^{N} \left(\mathbf{1}^i - \hat{\sigma}_z^i \right) = \omega_A \sum_{i=1}^{N} \hat{\sigma}_+^i \hat{\sigma}_-^i \,, \tag{3.1}$$

where ω_A is the bare atomic transition frequency and we are using the usual Pauli operators (1.8) defined with respect to the ith atom's ground, $|g\rangle_i$, and optically excited state, $|e\rangle_i$. Since the wavelength of light λ is much larger than all interatomic distances r_{ij}, the atoms become indistinguishable and light interacts with the system collectively. The dynamics are therefore best described by collective operators:

$$\hat{J}_\pm = \sum_{i=1}^{N} \hat{\sigma}_\pm^i \,, \tag{3.2}$$

$$\hat{J}_z = \sum_{i=1}^{N} \hat{\sigma}_z^i \,, \tag{3.3}$$

$$\hat{J}^2 = \sum_{i=1}^{N} \left(\hat{\sigma}_x^i \hat{\sigma}_x^i + \hat{\sigma}_y^i \hat{\sigma}_y^i + \hat{\sigma}_z^i \hat{\sigma}_z^i \right) \,, \tag{3.4}$$

which generate transitions between the eigenstates of the Hamiltonian (3.1) and obey $SU(2)$ commutation relations. These operators behave in the same way as those describing angular momentum in Quantum Mechanics [203]. Using these operators we can move from the 'site' basis, which best describes localised excitations, to the 'Dicke' basis, which is one of collective states of the ensemble of atoms. The Dicke basis is defined by the eigenvalues J and M of $\hat{J}^2$ and $\hat{J}_z$, respectively:

$$\hat{J}_z \left| J, M \right\rangle = M \left| J, M \right\rangle \,, \qquad \hat{J}^2 \left| J, M \right\rangle = J \left| J, M \right\rangle \,, \tag{3.5}$$

where J characterises the total angular momentum and M the degree of inversion (the number of atoms excited). Using the collective operators (3.2) we can succinctly express the light matter interaction Hamiltonian as:

$$\hat{H}_L = -\hat{E}\, d \left(\hat{J}_+ + \hat{J}_- \right) \,, \tag{3.6}$$

where $\hat{E}$ is the light field operator and d is the atomic dipole matrix element. In the absence of interactions between the atoms, $\hat{J}^2$ commutes with $\hat{H}_S + \hat{H}_L$ and thus its eigenvalue $\frac{N}{2}\left(\frac{N}{2}+1\right)$ is a conserved quantity. The Hamiltonian (3.6) causes the system to move along a ladder of optically accessible states called the 'Dicke' or 'bright' states. The rest of the 2^N states in the Hilbert space are decoupled and the system will not evolve into them unless some other interactions (such as dephasing)

are added. The Dicke ladder runs from $\left|J, -\frac{N}{2}\right\rangle$ to $\left|J, \frac{N}{2}\right\rangle$ shown in Fig. 3.1; the $N+1$ rungs correspond to the fully symmetric superpositions of $N/2 + M$ excited atoms for each value of M. For example the lowest two bright states in a system written in the site basis are:

$$|J, -N/2\rangle = |0, 0, 0...0\rangle \ , \tag{3.7}$$

$$|J, -N/2 + 1\rangle = \frac{1}{\sqrt{N}} |1, 1, 1, ...1\rangle \ . \tag{3.8}$$

The collective excitation operators explore this ladder of states, with matrix elements given by Clebsch-Gordan coefficients :

$$\hat{J}_+ |J, M\rangle = \sqrt{(J - M)(J + M + 1)}\, |J, M + 1\rangle \tag{3.9}$$

$$\hat{J}_- |J, M\rangle = \sqrt{(J - M + 1)(J + M)}\, |J, M - 1\rangle \tag{3.10}$$

and the transition rates between adjacent Dicke ladder states are then readily calculated:

$$\Gamma_{M \to M \pm 1} = \gamma \left(\frac{N}{2} \pm M + 1 \right) \left(\frac{N}{2} \mp M \right), \tag{3.11}$$

where $\gamma = 8\pi^2 d^2 / \left(3\epsilon_0 \hbar \lambda^3\right)$ is the free atom decay rate.

If the system is initialised in the fully excited state $\left|J, \frac{N}{2}\right\rangle$ and there are no photons to absorb, then the system cascades down the ladder, as shown by the red arrows in Fig. 3.1. Upon reaching the midway point ($M = 0$) its emission rate exceeds the rate γN expected of N uncorrelated atoms for $N > 2$. For a larger number of atoms the peak transition rate of Eq. (3.11) follows a quadratic dependence on N and is well approximated by

$$\Gamma_{M \to M-1} \approx \gamma \left(\frac{N}{2} \right)^2 . \tag{3.12}$$

This is the essence of superradiance: constructive interference between the different possible decay paths greatly enhances the emission rate, producing a high intensity pulse. The enhancement is the result of simple combinatorics: near the middle of the ladder, $|J, 0\rangle$, there are a large number of possible configurations of excited atoms that contribute to each respective Dicke state. Superradiance is not an intrinsically transient effect: steady state operation can occur through repumping [106], or in cavities [175, 10], and recently a superradiant laser with potential for extraordinary stability and narrow linewidth has been demonstrated [19].

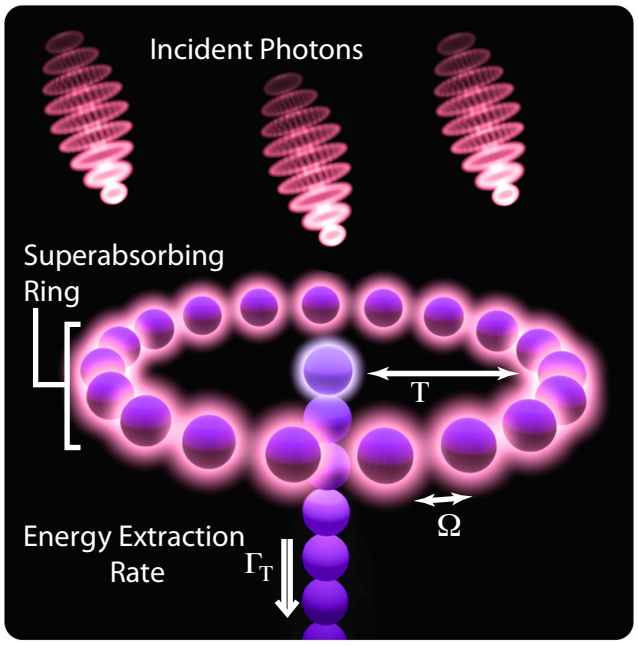

Figure 3.2: One potential realisation of superabsorption. Photons absorbed by the ring give rise to delocalised excitons; ideally the ring maintains a specific exciton population to achieve enhanced absorption. Combined with a suitable charge sensor (e.g. a quantum point contact) this enables photon sensing. We also model an application for photon harvesting, where newly created excitons are transferred from the ring to a central core absorber, followed by an irreversible process (e.g. one-way transfer down a strongly coupled chain) to a centre converting the exciton into stored energy.

3.4 Superabsorption

Time-reversal symmetry of quantum mechanics implies that systems with enhanced emission rates will also have enhanced absorption rates. Naturally emission dominates if an excited state of the collective emits into a vacuum, since there are no photons to absorb. Even in an intense light field where absorption and emission are closely balanced, a given transition remains more likely to emit than to absorb. These will always perform an (often strongly) biased random walk down the ladder of accessible states, being attracted by the bottom most rung. Strongly enhanced absorption near the middle of the Dicke ladder is thus an improbable process and can only last for a vanishingly short time. Thus it might seem that the inverse of superradiance is intrinsically ephemeral.

The crucial ingredient for achieving superabsorption is to engineer the transition rates in a way that primarily confines the dynamics to an *effective two-level system*

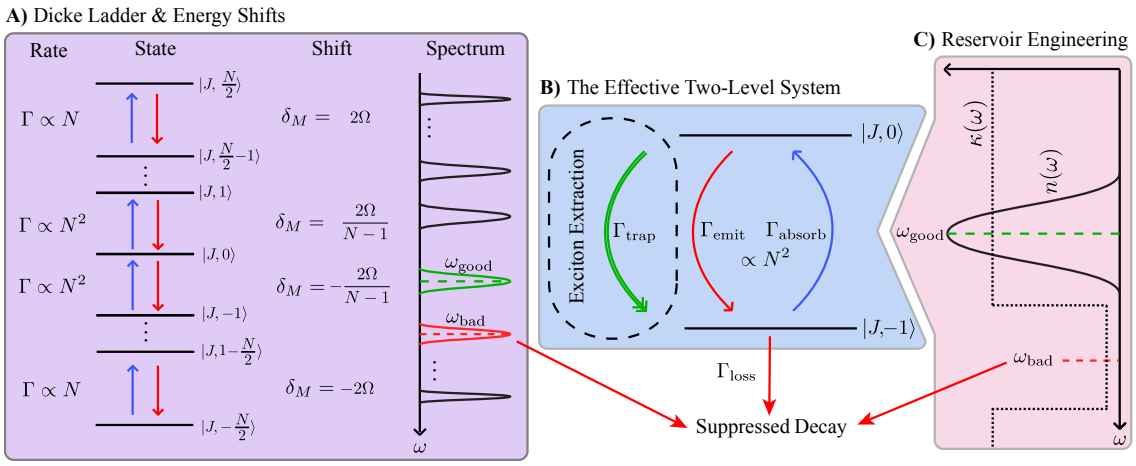

Figure 3.3: Engineering the Dicke Ladder. **A)** The ladder of Dicke states of an N atom system, with emission (red) and absorption (blue) processes. In the presence of interactions $\Omega \neq 0$, the frequency shift of each transition is given by $\omega_A + \delta_M$. **B)** The Effective Two-Level System (E2LS) picture with optional trapping process for energy extraction in the dashed box. **C)** A scheme for using the environment to confine the ladder of states into an effective two level system either by tailoring the spectral density $\kappa(\omega)$ or the mode occupation $n(\omega)$.

(E2LS) around the $M = 0$ transition (see Fig. 3.4b), which exhibits the required quadratic absorption rate. In order to ensure that most transitions take place within the E2LS we must either suppress the total loss rate from the E2LS or enhance the probability of transitions within it. This becomes possible if the frequency of the E2LS transition is distinct from that of other transitions, and in particular the one immediately below the targeted transition within the E2LS. This will never be the case for a non-interacting set of atoms, which must have a degenerate set of ladder transition energies, but it can occur once suitable interactions are included. Dicke physics requires that the atoms remain indistinguishable, but interactions are still permissible in certain symmetric geometries such as rings [51, 103], and these structures will continue to exhibit superradiance, and are therefore also capable of superabsorption. In the theory of superradiance this effect is called 'chirping' since each rung of the ladder has a unique frequency Fig. 3.4a), the frequency of the emitted light changes over the course of the superradiant pulse.

The required interactions are in fact the ever present field meditated dipole-dipole interactions, which are usually ignored, because they are usually small and have little effect on the dynamics. In general dipole-dipole interactions are deleterious to superradiance, as they tend to give each atom a unique environment which in turn makes the light they emit distinguishable. However, if the atoms are in a ring

structure that is strikingly reminiscent of the photosynthetic light harvesting complex LH1 [16, 69] (see Fig. 3.2) they retain Dicke physics.

3.4.1 Interactions

3.4.1.1 Field Induced Interactions

We shall now derive a master equation for the candidate superabsorber depicted in Fig. 3.2. We assume the interactions act between adjacent atoms only and are due to Förster type coupling. Following the general procedure of Section 1.5.2.1 and Ref. [103], we generalise from a vacuum environment to one with a population distribution and structured spectral density. This allows for the presence of the superabsorption term and introduces some additional complexities.

We consider the interaction picture with respect to $\hat{H}_S$ (3.1) and the free Hamiltonian of the electromagnetic field (1.75). After performing the standard Born-Markov approximation and tracing over the environment $\mathcal{E}$, the starting point for our derivation is [25] ($\hbar = 1$):

$$\frac{d}{dt}\tilde{\rho}_{\mathcal{S}}(t) = -\int_0^\infty dt' \mathrm{Tr}_{\mathcal{E}}[\tilde{H}_L(t), [\tilde{H}_L(t-t'), \tilde{\rho}_{\mathcal{S}}(t) \otimes \tilde{\rho}_{\mathcal{E}}]\,, \tag{3.13}$$

where $\tilde{\rho}_{\mathcal{S}}(t)$ is the reduced interaction picture density matrix and $\tilde{H}_L(t)$ denotes the interaction picture representation of the system-light-interaction Hamiltonian:

$$\hat{H}_L = -\sum_{i=1}^{N} \hat{\sigma}_-^i \, \boldsymbol{d} \cdot \hat{\boldsymbol{E}}(\boldsymbol{r}_i) + \hat{\sigma}_+^i \boldsymbol{d}^* \cdot \hat{\boldsymbol{E}}(\boldsymbol{r}_i)\,, \tag{3.14}$$

where $\boldsymbol{d}$ is the atomic dipole vector and the electric field operator is given by:

$$\hat{\boldsymbol{E}}(\boldsymbol{r}_i) = i \sum_{i=1}^{N} \sum_{\boldsymbol{k},\lambda} \sqrt{\frac{2\omega_k}{V}} \boldsymbol{e}_\lambda(\boldsymbol{k}) \left(\hat{b}_\lambda(\boldsymbol{k}) e^{i\boldsymbol{k}\cdot\boldsymbol{r}_i} - \hat{b}_\lambda^\dagger(\boldsymbol{k}) e^{-i\boldsymbol{k}\cdot\boldsymbol{r}_i} \right), \tag{3.15}$$

where $\boldsymbol{e}_\lambda(\boldsymbol{k})$ and $\hat{b}_\lambda^{(\dagger)}(\boldsymbol{k})$ are the polarisation vector of the field and its annihilation (creation) operator, respectively. The system dynamics is then generically determined by the following master equation [25]:

$$\frac{d}{dt}\rho_S(t) = -i[\hat{H}_S + \hat{H}_I, \rho_S(t)] + \sum_{\omega} \sum_{i,j} \left[\Gamma_{i,j}(\omega)(\hat{A}_j \rho_S(t) \hat{A}_i^\dagger - \hat{A}_i^\dagger \hat{A}_j \rho_S(t)) + \text{h.c.} \right], \tag{3.16}$$

where h.c. denotes the Hermitian conjugate. The $\hat{A}_i$ are the Lindblad operators given by $\hat{\sigma}_-^i$ and $\hat{\sigma}_+^i$, and $\Gamma_{i,j} = \int_0^\infty ds\, e^{i\omega s} \langle \boldsymbol{d}^* \cdot \hat{\boldsymbol{E}}(\boldsymbol{r}_i, s) \boldsymbol{d} \cdot \hat{\boldsymbol{E}}(\boldsymbol{r}_j, 0) \rangle$ is the spectral

correlation tensor, which will be calculated in the following. We start by considering the expression

$$\langle \boldsymbol{d}^* \cdot \hat{\boldsymbol{E}}(\boldsymbol{r}_i, s)\boldsymbol{d} \cdot \hat{\boldsymbol{E}}(\boldsymbol{r}_j, 0)\rangle = Tr_{\mathcal{E}}[\boldsymbol{d}^* \cdot \hat{\boldsymbol{E}}(\boldsymbol{r}_i, s)\boldsymbol{d} \cdot \hat{\boldsymbol{E}}(\boldsymbol{r}_j, 0)\rho_{\mathcal{E}}] \ , \tag{3.17}$$

where $\rho_{\mathcal{E}}$ is taken as the thermal state of the environment, though allowing filtered thermal light later will not change the form of the result [194, 3]. Generally, for a thermalised environment it is well known that [25]

$$\langle \hat{b}_\lambda(\boldsymbol{k})\hat{b}_{\lambda'}(\boldsymbol{k'})\rangle = \langle (\hat{b}^\dagger_\lambda(\boldsymbol{k})\hat{b}^\dagger_{\lambda'}(\boldsymbol{k'})\rangle = 0 \ , \tag{3.18}$$

$$\langle \hat{b}_\lambda(\boldsymbol{k})\hat{b}^\dagger_{\lambda'}(\boldsymbol{k'})\rangle = \delta_{\boldsymbol{k}\boldsymbol{k}'}\delta_{\hat{\lambda}\hat{\lambda}'} = (1 + n(\omega_k)) \ , \tag{3.19}$$

$$\langle \hat{b}^\dagger_\lambda(\boldsymbol{k})\hat{b}_{\lambda'}(\boldsymbol{k'})\rangle = \delta_{\boldsymbol{k}\boldsymbol{k}'}\delta_{\hat{\lambda}\hat{\lambda}'} = n(\omega_k) \ . \tag{3.20}$$

Using these, the spectral correlation tensor can written as:

$$\Gamma_{i,j} = \frac{2\pi}{V}\sum_{\boldsymbol{k},\lambda}(\boldsymbol{d} \cdot \boldsymbol{e}_\lambda(\boldsymbol{k}))^2\omega_k\Bigg((1 + n(\omega_k))e^{i\boldsymbol{k}\cdot\boldsymbol{r}_{ij}}\int_0^\infty ds\, e^{-i(\omega_k-\omega)s} + e^{-i\boldsymbol{k}\cdot\boldsymbol{r}_{ij}}n(\omega_k)\int_0^\infty ds\, e^{i(\omega_k+\omega)s}\Bigg) \ , \tag{3.21}$$

where $\boldsymbol{r}_{i,j}$ is the vector connecting atoms i and j. Converting the sum over $\boldsymbol{k}$ to an integral ($\omega_k = c|\boldsymbol{k}|$) yields

$$\frac{1}{V}\sum_{\boldsymbol{k}} \to \frac{1}{(2\pi)^3c^3}\int_0^\infty d\omega_k\, \kappa(\omega_k)\omega_k^2\int d\Omega \, , \tag{3.22}$$

where $\kappa(\omega)$ is the spectral density given by the density of states weighted by the coupling strength, $\kappa(\omega) = \sum_k |g_k|^2\delta(\omega - \omega_k) \equiv \chi(\omega)|g(\omega)|^2$. Considering for the moment only the angular part of the integration. We need to evaluate terms such as:

$$\int \left(\boldsymbol{d} \cdot \boldsymbol{d}^* + \frac{(\boldsymbol{k} \cdot \boldsymbol{d}^*)(\boldsymbol{k} \cdot \boldsymbol{d})}{|\boldsymbol{k}|^2}\right)e^{i\boldsymbol{k}\cdot\boldsymbol{r}_{ij}}d\Omega = \int_0^{2\pi}\int_0^\pi \sin\theta\, e^{i\boldsymbol{k}\cdot\boldsymbol{r}_{ij}}\, d\theta d\phi \tag{3.23}$$

Without loss of generality we can define $r_{i,j}$ as along the z axis such that ($|\boldsymbol{k}| \cdot \boldsymbol{r}_{ij} = k\cos\theta$). Then collating the results of the angular integration gives a diffraction-type function:

$$F(\omega\, \boldsymbol{r}_{ij}) = \frac{8\pi}{3}\left(j_0(\omega\,|\boldsymbol{r}_{ij}|) + \frac{1}{2}\left(3\cos^2(\theta_{\boldsymbol{d}\boldsymbol{r}_{ij}}) - 1\right)j_2(\omega\,|\boldsymbol{r}_{ij}|)\right) \ , \tag{3.24}$$

where $j_n(x)$ is the n^{th} spherical Bessel function and the angle $\theta_{\boldsymbol{d}\boldsymbol{r}_{ij}}$ between the atomic dipoles and pairwise connection vectors is

$$\cos^2\theta_{\boldsymbol{d}\boldsymbol{r}_{ij}} = \frac{|\boldsymbol{d} \cdot \boldsymbol{r}_{ij}^2|}{|\boldsymbol{d}^2||\boldsymbol{r}_{ij}{}^2|} \, . \tag{3.25}$$

Considering the geometry in Fig. 3.2. we assume that all dipoles are parallel, and perpendicular to the plane defined by the ring. In this case, and for only nearest neighbour interactions, $\theta_{\boldsymbol{d}\boldsymbol{r}_{ij}}$ is independent of i and j. Thus Eq. (3.21) becomes

$$\Gamma_{i,j} = \frac{|d|^2}{(2\pi)^2 c^3}\int_0^\infty d\omega_k\,\kappa(\omega_k)\omega_k^3\,F(\omega_k r_{ij})\bigg((1+n(\omega_k))\int_0^\infty ds e^{-i(\omega_k-\omega)s} + n(\omega_k)\int_0^\infty ds e^{i(\omega_k+\omega)s}\bigg), \tag{3.26}$$

which we separate into its real and imaginary parts $\Gamma_{i,j} = \frac{1}{2}\gamma_{i,j}(\omega) + iS(\omega)$ with the help of the identity

$$\int_0^\infty ds\, e^{\pm i\epsilon s} = \pi\delta(\epsilon) \pm iP\frac{1}{\epsilon}. \tag{3.27}$$

The real terms $\gamma_{i,j}(\omega)$ derive from the δ-functions and give rise to the dissipative dynamics; optical transitions in this case. In the remaining term, $F(\omega_k\, r_{ij})$ is evaluated at $\omega_k = \pm\omega$. We are working in the small sample limit, where the wavelength of light is far longer than the size of our nanostructure ($\omega\, r_{ij} \approx 0$), and so $F(\omega\, r_{ij}) \approx 8\pi/3$. Hence $\gamma_{i,j}$ is independent of the atomic indices to a good approximation:

$$\gamma_{i,j}(\omega) \approx \gamma(\omega) = \frac{4\omega^3|d|^2}{3c^3}\kappa(\omega)(1+n(\omega))\,. \tag{3.28}$$

The Planck distribution has the property that $n(-\omega) = -(1+n(\omega))$. Thus we can combine the terms arising from $\delta(\omega_k \pm \omega)$ and only run the sum over positive values. The second term on the righthand side of Eq. (3.16) thus becomes

$$D[\dot\rho] = \sum_{\omega>0}\sum_{i,j}\frac{4\omega^3|d|^2}{3c^3}\kappa(\omega)\bigg((1+n(\omega))(\hat\sigma_-^j\rho\hat\sigma_+^i - \frac{1}{2}\left\{\hat\sigma_+^i\hat\sigma_-^j,\rho\right\}) + n(\omega)(\hat\sigma_+^j\rho\hat\sigma_-^i - \frac{1}{2}\left\{\hat\sigma_-^i\hat\sigma_+^j,\rho\right\})\bigg). \tag{3.29}$$

By simply assuming all transitions have the same frequency splitting ($\omega = \omega_A$), a vacuum environment state $n(\omega) = 0$ and switching to the collective operators to express the sums $\hat J_- = \sum_i \hat\sigma_-^i$, we reproduce the ordinary superradiance master equation dissipator:

$$D[\dot\rho] = -\frac{\Gamma}{2}(\{\hat J_+\hat J_-,\rho\} - 2\hat J_-\rho\hat J_+) \tag{3.30}$$

We now turn to the imaginary part $S(\omega)$ of the spectral correlation tensor, which will be responsible for providing the detuning between different transitions; this is given by:

$$S(\omega) = \frac{|d|^2}{(2\pi)^2 c^3}P\int_0^\infty d\omega_k\,\kappa(\omega_k)\omega_k^3\,F(\omega_k\, r_{ij})\bigg(\frac{1+n(\omega_k)}{\omega-\omega_k} + \frac{n(\omega_k)}{\omega_k+\omega}\bigg). \tag{3.31}$$

The $i = j$ terms, for which $F(0) = 8\pi/3$, correspond to the ordinary Lamb shift of individual atom transitions; these can be accounted for by a renormalisation of the bare atomic frequency ω_A. By contrast, the $i \neq j$ terms correspond to the dipole-dipole interaction induced by the EM field. Evaluating this integral requires us to choose a specific form for the spectral density $\kappa(\omega)$. Here we consider two cases: first a flat spectral density, and second one that features a 'stop band' in the spectrum. We begin with the former case. We first separate out the term that is independent of $n(\omega)$, the Lamb shift S_L, and evaluate it. In the small sample limit ($\omega r_{ij} \ll 1$) we find

$$S_L = \frac{d^2}{4\pi\epsilon_0 r_{ij}^3}\left[1 - 3\cos^2(\theta_{dr})\right] . \tag{3.32}$$

After separating out the Lamb shift, we are left with the divergent integral corresponding to the Stark shift:

$$S_s(\omega) = \frac{|d|^2}{(2\pi)^2 c^3} P \int_0^\infty d\omega_k \, \kappa(\omega_k)\omega_k^3 \, F(\omega_k r_{ij}) \left(\frac{n(\omega_k)}{\omega - \omega_k} + \frac{n(\omega_k)}{\omega + \omega_k} \right) . \tag{3.33}$$

This is seldom evaluated in the literature and is usually assumed negligible. Here we are primarily concerned with controlling $n(\omega)$ so that it is only significant for one mode, which has frequency ω_g. In this case we set $n(\omega_k) = \delta(\omega_k - \omega_g)$ and take the small sample limit:

$$\begin{aligned} S_s(\omega) = \lim_{r\omega_g \to 0} \frac{4\pi\omega}{r^3(\omega - \omega_g)(\omega + \omega_g)} \Bigg(& \sin(r\omega_g)(\cos(2\theta_{dr})(3 - r^2\omega_g^2) + r^2\omega_g^2 + 1) \\ & - r\omega_g(3\cos(2\theta_{dr}) + 1)\cos(r\omega_g)) \Bigg) = 0 \end{aligned} \tag{3.34}$$

Hence we can neglect the Stark shift and only retain the Lamb shift. Returning to the other spectral density we consider, that with the stop band, we can express the stop band with the following, simplistic spectral density:

$$\kappa(\omega) = 1 - T(\omega_b, \sigma) , \tag{3.35}$$

where $T(\omega_b, \sigma)$ is the 'top hat' function centred on ω_b with a width σ. The factor of one produces the same result as for the flat spectral density $S_s(\omega)$. The top hat handles the effect of the gap $S_{gap}(\omega)$:

$$S(\omega) = S_s(\omega) - S_{gap}(\omega) . \tag{3.36}$$

The top hat has the effect of confining the integral to a window around ω_b:

$$S_{gap}(\omega) = \frac{|d|^2}{(2\pi)^2 c^3} P \int_{\omega_b-\sigma}^{\omega_b+\sigma} d\omega_k\, \omega_k^3\, F(\omega_k r_{ij}) \left(\frac{1+n(\omega_k)}{\omega-\omega_k} + \frac{n(\omega_k)}{\omega_k+\omega} \right). \tag{3.37}$$

This can be evaluated to yield a lengthly, but straightforward expression. For an ideal gap ($\sigma \to 0$), $S_{gap}(\omega) = 0$ and hence can be neglected. Collating these results, we are left with a familiar expression for the strength of the interaction between two dipoles (3.32) multiplied by a hopping term introduced via the EM field:

$$\hat{H}_I = \Omega_{i,j} \sum_{i \neq j}^{N} \left(\hat{\sigma}_+^i \hat{\sigma}_-^j + \hat{\sigma}_-^i \hat{\sigma}_+^j \right), \tag{3.38}$$

which describes energy conserving 'hopping' of excitons between sites mediated by virtual photon exchange. The hopping interaction strength $S_L = \Omega_{i,j}$ is given by:

$$\Omega(i,j) = \frac{d^2}{4\pi\epsilon_0 r_{ij}^3} \left[1 - \frac{3(\hat{\boldsymbol{\epsilon}}_a \cdot \boldsymbol{r}_{ij})^2}{r_{ij}^2} \right] \approx \frac{d^2}{4\pi\epsilon_0 r_{ij}^3} \tag{3.39}$$

with $\hat{\boldsymbol{\epsilon}}_a$ being a unit vector parallel to the direction of the dipoles. For a circular geometry with dipoles perpendicular to $\boldsymbol{r}_{ij}$ and retaining only nearest neighbour interactions [a good approximation for larger rings since $\Omega(i,j) \propto r_{ij}^{-3}$], $\Omega := \Omega(i, i+1)$ is a constant. Owing to the high degree of symmetry of the ring geometry, to first order $\hat{H}_I$ does not mix the $|JM\rangle$ eigenstates, only shifting their energies [103] according to

$$\delta E_M = \langle J, M | \hat{H}_I | J, M \rangle = \Omega \frac{J^2 - M^2}{J - \frac{1}{2}}. \tag{3.40}$$

The shift of the transition frequencies is given by the difference of two adjacent levels $E_M - E_{M-1}$:

$$\omega_{M \to M-1} = \omega_A - 4\Omega \frac{M - \frac{1}{2}}{N-1}. \tag{3.41}$$

These altered frequencies break the degeneracy in the Dicke ladder where each transition now has a unique frequency. For example the transition frequency from the ground state to the first Dicke state is $\omega_{-N/2+1 \to -N/2} = \omega_A - 2\Omega$. Crucially, the Dicke states still still represent a very good approximation of the eigenbasis of the system, yet each transition in the ladder now samples both $\kappa(\omega)$ and $n(\omega)$ at its own unique frequency. The highly symmetric geometry of our system means that the hopping interaction (3.38) does not cause mixing of Dicke levels, but only shifts their energies. Thus an effective Hamiltonian for the subspace consisting of only the fully symmetric states of the Dicke ladder can be written as :

$$\hat{H}_S + \hat{H}_I = \frac{E_M}{2} \sum_{M=-J}^{J} |J, M\rangle\langle J, M|, \tag{3.42}$$

where E_M is the energy of the $|J, M\rangle$ state now including the shift defined in Eq. 3.40. Instead of having a generic ladder operator $\hat{J}_\pm$ that moves any state $|J, M\rangle \rightarrow |J, M \pm 1\rangle$, with emission or absorption at ω_A, we now have to break up this operator, because the Dicke transitions are no longer degenerate in energy. The generic ladder operators are thus replaced by a sum over operators, which take us between specific Dicke states, sampling the spectral density at the requisite frequency ω_β:

$$\hat{L}_M = |J, M-1\rangle\langle J, M| \,, \tag{3.43}$$

which yields the result:

$$\dot{\rho} = -i[\hat{H}_S + \hat{H}_I, \rho] - \gamma \sum_\beta \kappa(\omega_\beta) \left((n(\omega_\beta) + 1) D[\hat{L}_\beta]\rho + n(\omega_\beta) D[\hat{L}_\beta^\dagger]\rho \right) . \tag{3.44}$$

3.4.1.2 Explicit Interactions

In the previous section the hopping interaction emerged from the derivation of the master equation, as a direct consequence of embedding the absorbers into a common electromagnetic environment. Alternatively, we could add an interaction directly to the system Hamiltonian, which may either be mediated by virtual photon exchange or have some other physical origin. The initial Hamiltonian then reads:

$$\hat{H}_S = \omega_A \sum_{m=1}^{N} \hat{\sigma}_+^m \hat{\sigma}_-^m + \Omega \sum_{i,j}^{N} (\hat{\sigma}_+^i \hat{\sigma}_-^j + \hat{\sigma}_-^j \hat{\sigma}_+^i) \,. \tag{3.45}$$

Such a Hamiltonian is a diagonalised using the Jordan-Wigner transformation [13]. For example, a four atom system has eigenvalues:

$$\left\{ 0, \omega_A - 2\Omega, 2\omega_A - 2\sqrt{2}\Omega, 3\omega_A - 2\Omega, 4\omega_A \right\} , \tag{3.46}$$

resulting in the following transition frequencies:

$$\omega = \left\{ \omega_A - 2\Omega, \omega_A - 2\Omega \left(1 + \sqrt{2}\right), \omega_A + 2\Omega \left(-1 + \sqrt{2}\right), \omega_A + 2\Omega \right\} . \tag{3.47}$$

These differ slightly from those derived using the approach in the earlier. Crucially, however, the degeneracy of the transition frequencies is broken in a similar way as before. For small length scale linear systems it has been noted that superradiance dynamics are not significantly altered [13], when compared to the traditional field mediated interaction approach [103].

3.4.1.3 Resolution of Frequency Shifts

The enhanced absorption and emission rate in the middle of the Dicke ladder implies an increased lifetime broadening. One might thus worry whether the detunings obtained courtesy of the hopping interaction are then still sufficient to completely resolve adjacent transitions. A simple analysis shows that this is indeed the case [103], and the natural width ($N^2\gamma$ around $M = 0$) remains smaller than the shift δ_ω provided the wavelength of the light is much greater than the size of the system. To see this, we shall assume that the transition is indeed well resolved, $N^2\gamma < \delta_\omega$, and show that is essentially equivalent to the 'small sample' condition, $r \ll \lambda$, which underlies the phenomenon of superradiance in the first place.

Using the definition of γ from as the free atom decay rate, the greatest broadening and smallest energy shift at $M = 0$ are, respectively,

$$N^2\gamma = \frac{8N^2\pi^2d^2}{3\epsilon_0\hbar\lambda^3}\,, \tag{3.48}$$

$$\delta_\omega = 4\frac{\Omega}{N-1} \approx \frac{d^2}{4\pi\hbar\epsilon_0 r^3}\,. \tag{3.49}$$

Substituting Eqs. (3.48) and (3.49), the inequality $N^2\gamma < \delta_\omega$ becomes

$$\frac{2N^3\pi^2d^2}{3\epsilon_0\hbar\lambda^3} < \frac{d^2}{4\pi\hbar\epsilon_0 r^3} \quad \Longleftrightarrow \quad 2N\pi r < \lambda\,, \tag{3.50}$$

where the righthand side follows after cancellation of several variables followed by taking the qubic root. This is equivalent to $r \ll \lambda$, up to moderate numerical factor (when N is not too large), accounted for by relaxing '$\ll$' to '$<$'. For the present discussion, r is understood to be the nearest neighbour distance, having assumed energy shifts appropriate for only nearest neighbour interactions (for other interaction models, the detunings would be larger). We note that distinct shifted lines have also already been observed — and resolved — experimentally [260].

3.4.1.4 Interactions beyond the nearest neighbour limit

Earlier we assumed only nearest neighbour interactions are significant. For a symmetric ring geometry relaxing this condition leads to the same qualitative behaviour, but results in slightly larger detunings between adjacent transitions in the Dicke ladder. First, let us consider the opposite limit to the nearest neighbour case and allow all pairwise interactions with equal strength:

$$\langle J, M|\hat{H}_H\,|J, M\rangle = \langle J, M|\Omega \sum_{i\neq j}(\hat{\sigma}^i_+\hat{\sigma}^j_- + \hat{\sigma}^i_-\hat{\sigma}^j_+)\,|J, M\rangle\,, \tag{3.51}$$

$$\delta E_m = \Omega\langle J, M| \sum_{i\neq j} (\hat{\sigma}^i_+ \hat{\sigma}^j_- + \hat{\sigma}^i_- \hat{\sigma}^j_+) \, |J, M\rangle \ , \tag{3.52}$$

which can be rewritten using the collective operators as follows

$$\delta E_m = \Omega\langle J, M| \hat{J}_+ \hat{J}_- + \hat{J}_- \hat{J}_+ - \sum_i (\hat{\sigma}^i_+ \hat{\sigma}^i_- + \hat{\sigma}^i_- \hat{\sigma}^i_+) \, |J, M\rangle \ . \tag{3.53}$$

The final two terms are added to remove the $i = j$ terms implicit in the $\hat{J}_+\hat{J}_-$ terms, which count the number of excited and unexcited atoms, respectively. Hence,

$$\delta E_m = \Omega(\langle J, M| \hat{J}_+ \hat{J}_- + \hat{J}_- \hat{J}_+ \, |J, M\rangle - 2J) \, . \tag{3.54}$$

The remaining two terms are easily calculated using (3.9), yielding:

$$\delta E_m = 2\Omega(J^2 - M^2) \, . \tag{3.55}$$

Thus the energy shifts are the same as in the nearest neighbour case Eq. (10) but lack the factor$(J - 1/2)^{-1}$. Therefore, unlike in the nearest neighbour limit, increasing the number of atoms does not reduce the size of the frequency shift, which could help in blocking the transition at ω_{bad} and ensuring frequency selectivity of a trapping mechanism.

The actual ring geometry with all pairwise dipole interactions included will fall somewhere in between these two limits, depending on ring size. The operators involved in the interaction remain the same, but their weights are altered as the size of the ring changes. The symmetry of the ring dictates that each atom will be subject to the same set of interactions with the rest of the ring. The condition of interchangeability of atoms is thus met regardless of the specific interaction model (i.e. nearest neighbour, next nearest neighbour etc.). For all cases, the hopping interaction only causes shifts of a variable size between the two limits we have discussed above; the size of the shifts given a particular ring size and interaction model is readily obtained numerically.

3.4.1.5 Summary

In the previous sections we've developed a model for our candidate superaborber, which corresponds to a Dicke ladder of non-degenerate transitions whose dynamics are found from a collective quantum optical master equation:

$$\begin{aligned} \dot{\rho} &= -i[\hat{H}_S + \hat{H}_I, \rho] \\ &- \gamma \sum_{\beta\in\omega} \kappa(\omega_\beta) \left((n(\omega_\beta) + 1) D[\hat{L}_\beta]\rho + n(\omega_\beta) D[\hat{L}^\dagger_\beta]\rho \right) \ . \end{aligned} \tag{3.56}$$

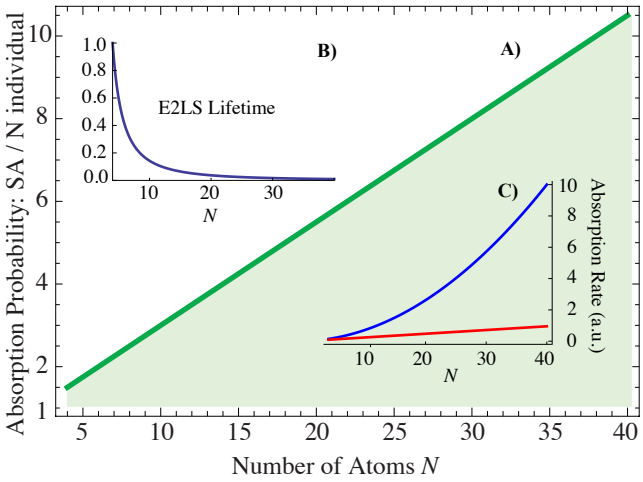

Figure 3.4: Enhanced absorption probability. **A)** the probability of absorbing a photon within the lifetime $\Gamma_{\text{loss}}^{-1}(N)$ of the superabsorbing E2LS comprising N atoms, compared to that of N individual atoms over the same duration. The relative advantage is linear in N as expected, and the coloured shading indicates the quantum advantage. **B)** lifetime of the E2LS for growing N relative to the four atoms case $\Gamma_{\text{loss}}^{-1}(N)/\Gamma_{\text{loss}}^{-1}(N=4)$. Note that the decrease in lifetime corresponds to an increasing time resolution of a superabsorbing photon detector: after initialisation the system is receptive to a photon of the requisite frequency only during this time window. **C)** absorption rate at the midpoint of the Dicke ladder (blue) and for N individual absorbers (red). The clearly visible N^2 scaling that is typical of superradiant pulses also applies to the absorption rate.

$\kappa(\omega) = \sum_k |g_k|^2 \delta(\omega - \omega_k) = \chi(\omega)|g(\omega)|^2$ is the spectral density at frequency ω; $n(\omega_\beta)$ is the occupation number of the ω_β mode, and $D[\hat{L}_\beta]\rho$ is the Lindbladian dissipator $\hat{L}_\beta \rho \hat{L}_\beta^\dagger - \frac{1}{2}\{\hat{L}_\beta^\dagger \hat{L}_\beta, \rho\}$. $L_\beta^\dagger$ moves the system up a Dicke ladder transition with frequency ω_β. Eq. (3.56) also features unitary dynamics due to the field interaction that comprises two components: the Lamb shift, accounted for by renormalising ω_A in the system Hamiltonian $\hat{H}_S$, and the field induced dipole-dipole interaction

3.4.2 Quantum Control

Our objective is to enhance transition rates at the frequency of the E2LS, which we shall call the 'good' frequency ($\omega_{0\to-1} =: \omega_{\text{good}}$) and suppress those for transitions directly out of the E2LS at the 'bad' frequency ($\omega_{-1\to-2} =: \omega_{\text{bad}}$). The required type of control of the environment is known as reservoir engineering [195]; in principle we have a choice between tailoring $\kappa(\omega)$, $n(\omega)$, or both. Tailoring the spectral density has the advantage that it can, in theory, completely eliminate the rate of loss from our E2LS when there is no mode of the right frequency present to allow decay. This requires

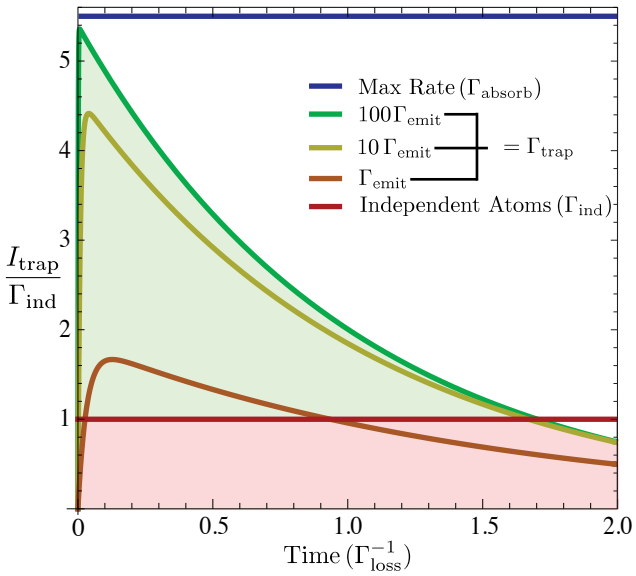

Figure 3.5: A superabsorption cycle. Superabsorption of the effective two level system indicated in Fig. 3.4. The green shading indicates the superabsorption region, the red when the extraction rate is below what could be extracted from uncorrelated atoms; both are for a system of twenty atoms and mode occupancy $n(\omega_{\text{good}}) = 10$. The maximum extraction possible from independent atoms ($\Gamma_{\text{ind}} = n(\omega_{\text{good}})N\gamma$) is used for comparison.

placing the device inside a suitably designed cavity or a photonic bandgap (PBG) crystal with a stop band at ω_{bad} (see Fig. 3.4c), where the required dimensionality of the PBG depends on the orientation of the optical dipoles. Suppression of emission rates by several orders of magnitude is then achievable with state-of-the-art systems [261, 187, 153, 88]. Photonic crystal cavities can offer both enhancement of a resonant transition (ω_{good}) and suppression of a off-resonant one (ω_{bad}) [78], making them ideal for the type of control required.

Control of $n(\omega)$ is technically easier to achieve, e.g. by using filtered thermal or pseudothermal [168, 97] light. However, this approach has the limitation that even in the optimal control regime, where $n(\omega) = 0$ everywhere except in a narrow region around ω_{good}, spontaneous emission will still cause loss from the E2LS.

Since both environmental control approaches rely on frequency selectivity, a sufficiently large detuning between adjacent Dicke transitions will be critical for achieving effective containment within the E2LS. Fortunately, this detuning is already within the frequency selectivity of current experimental controls for moderately sized rings, of say $N \sim 10$ see Section 3.5. In practice the environmental control will never be quite perfect and our system will, over long times, inevitably evolve away from the

E2LS. For example, one may only have control over $n(\omega)$ but not $\kappa(\omega)$, or an imperfect PBG with $\kappa(\omega_{\text{bad}}) > 0$, and both cases lead to an exponential decay of E2LS population with the lifetime $\Gamma_{\text{loss}}^{-1}$. Dephasing processes will also lead to leakage out of the fully symmetric subspace and thus shorten the effective lifetime of the E2LS. However, these imperfections need not dominate the behaviour and destroy the effect. We shall discuss the issue of sustained operation in the Reinitialisation Section 3.4.4.

Let us now consider the properties of the system immediately following initialisation: Fig. 3.4 shows the increased photon absorption rate of the superabsorbing E2LS compared to N uncorrelated systems, $\Gamma_{-1\to 0}/N$. Clearly, the probability of absorbing a photon within a given time window (up to the E2LS lifetime) is much higher in the superabsorbing configuration, providing an opportunity for photon dectection with improved sensitivity. The inset of Fig. 3.4 shows the lifetime of the E2LS, $\Gamma_{\text{loss}}^{-1} = (\gamma\Gamma_{-1\to -2}\kappa(\omega_{\text{bad}}))^{-1}$, as a function of N, here assumed to be limited by an imperfect PBG with $\kappa(\omega_{\text{bad}})/\kappa(\omega_{\text{good}}) = 1/100$. For photon sensing, the reduction of the operational window with increasing N may even be a desirable attribute (offering time resolved detection). Generally, the system we have so far described can function as a sensor as long as the temporary presence of an additional exciton can be registered, for example through continuously monitoring the system's charge state with a quantum point contact [105, 96, 76, 197].

3.4.3 Trapping

We have detailed how to create a photon sensor using superabsorption. We can also employ the superabsorption phenomenon in the context of energy harvesting if we can meet a further requirement: a non-radiative channel to extract excitons from the upper of these two levels, turning them into useful work as depicted in the dashed box of Fig. 3.4b. Specifically, we require an irreversible trapping process that extracts only the excitons that are absorbed by the E2LS, and does not extract excitons from levels below the E2LS. Moreover, the trapping process competes with the re-emission of the photons at a rate proportional to $n(\omega_{\text{good}}) + 1$, so that ideally it is much faster than that. Note that in this limit saturation is not an issue since absorbed photons are quickly transferred and converted, leaving the system free to absorb the next photon.

The excitons are delocalised across the ring and need to be extracted collectively to preserve the symmetry of the Dicke states. In designing this process we take inspiration from natural light harvesting systems: A 'trap' atom is located at the centre of the ring and symmetrically coupled via a resonant hopping interaction to

all the other atoms (see Fig. 3.2). In this case the interaction is mediated by the electromagnetic field as described in the previous section, but it could have other physical origins depending on the system of interest. Once an exciton has moved to the trap site we assume that it is then removed into the wider environment by a process which irreversibly absorbs its energy. We note that more exotic and potentially more efficient trapping implementations can be envisioned, such as e.g. a reservoir of excitons with an effective 'Fermi level' capable of accepting an excitons only above the energy level E_{-1}. However, at present our aim is to focus on the simplest system capable of exhibiting enhanced photon energy harvesting by superabsorption.

3.4.3.1 Phenomenological Model

The above trapping process can be described phenomenologically as collective exciton extraction from the mid point ($M = 0$) by adding the dissipator $D[\hat{L}_{\text{trap}}]\rho$ to the righthand side of Eq. (3.56) with $\hat{L}_{\text{trap}} = \sqrt{\Gamma_{\text{trap}}}\,|J,-1\rangle\langle J,0|$, and where Γ_{trap} is the rate of the trapping process. The rate of exciton extraction I_{trap} is then simply given by the population of the trapping level multiplied by the trapping rate:

$$I_{\text{trap}}(t) = \Gamma_{\text{trap}}\,\text{Tr}\left[|J,0\rangle\langle J,0|\rho(t)\right] . \tag{3.57}$$

Consider an ideal E2LS realised by a PBG completely blocking ω_{bad}, i.e. a vanishing $\Gamma_{\text{loss}} := \kappa(\omega_{\text{bad}})(n(\omega_{\text{bad}})+1)\Gamma_{-1\to-2}$. Assuming a faster trapping than emission rate, $\Gamma_{\text{trap}} \gg \Gamma_{\text{emit}} := \kappa(\omega_{\text{good}})(n(\omega_{\text{good}})+1)\Gamma_{0\to-1}$, our figure of merit I_{trap} matches the absorption rate $\Gamma_{\text{absorb}} := \kappa(\omega_{\text{good}})n(\omega_{\text{good}})\Gamma_{-1\to0}$ for all t:

$$I_{\text{trap}}(t) = I_{\text{max}} \approx \Gamma_{\text{absorb}} \approx \mu\left(\frac{N}{2} + \frac{N^2}{4}\right) , \tag{3.58}$$

where $\mu = \gamma\kappa(\omega_{\text{good}})n(\omega_{\text{good}})$. It is clear from this equation that under these conditions we achieve a superlinear scaling of the exciton current flowing out of the superabsorber. Trapping processes like the one described here have been demonstrated experimentally and meet the requirement $\Gamma_{\text{trap}} \gg \Gamma_{\text{emit}}$ see Section 3.5 .

The inevitable loss out of the E2LS entails an exponential decay of $I_{\text{trap}}(t)$ with the lifetime $\Gamma_{\text{loss}}^{-1}$, as shown in Fig. 3.5. The initial net superabsorption rate far exceeds that possible from uncorrelated atoms, however it is only a transient effect and the system needs to be reinitialised periodically to maintain its advantage. This aspect will be discussed in the next section.

We have detailed the case where a PBG is used to increase the lifetime of the E2LS. If instead intense filtered thermal light is used to ensure $n(\omega_{\text{good}}) \gg 1$, then

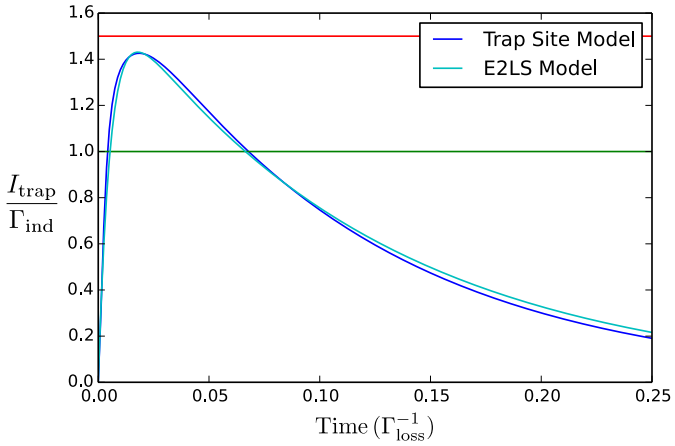

Figure 3.6: Comparison between the full trapping model discussed and the effective two level system model with adjusted rates. Parameters are: $d = 0.1, \gamma = 10^{-4}, g = 1$, and $\Gamma_{\text{trap}} = 4g$. In the phenomenological case Γ_{trap} takes the same value, whereas the effective Γ_{loss} rate was increased by a factor of five to account for additional leakage out of the E2LS due to detuned exciton extraction processes (see Fig. 3.7). Note that the shape of the E2LS curve can be made to look more similar to the full model by adjusting its Γ_{trap} and Γ_{loss} rates, but here we have chosen values giving rise to a similar peak height and enhancement area, indicative of a comparable collective advantage over one superabsorption lifetime cycle.

many absorption-trapping cycles can take place before a spontaneous emission event happens. This set-up would enable quantum enhanced light-based power transmission, where a large number of photons need to be harvested quickly in a confined area.

3.4.3.2 Full Model

In the previous section we describe the trapping process using a Lindblad operator, which takes the system from the state $|J, 0\rangle \rightarrow |J, -1\rangle$ by irreversibly removing one exciton from the system. Numerous microscopic mechanisms can be conceived of that would produce this effect; all will have to involve a collective coupling of the atoms of the ring, followed by a process (through coupling to a wider external environment) which prevents the return of exciton to the primary system, or at least renders it very unlikely.

Here, we give an account of the simplest scenario one can envision: all atoms of the ring are coupled to a 'trap' atom at the centre, whose role is to first localise the energy and then irreversibly remove it. This simple trapping model is schematically depicted in Fig. 3.7: The trap atom possesses a transition frequency $\omega_{\text{trap}} \approx \omega_{\text{good}}$

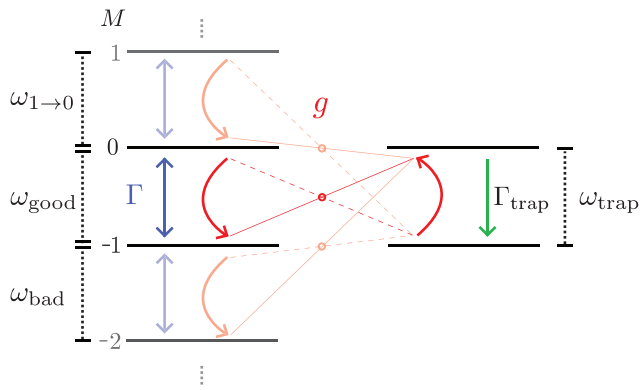

Figure 3.7: A trap site is connected to the Dicke ladder. The trap's transition frequency ideally matches that of the 'good' transition $\omega_{\text{trap}} \approx \omega_{\text{good}}$, and it is coupled to the Dicke transitions via a flip-flop interaction of strength g. This gives rise to 'see-saw' like oscillations between Dicke and trap transitions, but only the desired transition is resonant, all others are detuned and thus suppressed. To ensure that excitons hopping to the trap site are irreversibly removed instead of 'see-sawing' back and forth indefinitely, the trap is incoherently emptied at a rate Γ_{trap}. As long as Γ_{trap} is not so large that the trap transition experiences significant lifetime broadening approaching $|\omega_{\text{good}} - \omega_{\text{bad}}|$, and also assuming $|\omega_{\text{good}} - \omega_{\text{bad}}| > g$, the exciton extraction from the 'bad' transition in particular can be suppressed. The blue double-headed arrows indicate the (enhanced) optical emission and absorption processes.

and is coupled to the ring by a field mediated hopping interaction of strength g (i.e. the same type of interaction which couples the ring's atoms to each other). The Hamiltonian for such a setup is:

$$\hat{H}_{\text{T}} = g(\hat{J}_+\hat{\sigma}_-^T + \hat{J}_-\hat{\sigma}_+^T) + \omega_{\text{trap}}\hat{\sigma}_+^T\hat{\sigma}_-^T\,, \tag{3.59}$$

where the superscript T denotes the trap site, g is the strength of the coupling between the ring and the trap, and ω_{trap} is the trap's transition frequency, which ideally matches ω_{good}. An exciton 'hopping' onto the trap site is subjected to an irreversible decay with rate Γ_{trap}, e.g. by being linked to a chain of exciton sites acting as a wire or lead. In natural light harvesting systems the trap would be the reaction centre and the decay a photochemical process.

When the trapping rate Γ_{trap} is sufficiently fast only negligible population exists in the 2LS forming the trap, hence its effect can, to a good approximation, be considered that of a Lindblad operator acting on the main system, as in the previous section. For a slower rate Γ_{trap} a decaying Rabi oscillation may take place, moving the exciton back and forth between trap and ring. However, the presence or absence of these oscillations does not significantly affect the superabsorption process.

This simplistic trapping model introduces an extra contribution to the rate of loss from the E2LS: the finite lifetime $1/\Gamma_{\text{trap}}$ means the energy of the trap is not perfectly sharply defined, reducing the trap's frequency selectivity. Thus, it will occasionally also accept energy from the 'bad' transition ω_{bad}, which increases the effective loss rate Γ_{loss}. However, one can optimise the parameters (Γ_{trap} , g, ω_{trap}) to minimise this undesirable side effect, whilst still meeting the condition that $\Gamma_{\text{trap}} > \Gamma_{\text{emit}}$. With the addition of the trapping terms (3.59) the master equation is solved numerically. We compare this against the analytical expression for the trapping rate that can be derived for the E2LS model:

$$\rho_{\text{M=0}}(t) = \frac{\Gamma_{\text{absorb}}}{\sqrt{\Gamma_{\text{total}}^2 - 4\Gamma_{\text{loss}}(\Gamma_{\text{emit}} + \Gamma_{\text{trap}})}} \Bigg(e^{-\frac{1}{2}t(\Gamma_{\text{total}} - \sqrt{\Gamma_{\text{total}}^2 - 4\Gamma_L(\Gamma_{\text{emit}}+\Gamma_{\text{trap}})})} - e^{-\frac{1}{2}t(\Gamma_{\text{total}} + \sqrt{\Gamma_{\text{total}}^2 - 4\Gamma_L(\Gamma_{\text{emit}}+\Gamma_{\text{trap}})})} \Bigg), \tag{3.60}$$

$$I_{\text{trap}}(t) = \Gamma_{\text{trap}}\, \rho_{\text{M=0}}(t), \tag{3.61}$$

where $\Gamma_{\text{total}} = \Gamma_{\text{absorb}} + \Gamma_{\text{emit}} + \Gamma_{\text{loss}} + \Gamma_{\text{trap}}$ and with Γ_{trap} referring to the effective rate of a trapping Lindblad operator, which is related, but generally not necessarily equal to the decay rate of the trap site in the full model. This is due to the effect additional parameters such as the coupling strength g. By accounting for this and the additional contribution to Γ_{loss} described above, we can compare the trap site model against the E2LS. Fig. 3.6 shows the results of this comparison. The analytical results for the E2LS can thus provide an adequate and simple qualitative description of the dynamics that is brought about by a more complex and realistic trapping model.

3.4.4 Reinitialisation

Reinitialisation could be achieved by exploiting a chirped pulse of laser light to re-excite the system, or through a temporary reversal of the trapping process. In practice there will be an energy cost associated with reinitialisation but, as we show below, in all but the most severe cases this cost is more than offset by the faster photon to exciton conversion rate during the transient superabsorption periods. Furthermore, the frequency with which one has to reinitialise does not have a fundamental lower bound, it is limited only by the quality of the control one can apply.

Perhaps the most elegant way of implementing the reinitialisation step (short of self-initialisation, see below) would make use of quantum feedback control [267]: The superabsorption enhancement is derived from coherence between states that all

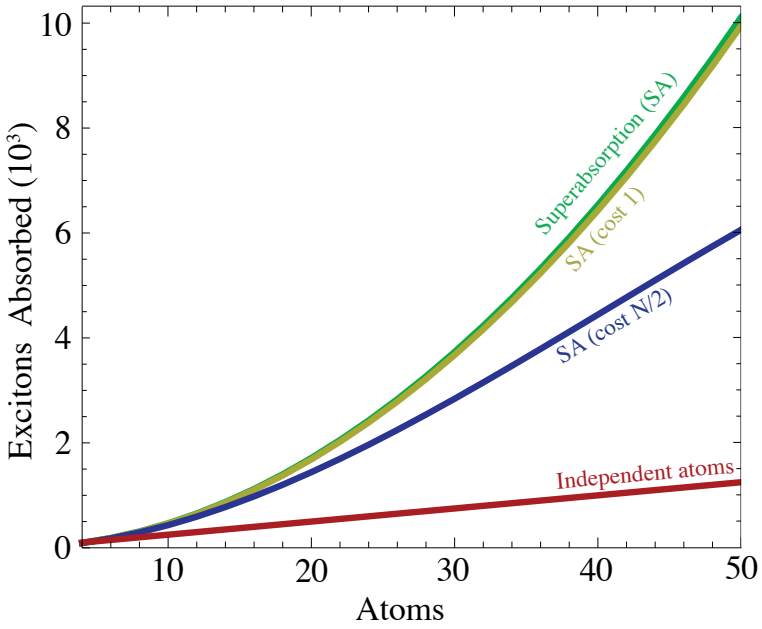

Figure 3.8: Superlinear exciton absorption. The total number of excitons absorbed within the common reference time $\Gamma_{\text{loss}}^{-1}(N = 4)$ as function of the number of atoms N. The coloured curves represent the reinitialisation cost models and the red line shows the maximum extracted from independent atoms for comparison. The scaling is superlinear in all coupled atom cases, approximately following the ideal N^2 law (green), except for large N in the pessimistic cost model of full reinitialisation (blue). If quantum feedback control enables the replacement of a single exciton as soon as a loss event has happened, then the nearly quadratic scaling persists up to arbitrary numbers of atoms (olive).

possess the same number of excitons. Therefore, the number of excitons could be continually monitored (e.g. by a quantum point contact or by monitoring fluorescence of a probe field tuned to a level or two below the desired manifold) without destroying the desired effect. A suitably designed feedback system could then feed in an excitation only when a loss event had occurred, providing optimal efficiency

$$I_{\text{trap}} = \Gamma_{\text{absorb}} - \Gamma_{\text{loss}} = (\mu - \sigma)\left(\frac{N}{2} + \frac{N^2}{4}\right) + 2\sigma\,, \tag{3.62}$$

where $\sigma = \gamma\kappa(\omega_{\text{bad}})(1 + n(\omega_{\text{bad}}))$. Provided $\mu > \sigma$ superabsorption will occur, and for $\sigma = 0$ we recover the theoretical maximum of the idealised case in Eq. (3.58).

A far simpler reinitialisation scheme would only require periodic reinitialisation following a fixed time interval, and does away with the need for feedback control. In order to account for the relative cost of such reinitialisation, we need to quantify the total number of excitons absorbed in a given time. Let us fix the time at which reinitialisation is performed to the natural lifetime of the E2LS, $\Gamma_{\text{loss}}^{-1}$. Integrating the trapping rate $I_{\text{trap}}(t)$ over one lifetime and subtracting the reinitialisation cost gives a fair measure of the number of excitons the system has absorbed within the given time. We can then consider the extreme limits of the reinitialization cost, from simply replacing a single lost exciton, to having to replace all of the $N/2$ excitons that make up the superabsorbing state. A larger system requires more frequent reinitialisations, since its loss rate is also enhanced by the system size. However, the bias in favour of absorption created by the environmental control is sufficient to ensure this does not negate the superabsorption process. Fig. 3.8 shows how the number of excitons absorbed in a given time scales with the number of atoms, and for all cost models we find a superlinear scaling.

3.5 Experimental Realisations

3.5.1 System

In this section we consider the parameters for various physical systems that could potentially demonstrate the superabsorption effect. In Table I we summarise key materials parameters for this system. Note that we use wavelength rather than frequency to characterise the good and bad transitions here, since these are more often quoted; $\omega = 2\pi c/n\lambda$, with n the material refractive index.

Quantum dots are a good candidate for their large transition dipole moments, continually improving spectral uniformity (low σ) and the recent progress in synthesising

Type	E (eV)	γ^{-1} (ns)	d (D)	r_{ij} (nm)	Ω (eV)	σ (meV)	$\delta\lambda$ (nm)
Quantum Dot (Förster)	1-2	$0.1-1$	20-100	10-50	0.001	$\lesssim 10$	< 1
Molecular Ring (B850)	1-2	1	5	$\lesssim 1$	0.05	$\lesssim 20$	~ 10
J-aggregate	2-3	$0.05-1$	10-15	$\lesssim 1$	0.1-0.2	$5-50$	~ 45

Table 3.1: Materials parameters comparison: Order of magnitude estimates of the relevant parameters for the superabsorption effect for different systems.

Type	λ	$\Delta\lambda$	Q	P_F^t	P_F^e	Γ^*_{absorb}	Γ^*_{loss}
Optical Microcavity [67]	637	$\lesssim 0.1$	10^4	70	20	P_F	~ 1
Photonic Crystal Cavity [8, 238, 78, 144, 249]	$900-1500$	$\lesssim 0.05$	10^3-10^6	10^2-10^4	$5-147$	P_F	~ 1
Photonic Bandgap Crystals [187, 261, 153, 88]	$400-1500$	n/a	n/a	n/a	n/a	~ 1	$0.01-0.1$
Concentrated filtered sunlight [71]	~ 650	~ 5	n/a	n/a	n/a	$\sim 10^4$	~ 1

Table 3.2: Materials parameters comparison for proposed control mechanisms. Where λ and $\Delta\lambda$ are the wavelength and linewidth in nm, Γ^*_{absorb} and Γ^*_{loss} are the enhancement or suppression relative to the respective rate in the absence of a cavity or photonic band gap environment, P_F^t is the theoretical Purcell factor defined in Eq. (3.63) and P_F^e is the current experimentally observed value.

highly ordered rings and arrays [55]. The main challenge facing this implementation is the relatively weak dipole-dipole interactions (Ω) that have thus far been observed (≈ 0.01 meV), although an order of magnitude improvement in this should be easily obtainable [247]. Furthermore, the interaction need not be of the field-induced character we focus on, chosen largely for the sake of simplicity. Any physical mechanism leading to an exciton number dependent shift of the Dicke states would suffice. For instance, in quantum dots the Coulomb interaction is known to be stronger (~ 10 meV) [155]. In general, engineering the strength and the scalability of dot to dot interactions is a key focus for the field, particularly for implementations of quantum information processing tasks. Progress in this area therefore seems very likely in the near future.

Molecular rings have the obvious advantage of possessing the required symmetry and the very close separation between sites, leading to large Ω. The values in the table correspond to the natural photosynthetic ring structure B850. It should be noted that lower disorder would be expected from artificially synthesised rings lacking the protein manifold found in natural systems. Furthermore, the dipole alignment of B850 (in plane) is least favourable for interactions with the field (B850 plays a storage and transfer role in photosynthesis) and therefore could be expected to increase by a factor of two if the dipoles were optimally oriented. Artificial porphyrin rings could alleviate both of these problems [191].

J-aggregates constitute a particularly promising candidate, having both highly delocalised excitations and very strong interactions between monomers [141]. Their interactions are sufficiently strong to overcome the typical values for disorder [11]. Collective effects such as superradiance and line narrowing have long been demonstrated in these systems. It is also possible to control geometry of J-aggregates chemically and deposit them on surfaces [138]. Integrating these structures with quantum control such as photonic bandgap crystals and optical microcavities is a new and developing area at the confluence of several fields. The objective of this effort is primarily the the study of exciton transport in photosynthesis, but at the same time, these systems provide an extremely promising platform for demonstrating superabsorption.

3.5.2 Control

We've described three different proposals for implementing the required environmental control over the system: optical cavities, photonic bandgap crystals and filtered

light. In Table 3.1 we gather the relevant material parameters from the literature, again using wavelength rather than frequency units; note that $\Delta\omega/\omega = \Delta\lambda/\lambda$.

The particular figures of merit are Γ^*_{absorb} and Γ^*_{loss}, which describe the relative suppression or enhancement of the 'good' and 'bad' transitions, respectively. In the case of cavities these are given by the Purcell factor [201], which describes enhancement of the rate of emission caused by coupling to a resonant cavity mode:

$$P_F = \frac{3}{4\pi^2}\left(\frac{\lambda_c}{n}\right)^3 \frac{Q}{V_m} \,, \tag{3.63}$$

where λ_c is the wavelength of the cavity, n is its refractive index, $Q = \omega_c/\Delta\omega$ its quality factor, and V_m its mode volume. For the results in the earlier in this section we allowed either a tenfold enhancement or suppression of Γ_{absorb} or Γ_{loss}, respectively. Table 3.1 shows that current experimental systems can easily surpass these requirements, assuming a typical separation of $\lambda_{\text{good}} - \lambda_{\text{bad}} > 10$ nm. Crucially, the structures listed here also remain large enough to accommodate our proposed absorber. For instance, a molecular ring with $N = 15$ would have a diameter of only ~ 5 nm. It is interesting to note that 2D and 3D photonic crystal cavities offer both enhancement of a resonant transition Γ_{absorb} and suppression of a non-resonant one Γ_{loss} [78], making them ideal for the type of control required.

3.5.3 Trapping

The trapping process is key for the application of superabsorption to light harvesting. Here the requirement is that the extraction process is fast enough to beat the rival emission process Γ_{emit}, which itself may be enhanced. Researchers concerned with creating new paradigms for solar cells by connecting quantum dots and J-aggregates (with their favourable and flexible absorption properties) to nanowires and bulk semiconductor have already been successful in realising fast and irreversible exciton extraction [157, 156]. The primary mechanism used for this purpose is Förster transfer, which is well known in both natural molecular structures like photosynthetic antennae and also artificial systems such as quantum dots. Förster transfer causes extremely fast exciton transitions (fs-ps) between monomers separated by nanometer distances. This mechanism for exciton extraction has been studied both theoretically and verified experimentally. Encouragingly, it has been shown to be capable of exceeding the reemission rate by up to three orders of magnitude [7, 72].

3.6 Imperfections

Any real physical system used to demonstrate superabsorption, or indeed superradiance, will have imperfections such as slightly varying frequencies for each atom, or a deviation away from perfect ring symmetry. In essence all such imperfections in superradiance are alike; they diminish the collective effect because they lead to the emission of distinguishable photons. It might therefore be a concern that these collective effects could only be realised in the ideal case. However, superradiant effects of molecular aggregates with a spatial extent smaller than the wavelength of light are known to possess a certain degree of robustness against inhomogenous broadening [237], dephasing processes [98], and exciton phonon coupling [236]. This is because the increased transition rates produced by superradiance serve to counterbalance the effect of disorder: the faster rate broadens the natural linewidth of the transitions, effectively masking the distinguishably introduced by the disorder. Intuitively, we expect a superabsorption advantage to be achievable whenever an imperfect system is still capable of displaying superradiant behaviour (of course with the additional requirement that the energy shifts of adjacent decay process are resolvable). In this section we model realistic imperfections by considering static energy disorder and show that superabsorption can still be realised in the presence of disorder.

In this Section we shall verify the analytical results of the previous sections using numerical approaches. As a first step, we investigate the validity of the master equation framework described previously. This is achieved with a Monte Carlo approach which allows the system to explore the entire Dicke ladder. In order to study disorder in the system Hamiltonian, we also present results from a completely independent model, which only builds on the physical Hamiltonian and makes no assumptions about the Dicke model being a good description of the system.

3.6.1 Monte Carlo

The Effective Two Level System (E2LS) model allowed us to reduce the complexity of the problem dramatically and made it analytically tractable. In order to verify this approach we here compare it to an independent numerical model: Figure 3.9 shows excellent agreement between the E2LS model and Monte Carlo simulations of the master equation (3.44) using QuTip [134]. Monte Carlo simulations of quantum systems use a time/memory tradeoff to allow large systems to be simulated. They do this by only storing and propagating the state vector rather than the entire density matrix, by averaging over many trajectories the results converge toward the dynamics

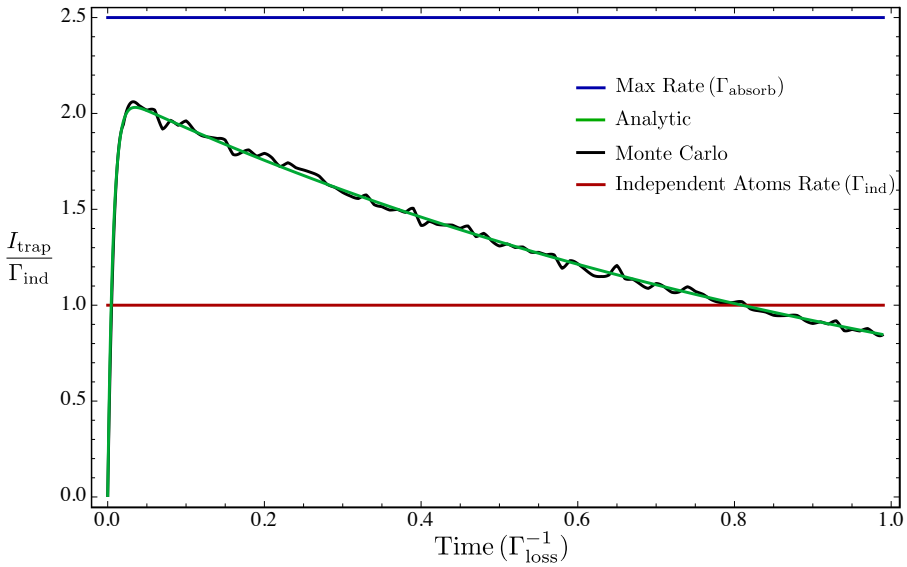

Figure 3.9: Numerical verification of the Effective Two Level System (E2LS). Comparison of the E2LS model with numerical results from Monte Carlo simulations done using the Quantum Optics Toolbox in Python (QuTip) [134]. Parameters: $N = 8$, $N(\omega_{\text{good}}) = 10$, $\Gamma_T = 10\,\Gamma_E$,$\gamma = 1$, trajectories 100,000.

that would have been obtained by numerical integrating the master equation as in the previous section. The numerical model uses a phenomenological trapping. The agreement with the E2LS can be made arbitrarily close with increasing numbers of trajectories. The same agreement was also seen for systems with larger numbers of atoms.

3.6.2 Numerical integration of Master Equation

We proceed by exploring the effect of disorder on both superradiance and superabsorption. To capture these effects we must use a more general, but less analytically informative approach to deriving the master equation than the one presented previously.

Starting with the implicit interaction model, we now allow the site energies to vary. We aim to simulate the effect of static energy disorder, which – to some extent – will be present in all physical implementations of superabsorption. To do this we draw the site frequencies ω_m from a Gaussian distribution with a mean given by the atomic frequency ω_A and a standard deviation given by σ. The system Hamiltonian is:

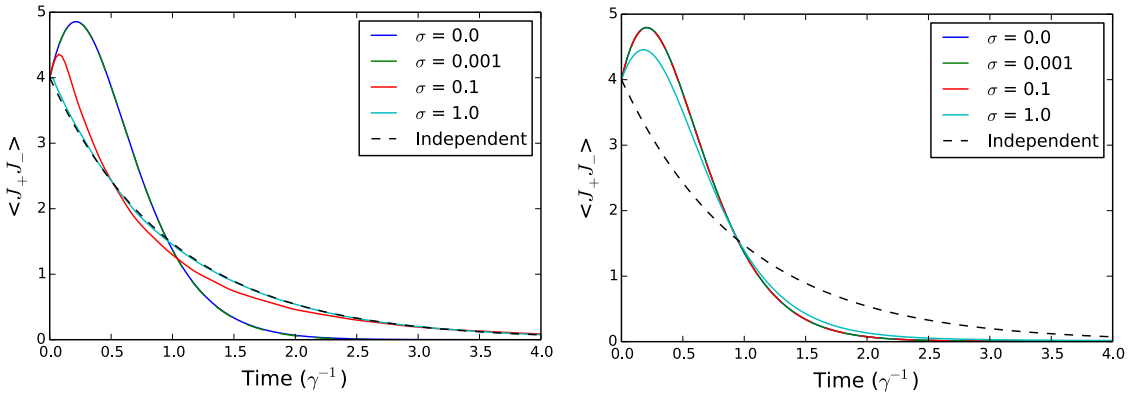

Figure 3.10: Disorder and Superadiance **Left:** The effect of increasing disorder (modelled as a Gaussian distribution with standard deviation σ) on a superradiant system without interactions ($\Omega = 0$). **Right:** The effect of increasing disorder (σ) on a superradiant system with hopping interaction strength $\Omega = -1$. Shared parameters: $\omega_A = 10, d = 1, \gamma = 0.01, N = 4$. Without interactions, the relevant energy scale characterising the transition from collective to independent emission is given by σ/γ. By contrast, when interactions are included the system eigenstates are intrinsically delocalised and the relevant energy scale becomes σ/Ω, leading to a significant increase in robustness against disorder.

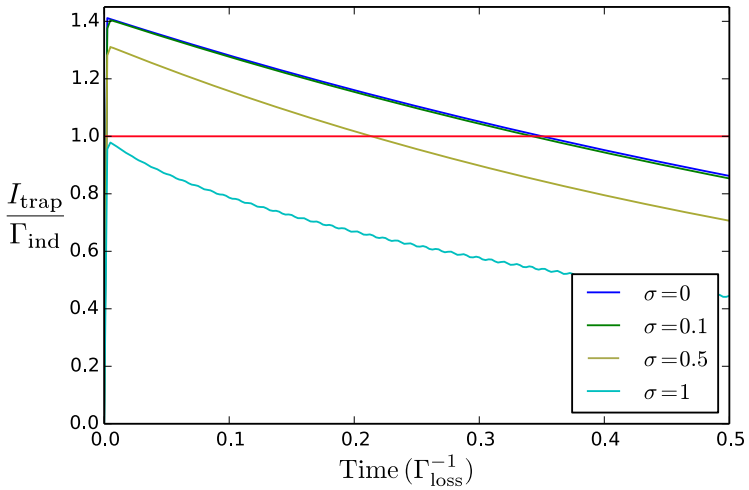

Figure 3.11: This figure shows that modest amounts of disorder will not significantly the superabsorption effect. Parameters: $\omega_A = 10$, d=1, $\gamma = 0.01$, N=4, $N(\omega_{\text{good}}) = 1$, $\kappa(\omega_{\text{bad}}) = 0.1\gamma$.

$$\hat{H}_S = \sum_{m=1}^{N} \omega_m \hat{\sigma}_+^m \hat{\sigma}_-^m + \Omega \sum_{i,j}^{N} (\hat{\sigma}_+^i \hat{\sigma}_-^j + \hat{\sigma}_-^j \hat{\sigma}_+^i) \,. \tag{3.64}$$

If the full trap model is to be used the extra terms are added. The Hamiltonian is then diagonalised numerically and the eigenoperators determined which project the dipole operator on the eigenspace of $\hat{H}_S$:

$$\hat{A}(\omega) = \sum_{e,e'} \delta(\omega = e - e') |e\rangle\langle e| (\hat{J}_- + \hat{J}_+) |e'\rangle\langle e'| \,, \tag{3.65}$$

where $|e\rangle\langle e|$ is a projector onto the a given eigenstate of the Hamiltonian (3.45). $\hat{A}_\alpha(\omega)$ is therefore an eigenoperator of $\hat{H}_S$, which causes a transition between two eigenstates of $\hat{H}_S$ sampling the environment at frequency ω. We construct the new master equation analogously to Eq. (3.13):

$$\frac{d}{dt}\tilde{\rho}_{\mathcal{S}}(t) = -i \int_0^\infty dt' \mathrm{Tr}_{\mathcal{E}}[\tilde{H}_I(t), [\tilde{H}_I(t-t'), \tilde{\rho}_{\mathcal{S}}(t) \otimes \tilde{\rho}_{\mathcal{E}}] \,, \tag{3.66}$$

and the standard procedure [25] straightforwardly yields

$$\frac{d}{dt}\rho_S(t) = \sum_{\omega,\omega'} \sum_{\alpha,\beta} e^{i(\omega-\omega')t} \Gamma_{\alpha,\beta}(\omega) (\hat{A}_\beta(\omega)\rho_S(t)\hat{A}_\alpha^\dagger(\omega') - \hat{A}_\alpha^\dagger(\omega')\hat{A}_\beta(\omega)\rho_S(t)) + \text{h.c.} \,. \tag{3.67}$$

Equation (3.67) could directly be solved numerically, but this is extremely computationally expensive even for small disordered systems, due the pathological scaling in the number of terms arising from the summation over ω, ω', α and β. To overcome this difficulty, (3.67) is traditionally simplified using the rotating wave approximation (RWA). This means neglecting the non-secular terms (where $\omega \neq \omega'$), leading to the canonical 'quantum optical master equation':

$$\frac{d}{dt}\rho_S(t) = \sum_{\omega} \sum_{\alpha,\beta} \Gamma_{\alpha,\beta}(\omega) (\hat{A}_\beta(\omega)\rho_S(t)\hat{A}_\alpha^\dagger(\omega) - \hat{A}_\alpha^\dagger(\omega)\hat{A}_\beta(\omega)\rho_S(t)) + \text{h.c.} \,. \tag{3.68}$$

In the case of ordinary superradiance, with no dipole-dipole interaction and consequent shifts, this step is unproblematic because there is in fact only one transition frequency (ω_A). However, for all other cases, care must be taken to apply the approximation selectively only where it is strictly justified. The RWA assumes that the fast oscillating terms $e^{i(\omega-\omega')t}$ effectively average to out to zero over the timescale relevant to the system dynamics τ_R. The fastest system dynamics timescale is given by the reciprocal of the lowest non-zero transition frequency ω_{min}^{-1}. However, there is

some subtlety to applying the RWA to collective transitions in disordered systems: Neglecting all non-secular terms instantly imposes the independent exponential decay type behaviour on the system. Applying no restriction is extremely computationally expensive, given that disorder calculation must be repeated many times and averaged to produce meaningful results. Removing too many non-secular terms causes an overestimation of the debilitating effect of disorder on the system: the dynamics to abruptly change from collective to independent behaviour with even the smallest amount of disorder. This is true of the commonly used order of magnitude separation between τ_R and ω_{min}^{-1}. Instead the criterion should made steadily more stringent until convergence is attained. By retaining these terms our model can smoothly interpolate between the limits of collective behaviour (superradiance/superabsorption) and independent exponential decay, which must emerge for strongly disordered systems. The resulting equation is then integrated numerically using the QuTip package [134]. The numerical calculation is then repeated many times in order to obtain the an ensemble average over different instances of disorder and smooth out the random oscillations introduced by any given instance.

Fig. 3.10 shows the effect of disorder on superradiance. As expected both plots show a certain robustness to disorder. This is because the increased transition rates produced by superradiance serve to counterbalance the effect of disorder: the faster rate broadens the natural linewidth of the transitions, effectively removing the distinguishability of atoms introduced by the disorder. The model with dipole-dipole interactions shows greater robustness, as might be expected because its eigenstates are intrinsically delocalised, whereas with no interactions there is less of a barrier to the localisation introduced by σ. Fig. 3.11 shows the effect of disorder on superabsorption. As expected from the argument above superabsorption also shows excellent robustness to disorder. It is slightly less robust than superradiance, because it relies on the Dicke ladder shifts not being too heavily altered by the level of static disorder characterised by σ. The ratio of static disorder to interaction strength needed for superabsorption, is well met by current experimental systems..

3.7 Discussion

We have shown that the absorptive analogue of quantum superradiance can be engineered in structures with suitably symmetric interactions. We have provided an intuitive explanation of this many-body light-matter effect by introducing an effective two-level system. Despite its simplicity this analytic model can provide highly

accurate predictions, as we have validated through the extensive exact numerical calculations. As we have already discussed, absorbing light beyond the limits of classical physics raises prospects for at least two new types of technology, and such superabsorption could be realised in a broad range of candidate systems.

The foremost application of the phenomenon may be in the context of optical or microwave sensors, either in future cameras or for scientific instruments. In addition to the obvious merits of being sensitive to low light levels, the frequency specificity of the superabsorber may be a desirable attribute. The small size of the ring structure and collective 'antenna array' could lead to high spatial and angular resolution, and the fact that the superabsorber is (re)initialised into its fully receptive state by an excitation pulse allows detection events to be confined into a narrowly defined time window. Note that for sensing applications the cost of (re)initialisation is likely unimportant, and a trapping mechanism is not required if the number of excitons in the system can be monitored differently, e.g. with a quantum point contact.

Light harvesting technologies represent another potential application, and indeed our Fig. 3.8 indicates that one can obtain a net increase in the number of exctions absorbed compared to conventional systems even allowing for the energy cost of sustaining the superabsorbing state. The technique would be particularly suited to wireless power transfer using narrowband light, e.g. for remote sensor or biologically implanted devices, where wired electrical power is impractical. For solar light harvesting a given superabsorber can only achieve optimal performance for a specific frequency range; however, one could engineer a range of different systems to jointly cover the solar spectrum.

There are multiple candidate systems for engineering the above applications. Molecular rings have the advantage of featuring a natural symmetry and intrinsically low levels of disorder. Taking $\Omega = 350$ cm^{-1} as appropriate for a B850 ring [251] with eight atoms produces transition wavelength shifts exceeding 6 nm, and a wavelength selectivity on the scale of nanometers is readily available with current laser and cavity linewidths. Of course, the dipole alignment of the B850 ring is not optimised for this purpose. However, complex ring structures can be designed and synthesised artificially (for example, porphyrin rings [191]) and this route should enable far superior properties. Self-assembly into much larger molecular J or H aggregates with established superradiant properties [174, 138] may provide further opportunities. Alternatively, superradiance, long-range interactions, and optical control have been demonstrated in quantum dots [218, 247], and there has been recent progress in synthesising ring like clusters with high spectral and spatial order [55]. Further,

suppression of the local density of optical states by two orders of magnitude at specific frequencies has been demonstrated in an appropriate semiconductor photonic crystal environment [261]. For typical parameters of those systems that would be consistent with the requirements for superabsorption.

To demonstrate the effect of superabsorption (i.e. sustained confinement into an E2LS with enhanced absorption and emission rates) as an instance of an engineered physical phenomenon, several additional possibilities present themselves. For example, circuit QED experiments possess long coherence times and have already demonstrated sub- and superradiant effects [83, 82] as well as tuneable cross Lamb shifts [148], and recent 3D structures [192] provide further flexibility. Bose Einstein Condensates offer similar properties but with much larger numbers of atoms [53, 180]. Dissipative Dicke model studies with nonlinear atom-photon interaction can enable a steady-state at the mid-point of the Dicke ladder ($M = 0$) [61, 102], which may provide a route to self-initialising superabsorbing systems.

CHAPTER 4

Enhanced Absorption Using Ratchet States

4.1 Summary

In the previous chapter we introduced one method of enhancing light absorption: by using a collective effect increase the matrix elements of optical transitions. In this chapter we will discuss an alternative approach that is instead based on the idea of removing a fundamental source of inefficiency: radiative recombination. Once again we take inspiration from the ring structures found in natural light harvesters. There is evidence that photosynthetic ring structures use a process of excitation followed by very rapid transfer into a long lived 'dark state', from which energy is then extracted [101]. In this chapter we develop a theoretical model of this process. In doing so we find that ring structures exhibit dark state protection, but instead of having fully dark states, they have what we term 'ratchet' states: excited states that can absorb light, but do not emit it. An absorber using a dark state has the disadvantage that any time spent in the dark state is dead time with respect to absorbing more photons. Thus if two photons arrive in quick succession the second will be lost. We generalise the previous studies of dark state protection from in dimers [56] to many sites and in so doing realise the potential advantages of these ratchet states to enhance current and power produced by a ring photocell. Of course the collective enhancement effects detailed in the previous chapter will still be present and integrating the two, would result in a quantum absorber effective at both low and high light intensity. The transfer into ratchet states is a decoherence assisted process, where naturally present dephasing and dissipation caused by a wider environment enhance the efficiency of the absorber. Our work therefore fits into a growing area of quantum technologies research, which uses biologically inspired designs and also harness decoherence to positive effect. We show that enhancements upwards of 200% in current and power

are possible for ring photocells under ambient conditions. Further enhancements may be possible in more exotic parameter regimes.

4.2 Introduction

Efficient absorption of energy for light is critical to both natural processes like photosynthesis as well as artificial technologies like photovoltaics. The revelation of quantum effects in photosynthesis, spurred research into biologically inspired systems, making use of proposed natural phenomena to enhance artificial photovoltaics [17]. There is also long standing research into alternative solar cell paradigms, which more closely mimic Nature's antenna and exciton transport model rarther than the p-n junctions at the heart of conventional solar cells [156].

As we discussed in Section 1.3 there are many causes for inefficiency in such processes, but few are as fundamental and apparently insurmountable as loss via radiative recombination. This is because any absorption process must have a companion emission process, which allows excitons to leave the absorber without producing useful work. The inherent inefficiency produced by such a process is referred to as 'detailed balance' and is makes a key contribution to the famous Shockley-Quiesser Limit [234] on the efficiency of solar cells. Pioneering work by Scully [227] showed that it is possible to break detailed balance by blocking reemission using the inverse phenomenon of lasing without inversion. This approach requires an external driving field to create coherence in the system. Although it can be shown that the enhancement persists once the energy of creating this field is accounted for [70], the requirement is clearly undesirable. It has been suggested that the same effect could be mediated by a Fano interference produced by coupling to an incoherent bath rather than a coherent field [71], but the validity of this has been questioned [56].

An alternative approach, which dispenses with this requirement, is to block remission via a transition into an optical dark state [56]. Since molecular dark state can have a lower energy than the bright state, a passive decay process will drive these transitions without the need for externally created coherence. Furthermore, the energy separation between these states in molecular systems is very low in comparison to the exciton energy. Thus dissipation can mediate transfer into states that do not decay, without much loss in total energy. This was demonstrated theoretically to create enhanced current and power output from such photocells [56]. However, dark states have the disadvantage that any time spent in them is 'dead time' with respect to absorbing further photons. The arrival times of photons at the absorber

are governed by a Poisson distribution. This means that even at low light intensity there will always be some incident photons lost due to near simultaneous arrival.

It is therefore important to minimise the amount of time spent in such a state. However, in natural light harvesters and organic semiconductor the time needed to extract the exciton and turn it into useful energy is often orders of magnitude slower than the optical processes [16]. This means loosing many more incident photons if the light is intense. This is particularly problematic if the incident sunlight is concentrated using optics prior to exposure to the photocell [268]. Both Refs. [56] and [227] make use of highly concentrated light ($n(\omega_A) = 60,000$ relative to ambient sunlight ($n(\omega_A) \approx 0.03$) for $\omega_A = 1.8$ eV) although this is not required in the later case as the effect is not dependent on the absolute magnitude of the photon transition rates. The ratchet states approach thus offers two regimes of enhancement: for low intensity light the suppression of reemission, and for high intensity light the ability of these states to further absorb.

4.3 Model

4.3.1 System

Our system consists of a ring of sites connected via a dipole-dipole hopping interaction. The Hamiltonian is given by (with a periodic boundary condition ($\sigma_{N+1} = \sigma_1$):

$$H_S = \epsilon \sum_{i=1}^{N} \sigma_i^+ \sigma_i^- + S \sum_{i=1}^{N} (\sigma_i^+ \sigma_{i+1}^- + \sigma_{i+1}^+ \sigma_i^-)\,, \tag{4.1}$$

where ϵ is the site energy splitting and S is the hopping strength. The Hamiltonian of a chain with free ends can be diagonalised by the successive application of the Jordan-Wigner and Fourier transforms. The Jordan-Wigner transform maps the Paul spin system on to a 'hard-core' boson model [137]. This gives the feature that collective excitons behave bosonicly, but maintains the exclusion principle that forbids double excitation of a single site. The transformation is defined by:

$$c_l^\dagger = \sigma_l^+ e^{i\pi \sum_{j=1}^{l-1} \sigma_j^\dagger \sigma_j}\,, \tag{4.2}$$

$$c_l = e^{-i\pi \sum_{j=1}^{l-1} \sigma_j^\dagger \sigma_j} \sigma_l^-. \tag{4.3}$$

Here the $e^{i\pi \sum_1^{n-1} \sigma_j^\dagger \sigma_j}$ factors are known as "strings" and are necessary to produce the anti-commutation of fermions:

$$\{c_\alpha, c_\beta^\dagger\} = \delta_{\alpha,\beta}\,, \tag{4.4}$$

$$\{c_\alpha^\dagger, c_\beta^\dagger\} = \{c_\alpha, c_\beta\} = 0 \tag{4.5}$$

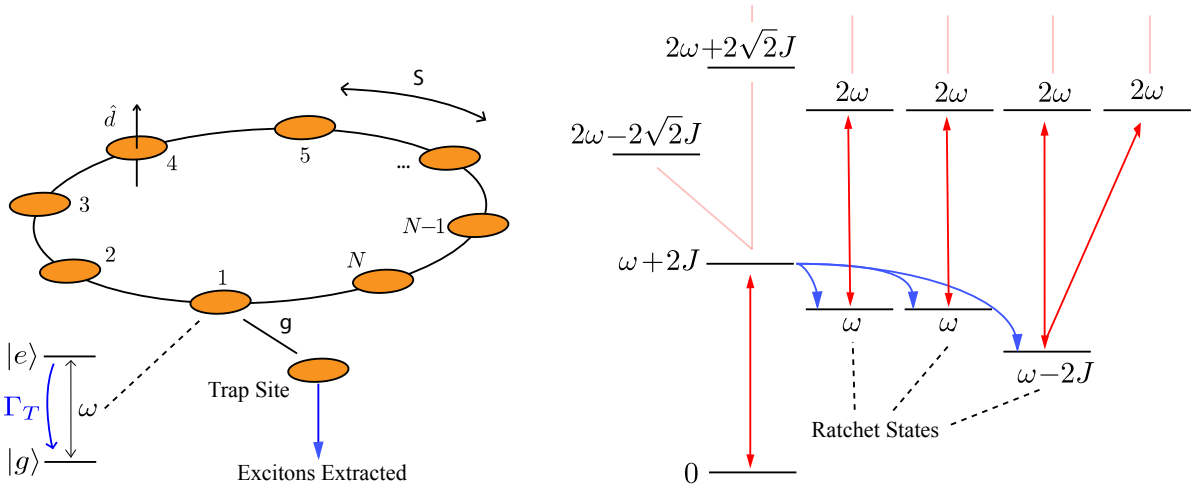

Figure 4.1: Schematic of the ring and energy level diagram with optical (red) and phononic (blue) transitions indicated. The upper half of the energy level diagram is symmetric to the lower.

The ring introduces the additional complexity of an alternating periodic or anti-periodic boundary condition. After performing the transform (4.2) the Hamiltonian is given by:

$$H_S = \omega\hat{n} - S\sum_{j=1}^{N}(c_j^\dagger c_{j+1} + c_{j+1}^\dagger c_j) + S(e^{i\pi\hat{n}}+1)(c_N^\dagger c_1 + c_1^\dagger c_N) \tag{4.6}$$

where $\hat{n} = i\sum_j^N c_j^\dagger c_j$ counts the number excitons. The final term handles the alternating boundary condition. This is an elegant form of the Hamiltonian, although it double counts for (N=2), but this is not the case that concerns us. The operator $e^{i\pi\hat{n}}$ commutes with the Hamiltonian, making the eigenvalues of $e^{i\pi\hat{n}}$ a good quantum number. The system can thus be broken into two parity subspaces of even and odd exciton number (n) and solved separately. We complete the diagonalisation using the Fourier transform:

$$c_k^\dagger = \tfrac{1}{\sqrt{N}}\textstyle\sum_{j=1}^{N} e^{ikj}c_j^\dagger \tag{4.7}$$

$$c_k = \tfrac{1}{\sqrt{N}}\textstyle\sum_{j=1}^{N} e^{-ikj}c_j\,, \tag{4.8}$$

where:

$$k_i = \tfrac{2\pi}{N}i \ (\text{n odd}) \tag{4.9}$$

$$k_i = \tfrac{\pi(2i+1)}{N} \ (\text{n even})\,. \tag{4.10}$$

The possible k values $S = \{k_i\}_{\{i=0,1,..,N-1\}}$ correspond to the single exciton states of the system. The eigenstates of the full multi-excitonic system are given by combinations of these states. The eigenstates are thus defined by sets K whose elements are k's. The size of K is equal to the number of excitons in the state ($|K| = n$). The Pauli exclusion principle manifests itself by allowing only different single exciton states to combine and form a multiple exciton state. The eigenvalues are then given by

$$\lambda_K = \sum_{k \in K} (\omega - 2S \cos k) \tag{4.11}$$

and the eigenstates

$$|\epsilon_K\rangle = c^\dagger_{K_1} ... c^\dagger_{K_n} |0\rangle \ , \tag{4.12}$$

where $|0\rangle$ is the ground state . Equation (4.12) yields an eigenstate with n excitations. Each band contains $\frac{N!}{n!(N-n)!}$ states, generated by (4.12). In its diagonalised form the Hamiltonian is given by

$$H_S = \sum_K \lambda_K \ |\epsilon_K\rangle \langle \epsilon_K| \, . \tag{4.13}$$

4.3.2 Ratchet States

We have obtained analytical expressions for the eigenvalues and eigenvectors of the system. We can now evaluate the optical properties of these states by thier matrix elements with respect to the optical transition operator:

$$\hat{J}_\pm = \sum_{i=1}^{N} \hat{\sigma}^i_\pm \, , \tag{4.14}$$

$$\Gamma_{K,K'} = |\langle \epsilon_{K'} | J_+ | \epsilon_K \rangle|^2 \, . \tag{4.15}$$

The transition optical transition rate between two arbitrary eigenstates can be derived using slater determinants [243, 236] :

$$\Gamma_{K,K'} = \left| 2^n N^{(-n+\frac{1}{2})} \delta \left(\sum_j k'_j, \sum_i k_i \right) \frac{\Pi_{i>i'} (e^{ik_i} + e^{ik_{i'}}) \Pi_{j>j'} (e^{-ik'_j} + e^{-ik'_{j'}})}{\Pi_{i=1}^{n} \Pi_{j=1}^{n+1} (1 - e^{i(k'_j - k_j)})} \right|^2 \tag{4.16}$$

where $\delta(x, y)$ is 1 if $x = y + 2\pi m$ for integer m, zero otherwise. Using equation (4.16) we can trivially compute the transfer rate between two eigenstates. The optical transitions connect eigenstates that differ by one exciton. Evaluating (4.16) for $N = 4$ reveals the first exciton band contains three states with a zero downward (emission) matrix element, but a finite upward (absorption) matrix element, see Fig. 4.1. These are the states with energy ω_A, ω_A and $\omega_A - 2S$, respectively. Each has an absorption

matrix element of $\sqrt{2}$. In general, the N-1 states below the highest energy state in the first band $\omega_A + 2S$ will be ratchet states, since the ground state can only be excited into the optical active bright state at the top of the band, none of the lower states have decay pathways back to the ground state.

4.4 Dynamics

4.4.1 Optical

As in the previous chapter we use the standard light matter interaction Hamiltonian (3.6) to describe the coupling of our ring of two level systems to a light field. The optical processes lead to a dissipator of the form:

$$D_{opt} = -\gamma \left((N(\omega_a) + 1) D[\hat{J}^-]\rho + N(\omega_a) D[\hat{J}^+]\rho \right) . \tag{4.17}$$

where $N(\omega)$ is the occupation number of the ω mode, and $D[\hat{L}]\rho$ is the Lindbladian dissipator $\hat{L}\rho\hat{L}^\dagger - \frac{1}{2}\{\hat{L}^\dagger\hat{L}, \rho\}$. This equation describes the collective optical transitions, which primarily cause interband transitions.

4.4.2 Phononic

We imagine that the system transitions into its ratchet states via coupling to a local bath of phonons:

$$\hat{H}_{s-ph} = g_{phonon} \sum_k \sum_{i=1}^{N} \hat{\sigma}_z^i (\hat{a}_k + \hat{a}_k^\dagger) \tag{4.18}$$

Clearly this type of coupling conserves the number of excitons in the system. Therefore it must only mediate transitions within the exciton bands:

$$\hat{A}_i(\omega) = \sum_{e,e'} \delta_{(\omega = e - e')} |e\rangle\langle e| \hat{\sigma}_z^i |e'\rangle\langle e'|, \tag{4.19}$$

where $|e\rangle\langle e|$ is a projector onto the a given eigenstate of the Hamiltonian, $\hat{A}_\alpha(\omega)$ is therefore an eigenoperator of $\hat{H}_S$, which causes a transition between two eigenstates of $\hat{H}_S$ sampling the environment at frequency ω. We construct the new master equation analogously to Eq. (3.13):

$$D_{pho} = \gamma_{ph} \sum_\omega \sum_{\alpha,\beta} n_{pho}(\omega) \left(\hat{A}_\beta(\omega)\rho_S(t)\hat{A}_\alpha^\dagger(\omega) - \hat{A}_\alpha^\dagger(\omega)\hat{A}_\beta(\omega)\rho_S(t) \right) + \text{h.c.} . \tag{4.20}$$

where ϵ and ϵ' are two eigenstates from the band n, $N(\omega) = (e^{\omega\beta} - 1)^{-1}$, and $\beta = (k_b T)^{-1}$. Every state in the band is coupled to every other (non-degenerate) state with a temperature dependent rate. Such a model is phenomenological, although well founded: experimentalists often ignore the existence of all but the lowest energy state in the band because all others are so rapidly damped into it. We improve on this accounting for the fully band of states and their energy and temperature dependent transition rates, however further work is needed to move towards a microscopic model of the phonon processes. Phonon relaxation processes are known to proceed far faster than optical transitions, allowing the population to move to the bottom of the band before there is time to reemit. To account for this difference in timescales we set the phonon transition rates to be several orders of magnitude higher than the optical $\gamma_{pho} = 1000\gamma$, where γ is the free atom decay rate.

4.4.3 Exciton Extraction

We have explained how absorbed excitons are transferred into ratchet states through the phonon assisted relaxation, which offer both dark state protection and subsequent absorption. In this section we detail how these absorbed excitons can be extracted to produce current. In this Section we develop two methods for exciton extraction, the first uses a simple Lindblad operator, the second expands the system to have an extra 'trap site', from which excitons are extracted. This allows us to differentiate between the enhancement effects offered by the ring structure and ratchet states alone and those effects arising purely due to the coupling to a coherent trap.

4.4.3.1 Lindblad Extraction

The Lindblad extraction mechanism offers an idealised case where population is extracted directly from a target level and only this level. As we saw in the previous chapter targeted coupling to particular states can be engineered, by the positioning of the extraction site. In the superabsorption case we wanted to extract from a symmetric state, so the trap site was placed at the centre of the ring and equally coupled to all. For the more complex anti-symmetric ratchet states it is difficult to see how such a targeted spatial coupling could be achieved. For the dimer case having a different sign on the interaction to the alternate sites gives such a coupling [56], but it is unclear how this could be generalised.

The Lindblad extraction mechanism does not have an explicit level structure, so it does not involve expanding the Hilbert space or extra unitary dynamics. Instead an

additional dissipator is used to move population from the ratchet state to the ground state:

$$D_T[\rho_S] = \gamma_T \left(\hat{L}\rho_S \hat{L}^\dagger + \frac{1}{2}\hat{L}^\dagger \hat{L}\rho_S + \frac{1}{2}\rho_S \hat{L}^\dagger \hat{L} \right) \tag{4.21}$$

where $\hat{L} = \hat{L}_{r/b}$. The level from which excitons are extracted depends on the specifics of the model. In the no dephasing / no phonons case, where $\gamma_{pho} = 0$ excitons are extracted from the first Dicke or bright state of the ring. In the general case $\gamma_{pho} \neq 0$ they are extracted from the ratchet state at the bottom of the first exciton band Fig 4.1. The extraction process is implemented as a Lindblad operator, which moves population from the relevant level to the ground state:

$$L_{\mathrm{r}} = |\mathrm{ground}\rangle\langle \mathrm{ratchet}| \ \text{ or } \ \mathrm{L_b} = |\mathrm{ground}\rangle\langle \mathrm{bright}|\,, \tag{4.22}$$

where $|\mathrm{ground}\rangle$ denotes the system ground state. Current and voltage are then calculated from the steady state population of these levels using the results of Section 4.4.4.

4.4.3.2 Coherent

Unlike in the previous chapter , in order to model the extraction of excitons from the system we couple only one of the site to an external trap site as depicted in Fig. 4.1. We couple the trap to an arbitrary site yielding the Hamiltonian:

$$\hat{H}_{\mathrm{T}} = g_{trap}(\hat{\sigma}_+^0 \hat{\sigma}_-^T + \hat{\sigma}_-^0 \hat{\sigma}_+^T) + \omega_{trap} \hat{\sigma}_+^T \hat{\sigma}_-^T\,, \tag{4.23}$$

where the superscript T denotes the trap site, g_{trap} is the strength of the coupling between the ring and the trap, and ω_{trap} is the trap's transition frequency. Excitons on the trap site under go charge separation at rate Γ_T. We model this as an irreversible decay process mediated by $\hat{L}^T = \hat{\sigma}_-^T$, which takes population from the trap excited state to its ground state. In the next section we will develop a formalism for assessing the voltage, current and power that can be extracted from such a photocell. The trap site energy ω_{trap} is made resonant with the target level for extraction. In the phonon assisted case ($\gamma_{pho} \neq 0$) the trap energy level is resonant with the lowest state in the first exciton band $\omega_A - 2S$, in the $\gamma_{pho} = 0$ case it is resonant with the bright state $\omega_A + 2S$.

Parameter	Symbol	Typical value E (eV)
Atomic transition frequency	ω_A	1.8
Hopping interaction strength	S	0.02
Trap coupling strength	g	$S/10$
Free decay rate	γ	10^{-6}
Trapping rate	γ_T	10^{-7}

Table 4.1: Table of parameters default parameters for the model [56]

4.4.4 Quantum Heat Engine

The field of quantum optics, like much of physics, has deep connections to thermodynamics. The relevance to Planck's work is very clear, but Einstein was also able to derive the spontaneous emission rate of an atom by using the thermodynamic principles a decade before Dirac arrived at the same result from a purely quantum treatment [74, 64]. In the 1960's it was first shown that treating lasers and masers as quantum heat engines allowed their maximal efficiency to be easily calculated [225, 94]. This approach has had a recent revival in the area of solar cell physics, where Quantum Heat Engine (QHE) theory is used to assess the power and efficiency of various candidate technologies [228, 56, 71].

QHE theory uses the analogy between a quantum absorber and a three or four level laser to give the expressions for current and voltage output for such a device. The current is given by the population of the trap excited state multiplied by the trapping rate:

$$I = e\Gamma_T \langle \rho_\alpha \rangle_{ss} \tag{4.24}$$

where e is the charge of an electron and Γ_T is the extraction or trapping rate and $\langle \rho_\alpha \rangle_{ss}$ is the steady state population of the trap site. The trap site is connected to a load, by passing electrons from the upper excited state to the lower ground state $|\beta\rangle$ useful work is extracted from the system. The system is thus performing a Carnot cycle between two heat baths, one the incidence solar photons and the other the local ambient bath of phonons. The voltage produced by the system is [71, 56]:

$$eV = E_\alpha - E_\beta + k_b T_a \ln\left(\frac{\langle \rho_\alpha \rangle_{ss}}{\langle \rho_\beta \rangle_{ss}}\right), \tag{4.25}$$

where E_α and E_β are the energy of the excited and ground state of the trap, k_b is the Boltzmann constant and T_a is the ambient temperature. We since we do not have direct control over the voltage, so in order to study the relationship between current

and voltage, we vary the trapping rate Γ_T. There are two limits to the behaviour of the system and sweeping Γ_T moves between them. One is the 'open circuit' regime:

$$\Gamma_T \to 0\,, \quad I \to 0\,, \quad eV \to E_{trap}\left(1 - \frac{T_A}{T_S}\right) \approx E_{trap} \tag{4.26}$$

where T_S is the temperature of the photon bath and T_A is the temperature of the phonon bath. The second is the short circuit regime:

$$\Gamma_T \to \infty\,, \quad V \to 0 \tag{4.27}$$

The power is naturally given by:

$$P = IV \tag{4.28}$$

4.5 Results

In order to evaluate the performance of the ratchet based absorber we need to find the state state of the following master equation incorporating both optical dissipator, phononic dissipator, and trap:

$$\dot{\rho}_S = -i[H_S + H_T, \rho_S] - D_{opt}[\rho_S] - D_{pho}[\rho_S] - D_T[\rho_S]\,. \tag{4.29}$$

To elucidate the effect of the ratchets we shall compare the full model (4.29) with two specific cases. One in which phonon process removed ($\gamma_{ph} = 0$). In this case the system undergoes optical transitions along the Dicke ladder of bright states discussed in the previous chapter. The other case, has the ratchet states artificially prevented from absorbing light to make them behave as fully dark states. This case shall be referred to as 'forced dark'. All the results in this section are based on calculating the steady state of the system using an iterative numerical method starting from the ground state of the system. The simulation of the system was done in QuTip [134]. These results all use the full coherent trap model and the default parameters given in Table 4.4.3.2 unless otherwise stated.

Figures 4.2, 4.3 and 4.4 demonstrate the effect of the ratchet states on the steady state exciton population of the system without trapping. The steady state population is a function of the optical T_{opt} and phononic bath temperatures T_{pho}, where T_{opt} is given in units of the solar temperature $K_S = 5800$ K. As expected the ratchet enhancement is greatest in the hot photons, cold phonons regime, where the forced dark states are unable to absorb any further light, making their steady state population

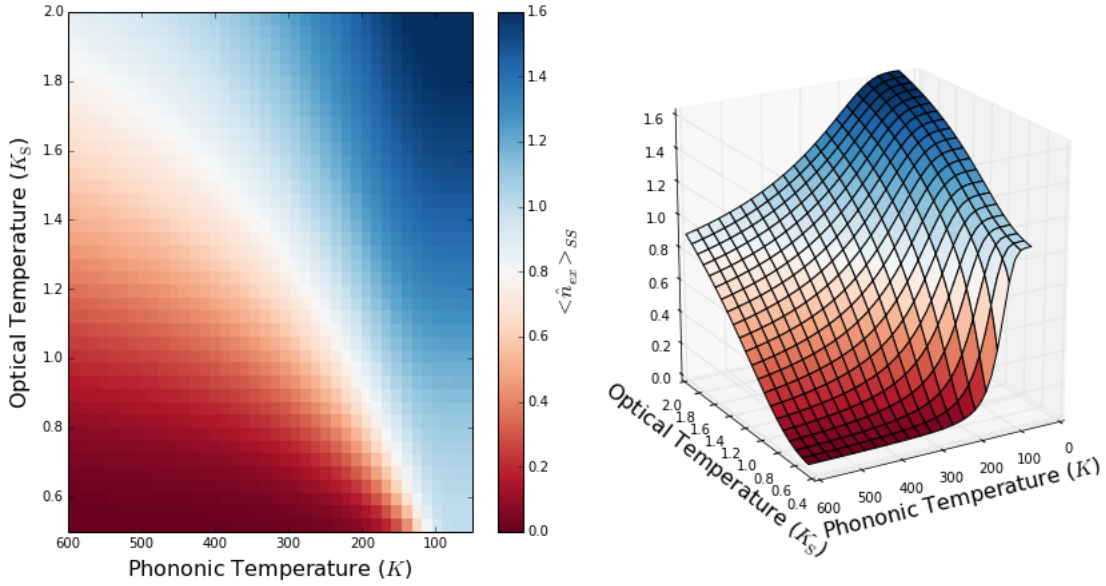

Figure 4.2: Contour and 3D plot of the steady state exciton population of ring of four sites with ratcheting. Parameters $S = 0.02$ eV and $\gamma_{pho} = 1000\gamma$.

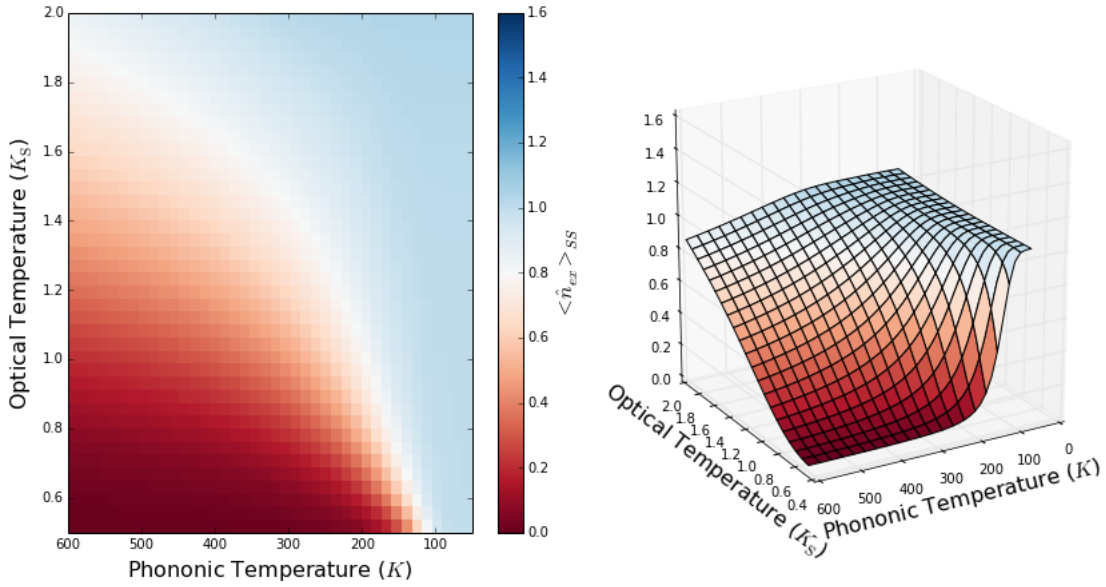

Figure 4.3: Contour and 3D plot of the steady state exciton population of ring of four sites, with forced dark states. Parameters $S = 0.02$ eV and $\gamma_{pho} = 1000\gamma$.

plateau at 1. In contrast, the ratchet states keep absorbing and the steady state population rises toward the infinite temperature limit of $\langle n_{ex} \rangle = 2$.

Figures 4.5, 4.6 and 4.7 compare the current output from the system when using the ratchet approach, to having no phonon processes. As expected the current has a similar behaviour to the steady state because of their close interdependence (4.24).

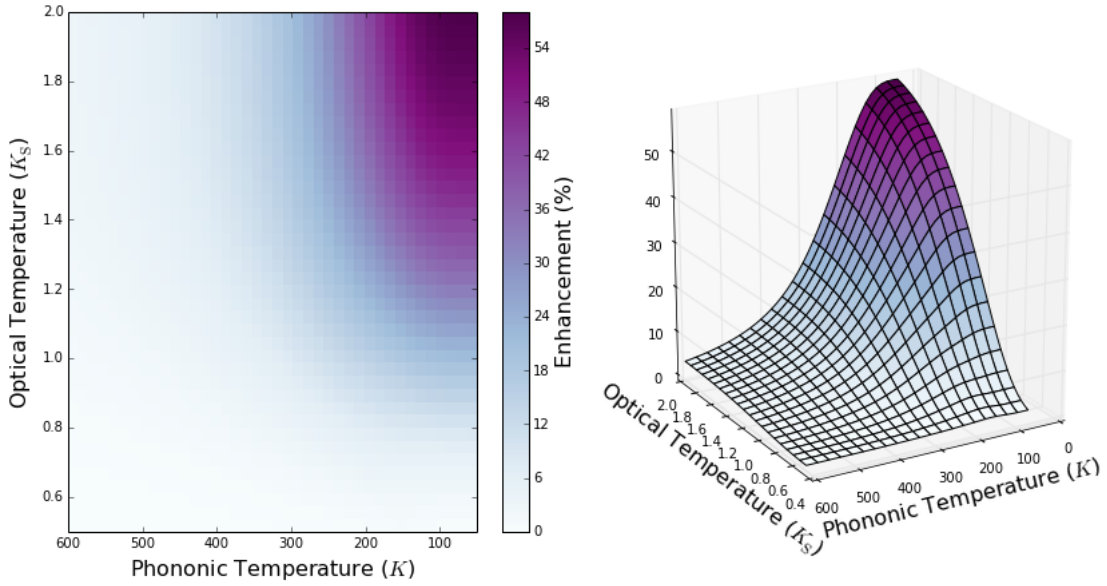

Figure 4.4: Contour and 3D plot showing the relative enhancement in steady state exciton population for ratcheting vs forced dark states. Parameters $S = 0.02$ eV and $\gamma_{pho} = 1000\gamma$.

With no phonon processes the steady state of the system with no trapping is a Boltzmann distribution across the ladder of bright states. In the presences of slow trapping the $\gamma_{pho} = 0$ results are not significantly altered and are naturally independent of the phonon temperature 4.6. Figure 4.7 shows that transitioning into ratchet states is always beneficial to absorption, at least in the relevant limit of extraction rate being a limitation $\gamma_T = \gamma/10$. The enhancement is greatest in the cold phonon regime where transitions away from the bright state, which is vulnerable to recombination, become essentially one way. The point where this transition into directional behaviour occurs depends not only on the phonon temperature, but also the strength of the hopping interaction S:

$$n_{pho}(S) = \frac{1}{e^{-S/(k_B T_{pho})} - 1}\,. \tag{4.30}$$

As S gets larger or T_A falls $n_{pho}(S) \to 0$ and the difference between the phonon emission rate $\approx \gamma_{pho}(1 + n_{pho}(S))$ and the absorption rate $\approx \gamma_{pho} n_{pho}(S)$ grows until the transitions are effectively unidirectional.

The enhancement offered by the ratchet approach is contingent on the exciton extraction rate being a limiting factor. In the case where γ_T can take any value it can simply be made high enough that any absorbed exciton will be extracted far faster than the deleterious reemission process can effect it. Figure 4.8 demonstrates

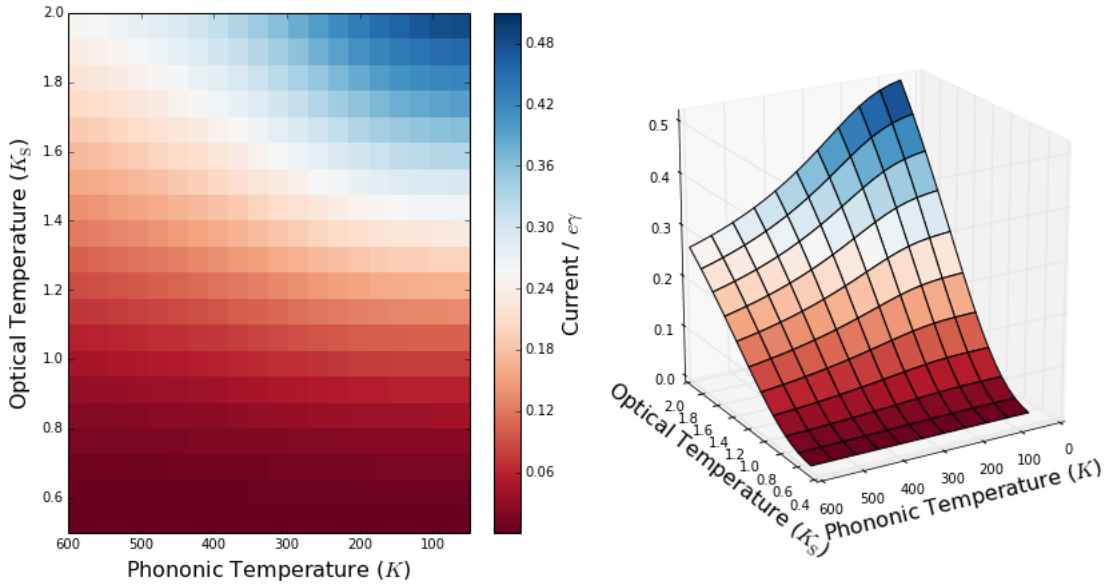

Figure 4.5: Contour and 3D plot of the current from ring of four sites with ratcheting. Parameters: $S = 0.02$ eV, $g = S/2$, $\gamma_{pho} = 1000\gamma$, coherent trap site extraction with $\gamma_T = \gamma/10$.

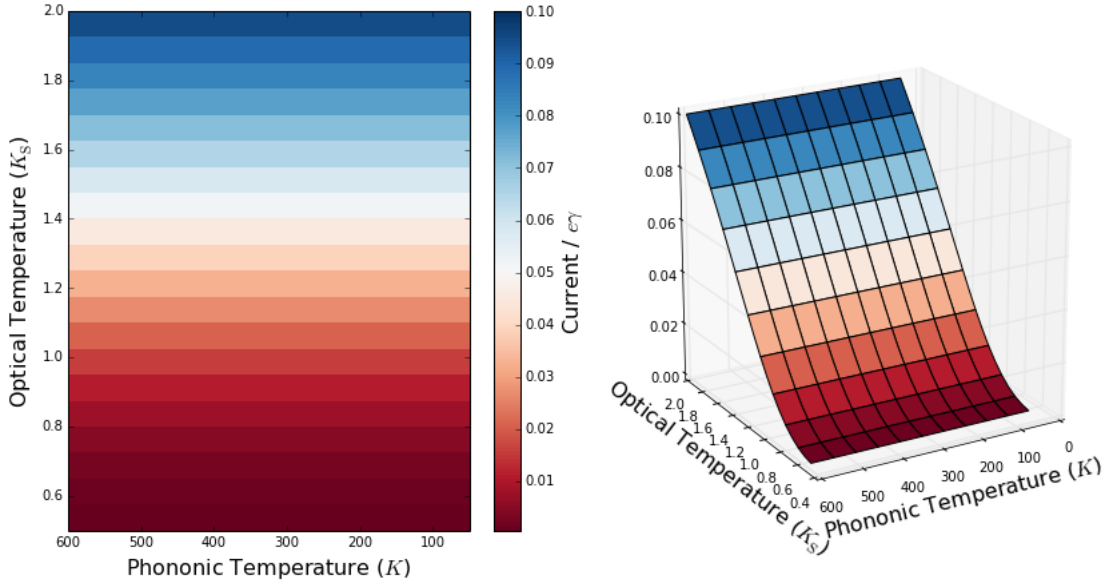

Figure 4.6: Contour and 3D plot of the current from ring of four sites with no phonon processes ($\gamma_{pho} = 0$). Parameters: $S = 0.02$ eV, $g = S/2$, coherent trap site extraction with $\gamma_T = \gamma/10$.

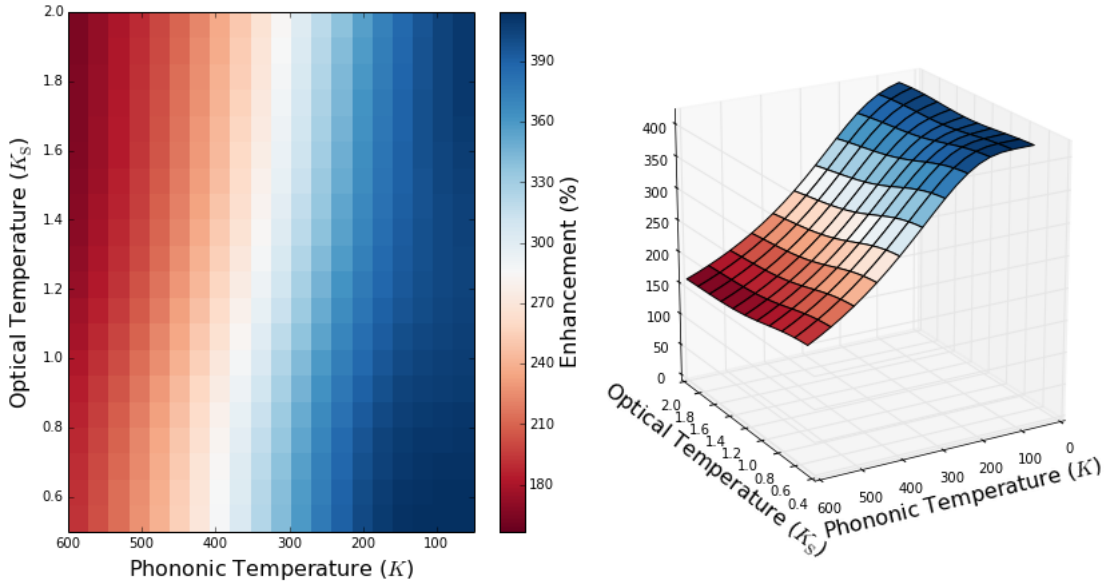

Figure 4.7: Contour and 3D plot of the relative current enhancement produced by ratchet states relative to no phonons. Parameters: $S = 0.02$ eV, $g = S/10$, coherent trap site extraction with $\gamma_T = \gamma/10$.

this effect, as γ_T is made an increasingly large fraction of the free decay rate γ, the relative enhancement offered by the phonon processes is diminished.

In figures 4.9 and 4.10 compare the power, current and voltage of Lindblad extraction with the full coherent model as a function of the hopping strength S. In figure 4.9 we use ambient conditions of room temperature phonons and unconcentrated sunlight $n(\omega_A) = 0.03$. Both the trapping models produce an increasing current and thus power, as S is increased. This is due the directional argument presented above population is channeled toward the bottom of the band. The coherent trap produces higher current than the Lindblad extraction because it can extract excitons from many different states, not only the targeted lowest band state. The difference between the two levels off as all population ends up in the target state for both models. The $\gamma_{pho} = 0$ results are unaffected by changing S, with the coherent current slightly higher, for the same reason as above. The voltages for diverge for the two different cases: this is because the trap site energy is tuned to $\omega_A - 2S$ for ratcheting and $\omega_A + 2S$ for $\gamma_{pho} = 0$. The trap energy has a major contribution to the voltage see Eqn. (4.25), hence the divergence. The power is given by the product of these two results, which yields an initial peak for the ratcheting, which is later diminished by the decreasing voltage.

Figure 4.10 is the same system, but with concentrated incident light $n(\omega_A) = 10$.

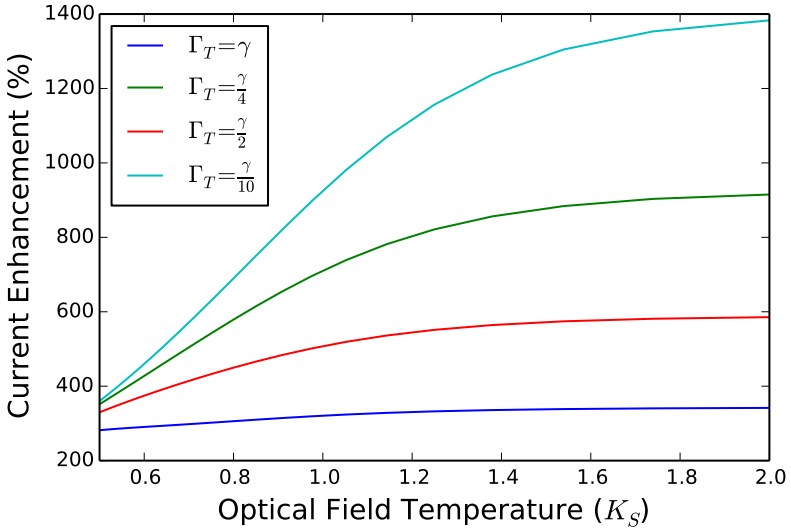

Figure 4.8: The effect of the trapping rate on the relative current enhancement for ratcheting vs. no phonons. Parameters: $S = 0.02$ eV, $g = S/2$, $T_{pho} = 300K$ and coherent trap site extraction.

Again the ratchet approach with a coherent trap offers the highest current and power. The main difference between these and the previous plots is that the ratcheting approach with Lindblad extraction is now producing less current than the $\gamma_{pho} = 0$ case. This is because the bright state has a higher population due to the increased light intensity, therefore extracting from it directly is more efficient than spreading population across the many non-bright states and extracting from only one. In any case the Lindblad approach is intended only as a benchmark, so its potential limitations are not a concern.

Figure 4.11 shows an IV curve for the the ratchet states approach compared to $\gamma_{pho} = 0$ case. The voltage defined in Equation (4.25) can not be varied directly; the IV curve is generated by using a range of different trapping rates γ_T, which produce a different ratio of level population. As we have discussed earlier if the trapping rate takes very large values there is no difference between the ratcheting and the no phonon approach. This is not the case that interests us, we therefore have to introduce an extra rate limiting step, which we call the transfer to trap rate γ_{T-T}. This is the rate at which population is incoherently moved from the ring to an uncoupled external trap site, using a Lindblad operator. The transfer to trap time does not need to be particularly restrictive, in fact the value used is 100 times the spontaneous emission rate. However, an extra process of some kind is needed to prevent the extraction rate completely saturating the rate of photon absorption. As

expected the ratcheting approach attains higher current maximum current, due to the avoidance of reemission. However the higher energy of the trap site in the $\gamma_{pho} = 0$ case allows it to draw current at higher voltages. Despite this the ratchet approach yields a higher maximum power output, because the higher current outweighs the the lower maximum voltage.

The IV curve for the coherent trap case is not presented, because in order to span a meaningful range of V the trapping rate must be made many orders of magnitude higher than any other rate in the system. This removes the trap's energy selectivity and renders the model questionable. In any case, the limit of large trapping is not one in which we would expect the ratcheting approach to be useful.

4.6 Conclusion

In this chapter we have investigated the absorption properties of a ring of sites interacting via an exciton hopping process, such as the molecular rings that serve an antennae in photosynthesis. By coupling to a phonon bath as well as to an optical field the system dynamics explore the full Hilbert space rather than just the Dicke ladder of allowed optical transitions. These off ladder states have interesting properties, which effect the current and voltage produced when coupling the ring to a trap site. In the first exciton band these states exhibit dark state protection, but they also still absorb light, making them one way or ratchet states. This means that the phononic transitions into such states create enhancement both when the photon flux is high and when its low. When the system is limited to extraction rates slower than the photon absorption rate, it is always advantageous to make use of these states. We demonstrated that an idealised Lindblad operator extraction method is in fact less efficient than coherently coupling a single site to a trap. This goes against what one might naively expect. Instead the coherent extraction is enhanced by its coupling to many different excited states. Future work could develop a more realistic model of the phonon processes, such as incorporating an appropriate spectral density. Further study of incoherent extraction and a comparison to coherent methods is needed to elucidate the optimal method of exciton extraction from ring structures. The long term goal would be to combine the suppression of reemission using dark states with superabsorption to create an ultimate quantum absorber.

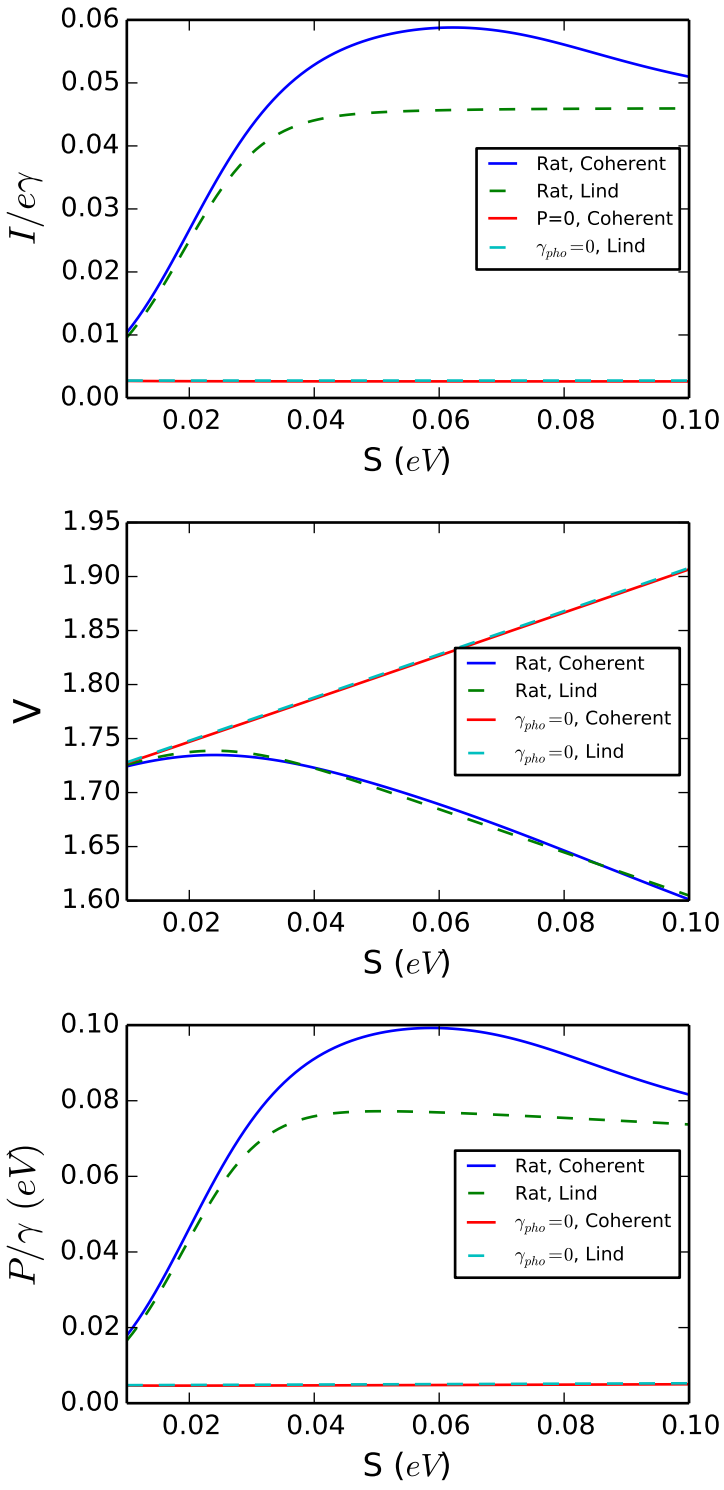

Figure 4.9: Comparison of Current, voltage and power as a function of the hopping interaction strength S for the lindblad trapping model and the coherent extraction model. Unconcentrated sunlight $n_{\omega_A} = 0.03$. Parameters: $S = 0.02$ eV, $g = S/10$, $N = 4$,$T_{pho} = 300K$, $n_{\omega_A} = 0.03$ and $\gamma_T = \gamma/10$.

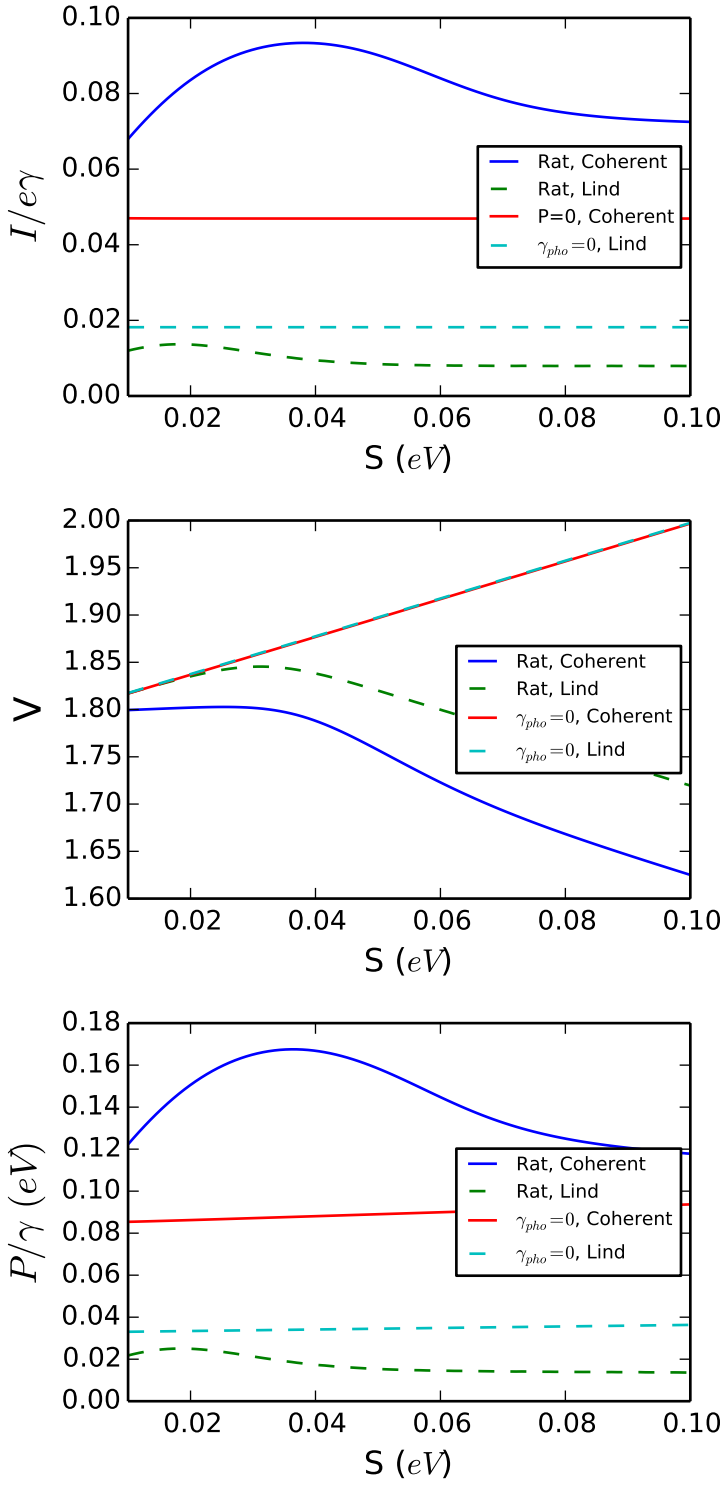

Figure 4.10: Comparison of Current, voltage and power as a function of the hopping interaction strength S for the lindblad trapping model and the coherent extraction model. Concentrated sunlight $n_{\omega_A} = 10$. Parameters: $S = 0.02$ eV, $g = S/10$, $N = 4$, $T_{pho} = 300K$ and $\gamma_T = \gamma/10$.

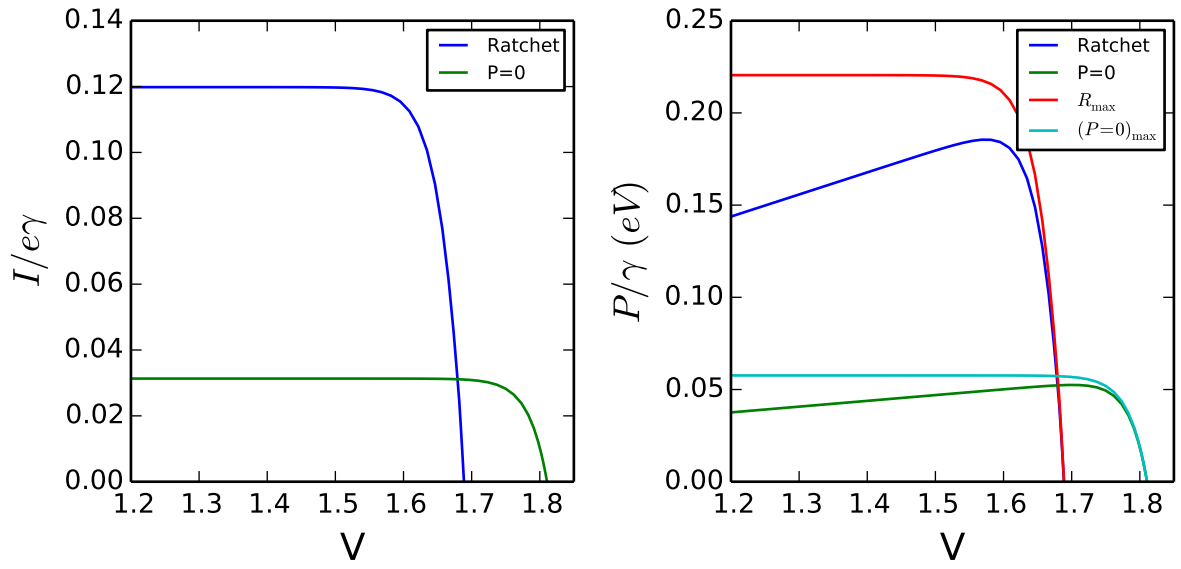

Figure 4.11: Current and power as a function of voltage for ratcheting ($\gamma_{pho} = 1000\gamma$) with Lindblad extraction. Parameters: $S = 0.02$ eV, $g = S/10$, $N = 4$, $\gamma_{T-T} = 100 n_{\omega_A}\gamma$, $T_{pho} = 300K$, $n_{\omega_A} = 0.03$ and $\gamma_T = \gamma/10$.

Bibliography

[1] D. Abbott, P. C. W. Davies, and A. K. Pati. *Quantum Aspects of Life*. Imperial College Press, 2008.

[2] I. I. Abram and R. Silbey. Energy transfer and spectral line shapes of impurities in crystals. *The Journal of Chemical Physics*, 63(6):2317–2328, 1975.

[3] L. Accardi, Y. G. Lu, and I. Volovich. *Quantum theory and its stochastic limit*. Springer Verlag, 2002.

[4] S. L. Adler and A. Bassi. Is quantum theory exact? *Science*, 325(5938):275–276, 2009.

[5] J. Adolphs and T. Renger. How proteins trigger excitation energy transfer in the fmo complex of green sulfur bacteria. *Biophysical Journal*, 91(8):2778 – 2797, 2006.

[6] G. S. Agarwal. Rotating-wave approximation and spontaneous emission. *Phys. Rev. A*, 4:1778–1781, Nov 1971.

[7] V. Agranovich, Y. N. Gartstein, and M. Litinskaya. Hybrid resonant organic–inorganic nanostructures for optoelectronic applications. *Chemical Reviews*, 111(9):5179–5214, 2011.

[8] Y. Akahane, T. Asano, B.-S. Song, and S. Noda. High-q photonic nanocavity in a two-dimensional photonic crystal. *Nature*, 425(6961):944–947, 10 2003.

[9] A. D. Armour, M. P. Blencowe, and K. C. Schwab. Entanglement and decoherence of a micromechanical resonator via coupling to a cooper-pair box. *Physical Review Letters*, 88:148301, Mar 2002.

[10] A. Auffèves, D. Gerace, S. Portolan, A. Drezet, and M. F. Santos. Few emitters in a cavity: from cooperative emission to individualization. *New Journal of Physics*, 13(9):093020, 2011.

[11] G. Bassani and V. Agranovich. *Electronic Excitations in Organic Based Nanostructures*. Thin Films and Nanostructures. Elsevier Science, 2003.

[12] J. Bell. On the einstein-podolsky-rosen paradox. *Physics*, 1:195–200, 1964.

[13] M. G. Benedict. *Super-radiance: Multiatomic coherent emission*. Taylor & Francis, 1996.

[14] B. Bhushan, editor. *Springer Handbook of Nanotechnology*. Springer, 3rd edition, 2010.

[15] R. Blankenship, J. Olson, and M. Miller. Antenna complexes from green photosynthetic bacteria. In R. Blankenship, M. Madigan, and C. Bauer, editors, *Anoxygenic Photosynthetic Bacteria*, volume 2 of *Advances in Photosynthesis and Respiration*, pages 399–435. Springer Netherlands, 2004. 10.1007/0-306-47954-0-20.

[16] R. E. Blankenship. *Molecular Mechanisms of Photosynthesis*. Blackwell Science, 1st edition, 2002.

[17] R. E. Blankenship, D. M. Tiede, J. Barber, G. W. Brudvig, G. Fleming, M. Ghirardi, M. R. Gunner, W. Junge, D. M. Kramer, A. Melis, T. A. Moore, C. C. Moser, D. G. Nocera, A. J. Nozik, D. R. Ort, W. W. Parson, R. C. Prince, and R. T. Sayre. Comparing photosynthetic and photovoltaic efficiencies and recognizing the potential for improvement. *Science*, 332(6031):805–809, 2011.

[18] K. Blum. *Density Matrix Theory and Applications*. Springer, 2nd edition, 1996.

[19] J. G. Bohnet, Z. Chen, J. M. Weiner, D. Meiser, M. J. Holland, and J. K. Thompson. A steady-state superradiant laser with less than one intracavity photon. *Nature*, 484(7392):78–81, 04 2012.

[20] P. Borri, W. Langbein, S. Schneider, U. Woggon, R. L. Sellin, D. Ouyang, and D. Bimberg. Ultralong dephasing time in ingaas quantum dots. *Physical Review Letters*, 87:157401, Sep 2001.

[21] D. Braak. Integrability of the rabi model. *Physical Review Letters*, 107:100401, Aug 2011.

[22] T. Brandes. Coherent and collective quantum optical effects in mesoscopic systems. *Physics Reports*, 408(5-6):315–474, 2005.

[23] T. Brandes and N. Lambert. Steering of a bosonic mode with a double quantum dot. *Physical Review B*, 67(12):125323, Mar 2003.

[24] H.-P. Breuer, B. Kappler, and F. Petruccione. The time-convolutionless projection operator technique in the quantum theory of dissipation and decoherence. *Annals of Physics*, 291(1):36 – 70, 2001.

[25] H. P. Breuer and F. Petruccione. *The Theory of Open Quantum Systems*. Oxford University, 2002.

[26] T. Brixner, T. Mančal, I. V. Stiopkin, and G. R. Fleming. Phase-stabilized two-dimensional electronic spectroscopy. *The Journal of chemical physics*, 121(9):4221–4236, 2004.

[27] J. C. Brookes, F. Hartoutsiou, A. P. Horsfield, and A. M. Stoneham. Could humans recognize odor by phonon assisted tunneling? *Physical Review Letters*, 98:038101, Jan 2007.

[28] M. Brunelli, S. Olivares, and M. G. A. Paris. Qubit thermometry for micromechanical resonators. *arXiv*, 03 2011.

[29] M. Brunelli, S. Olivares, M. Paternostro, and M. G. A. Paris. Qubit-assisted thermometry of a quantum harmonic oscillator. *ArXiv e-prints*, May 2012.

[30] L. Buck and R. Axel. A novel multigene family may encode odorant receptors: A molecular basis for odor recognition. *Cell*, 65(1):175 – 187, 1991.

[31] T. P. Burg, M. Godin, S. M. Knudsen, W. Shen, G. Carlson, J. S. Foster, K. Babcock, and S. R. Manalis. Weighing of biomolecules, single cells and single nanoparticles in fluid. *Nature*, 446(7139):1066–1069, 04 2007.

[32] A. Caldeira and A. Leggett. Quantum tunneling in a dissipative system. *Ann. Phys. (N.Y.)*, 149:374–456, 1983.

[33] A. O. Caldeira and A. J. Leggett. Influence of damping on quantum interference: An exactly soluble model. *Physical Review A*, 31:1059–1066, Feb 1985.

[34] T. R. Calhoun, N. S. Ginsberg, G. S. Schlau-Cohen, Y.-C. Cheng, M. Ballottari, R. Bassi, and G. R. Fleming. Quantum coherence enabled determination of the energy landscape in light-harvesting complex ii. *The Journal of Physical Chemistry B*, 113(51):16291–16295, 2011/09/28 2009.

[35] G. A. Campbell and R. Mutharasan. Use of piezoelectric-excited millimeter-sized cantilever sensors to measure albumin interaction with self-assembled monolayers of alkanethiols having different functional headgroups. *Analytical Chemistry*, 78(7):2328–2334, 2006.

[36] J. Cao. A phase-space study of bloch-redfield theory. *The Journal of Chemical Physics*, 107(8):3204–3209, 1997.

[37] V. Čápek. Generalized haken-strobl-reineker model of excitation transfer. *Zeitschrift fr Physik B Condensed Matter*, 60:101–105, 1985. 10.1007/BF01312648.

[38] H. Carmichael. *An Open Quantum Systems Approach to Quantum Optics*. Springer, 1st edition, 1993.

[39] S. Chaturvedi and F. Shibata. Time-convolutionless projection operator formalism for elimination of fast variables. applications to brownian motion. *Zeitschrift für Physik B Condensed Matter*, 35:297–308, 1979. 10.1007/BF01319852.

[40] Q.-H. Chen, C. Wang, S. He, T. Liu, and K.-L. Wang. Exact solvability of the quantum rabi model using bogoliubov operators. *Phys. Rev. A*, 86:023822, Aug 2012.

[41] Y.-C. Cheng and G. R. Fleming. Coherence quantum beats in two-dimensional electronic spectroscopy. *The Journal of Physical Chemistry A*, 112(18):4254–4260, 2011/09/28 2008.

[42] Y.-C. Cheng and G. R. Fleming. Dynamics of light harvesting in photosynthesis. *Annual Review of Physical Chemistry*, 60(1):241–262, 2009. PMID: 18999996.

[43] A. Chin, J. Prior, R. Rosenbach, F. Caycedo-Soler, S. Huelga, and M. Plenio. The role of non-equilibrium vibrational structures in electronic coherence and recoherence in pigment-protein complexes. *Nature Physics*, 9(2):113–118, 2013.

[44] A. W. Chin, A. Datta, F. Caruso, S. F. Huelga, and M. B. Plenio. Noise-assisted energy transfer in quantum networks and light-harvesting complexes. *New Journal of Physics*, 12(6), 2010.

[45] A. W. Chin, A. Datta, F. Caruso, S. F. Huelga, and M. B. Plenio. Noise-assisted energy transfer in quantum networks and light-harvesting complexes. *New Journal of Physics*, 12(6):065002, 2010.

[46] M. Cho. Coherent two-dimensional optical spectroscopy. *Chemical Reviews*, 108(4):1331–1418, 2008. PMID: 18363410.

[47] K. Chopra, P. Paulson, and V. Dutta. Thin-film solar cells: an overview. *Progress in Photovoltaics: Research and Applications*, 12(2-3):69–92, 2004.

[48] A. N. Cleland. *Foundations of Nanomechanics*. Springer, 1st edition, 2003.

[49] A. N. Cleland and M. R. Geller. Superconducting qubit storage and entanglement with nanomechanical resonators. *Physical Review Letters*, 93:070501, Aug 2004.

[50] A. N. Cleland, M. Pophristic, and I. Ferguson. Single-crystal aluminum nitride nanomechanical resonators. *Applied Physics Letters*, 79(13):2070–2072, 2001.

[51] B. Coffey and R. Friedberg. Effect of short-range coulomb interaction on cooperative spontaneous emission. *Physical Review A*, 17:1033–1048, Mar 1978.

[52] E. Collini, C. Y. Wong, K. E. Wilk, P. M. G. Curmi, P. Brumer, and G. D. Scholes. Coherently wired light-harvesting in photosynthetic marine algae at ambient temperature. *Nature*, 463(7281):644–647, 02 2010.

[53] Y. Colombe, T. Steinmetz, G. Dubois, F. Linke, D. Hunger, and J. Reichel. Strong atom-field coupling for bose-einstein condensates in an optical cavity on a chip. *Nature*, 450(7167):272–276, 11 2007.

[54] L. N. Cooper. Bound electron pairs in a degenerate fermi gas. *Physical Review*, 104:1189–1190, Nov 1956.

[55] M. Creasey, J.-H. Lee, Z. Wang, G. J. Salamo, and X. Li. Self-assembled InGaAs quantum dot clusters with controlled spatial and spectral properties. *Nano Letters*, 12(10):5169–5174, 2012.

[56] C. Creatore, M. A. Parker, S. Emmott, and A. W. Chin. Efficient biologically inspired photocell enhanced by delocalized quantum states. *Physical Review Letters*, 111:253601, Dec 2013.

[57] M. D. Crisp. Application of the displaced oscillator basis in quantum optics. *Physical Review A*, 46(7):4138–4149, Oct 1992.

[58] G. C. de Oliveira, A. R. de Almeida, I. P. de Queiros, A. M. Moraes, and C. M. A. Dantas. Alternative proposal for the generation of the displaced number state;. *Physica A: Statistical Mechanics and its Applications*, 351(2-4):251–259, 2005.

[59] A. de Vos and H. Pauwels. On the thermodynamic limit of photovoltaic energy conversion. *Applied Physics*, 25:119–125, June 1981.

[60] R. H. Dicke. Coherence in spontaneous radiation processes. *Physical Review*, 93:99–110, Jan 1954.

[61] F. Dimer, B. Estienne, A. Parkins, and H. Carmichael. Proposed realization of the dicke-model quantum phase transition in an optical cavity qed system. *Physical Review A*, 75(1):013804, 2007.

[62] L. Diósi. Non-markovian open quantum systems: Input-output fields, memory, monitoring. *Physical Review A*, 08 2011.

[63] L. Diósi and W. T. Strunz. The non-markovian stochastic schrdinger equation for open systems. *Physics Letters A*, 235(6):569 – 573, 1997.

[64] P. A. M. Dirac. The Quantum Theory of the Emission and Absorption of Radiation. *Royal Society of London Proceedings Series A*, 114:243–265, Mar. 1927.

[65] P. A. M. Dirac. *The Princples of Quantum Mechanics*. Oxford University Press, 4th edition, 1988.

[66] D. P. DiVincenzo. The physical implementation of quantum computation. *Fortschritte der Physik*, 48(9-11):771–783, 2000.

[67] P. R. Dolan, G. M. Hughes, F. Grazioso, B. R. Patton, and J. M. Smith. Femtoliter tunable optical cavity arrays. *Optics Letters*, 35(21):3556–3558, 2010.

[68] F. Dolde, H. Fedder, M. W. Doherty, T. Nobauer, F. Rempp, G. Balasubramanian, T. Wolf, F. Reinhard, L. C. L. Hollenberg, F. Jelezko, and J. Wrachtrup. Electric-field sensing using single diamond spins. *Nat Phys*, 7(6):459–463, 06 2011.

[69] H. Dong, D.-Z. Xu, J.-F. Huang, and C.-P. Sun. Coherent excitation transfer via the dark-state channel in a bionic system. *Light: Science & Applications*, 1(3):e2, 2012.

[70] K. E. Dorfman, M. B. Kim, and A. A. Svidzinsky. Increasing photocell power by quantum coherence induced by external source. *Physical Review A*, 84:053829, Nov 2011.

[71] K. E. Dorfman, D. V. Voronine, S. Mukamel, and M. O. Scully. Photosynthetic reaction center as a quantum heat engine. *Proceedings of the National Academy of Sciences*, 110(8):2746–2751, 2013.

[72] A. Dorn, D. B. Strasfeld, D. K. Harris, H.-S. Han, and M. G. Bawendi. Using nanowires to extract excitons from a nanocrystal solid. *ACS Nano*, 5(11):9028–9033, 2011.

[73] A. Einstein. The photoelectric effect. *Ann. Phys*, 17:132, 1905.

[74] A. Einstein. Strahlungs-emission und absorption nach der quantentheorie. *Deutsche Physikalische Gesellschaft*, 18:318–323, 1916.

[75] A. Einstein, B. Podolsky, and N. Rosen. Can quantum-mechanical description of physical reality be considered complete? *Physical Review*, 47:777–780, May 1935.

[76] J. Elzerman, R. Hanson, J. Greidanus, L. W. Van Beveren, S. De Franceschi, L. Vandersypen, S. Tarucha, and L. Kouwenhoven. Few-electron quantum dot circuit with integrated charge read out. *Physical Review B*, 67(16):161308, 2003.

[77] G. S. Engel, T. R. Calhoun, E. L. Read, T.-K. Ahn, T. M. Mancal, Y.-C. Cheng, R. E. Blankenship, and G. R.Fleming. Evidence for wavelike energy transfer through quantum coherence in photosynthetic systems. *Nature*, 446(7137):782–786, 04 2007.

[78] D. Englund, D. Fattal, E. Waks, G. Solomon, B. Zhang, T. Nakaoka, Y. Arakawa, Y. Yamamoto, and J. Vučković. Controlling the spontaneous emission rate of single quantum dots in a two-dimensional photonic crystal. *Physical Review Letters*, 95(1):013904, 2005.

[79] D. Farrell, Y. Takeda, K. Nishikawa, T. Nagashima, T. Motohiro, and N. Ekins-Daukes. A hot-carrier solar cell with optical energy selective contacts. *Applied Physics Letters*, 99(11):111102, 2011.

[80] R. E. Fenna and B. W. Matthews. Chlorophyll arrangement in a bacteriochlorophyll protein from chlorobium limicola. *Nature*, 258(5536):573–577, 12 1975.

[81] R. Feynman and F. V. Jr. The theory of a general quantum system interacting with a linear dissipative system. *Annals of Physics*, 281(1-2):547 – 607, 1963.

[82] S. Filipp, A. F. van Loo, M. Baur, L. Steffen, and A. Wallraff. Preparation of subradiant states using local qubit control in circuit qed. *Physical Review A*, 84:061805, Dec 2011.

[83] J. M. Fink, R. Bianchetti, M. Baur, M. Göppl, L. Steffen, S. Filipp, P. J. Leek, A. Blais, and A. Wallraff. Dressed collective qubit states and the tavis-cummings model in circuit qed. *Physical Review Letters*, 103:083601, Aug 2009.

[84] P. Forn-Díaz, J. Lisenfeld, D. Marcos, J. J. Garc'ıa-Ripoll, E. Solano, C. J. P. M. Harmans, and J. E. Mooij. Observation of the bloch-siegert shift in a qubit-oscillator system in the ultrastrong coupling regime. *Physical Review Letters*, 105:237001, Nov 2010.

[85] T. Förster. Zwischenmolekulare energiewanderung und fluoreszenz. *Annalen der Physik*, 437(1-2):55–75, 1948.

[86] M. I. Francoa, L. Turina, A. Mershinb, and E. M. C. Skoulakisa. Molecular vibration-sensing component in drosophila melanogaster olfaction. *PNAS*, 108(9):3797–3802, 2011.

[87] A. Freiberg, S. Lin, K. Timpmann, and R. E. Blankenship. Exciton dynamics in fmo bacteriochlorophyll protein at low temperatures. *The Journal of Physical Chemistry B*, 101(37):7211–7220, 1997.

[88] A. Frölich, J. Fischer, T. Zebrowski, K. Busch, and M. Wegener. Titania woodpiles with complete three-dimensional photonic bandgaps in the visible. *Advanced Materials*, 25(26):3588–3592, 2013.

[89] R. L. Fulton and M. Gouterman. Vibronic coupling. i. mathematical treatment for two electronic states. *Journal of Chemical Physics*, 35(3):1059–1071, 1961.

[90] M. R. Gallis and G. N. Fleming. Environmental and spontaneous localization. *Physical Review A*, 42:38–48, Jul 1990.

[91] C. W. Gardiner and P. Zoller. *Quantum Noise*. Springer, 2nd edition, 1999.

[92] B. M. Garraway. Nonperturbative decay of an atomic system in a cavity. *Physical Review A*, 55(3):2290–2303, Mar 1997.

[93] E. M. Gauger, E. Rieper, J. J. L. Morton, S. C. Benjamin, and V. Vedral. Sustained quantum coherence and entanglement in the avian compass. *Phys. Rev. Lett.*, 106:040503, Jan 2011.

[94] J. Geusic, E. Schulz-DuBios, and H. Scovil. Quantum equivalent of the carnot cycle. *Physical Review*, 156(2):343, 1967.

[95] F. Giraldi and F. Petruccione. Reservoir for inverse-power-law decoherence of a qubit. *Physical Review A*, 83:012107, Jan 2011.

[96] H.-S. Goan. Continuous measurements of electron tunneling through a quantum dot by a quantum point contact. *Bulletin of the American Physical Society*, 56, 2011.

[97] J. W. Goodman. Statistical optics. *New York, Wiley-Interscience, 1985, 567 p.*, 1, 1985.

[98] J. Grad, G. Hernandez, and S. Mukamel. Radiative decay and energy transfer in molecular aggregates: The role of intermolecular dephasing. *Physical Review A*, 37(10):3835, 1988.

[99] M. Grätzel. Dye-sensitized solar cells. *Journal of Photochemistry and Photobiology C: Photochemistry Reviews*, 4(2):145–153, 2003.

[100] M. A. Green, K. Emery, Y. Hishikawa, W. Warta, and E. D. Dunlop. Solar cell efficiency tables (version 44). *Progress in Photovoltaics: Research and Applications*, 22(7):701–710, 2014.

[101] B. Grimm. *Chlorophylls and bacteriochlorophylls: biochemistry, biophysics, functions and applications*, volume 25. Springer, 2007.

[102] A. L. Grimsmo and S. Parkins. Cavity-qed simulation of qubit-oscillator dynamics in the ultrastrong-coupling regime. *Physical Review A*, 87(3):033814, 2013.

[103] M. Gross and S. Haroche. Superradiance: An essay on the theory of collective spontaneous emission. *Physics Reports*, 93:301–396, Dec. 1982.

[104] L. K. Grover. A fast quantum mechanical algorithm for database search. *Proceedings, 28th Annual ACM Symposium on the Theory of Computing (STOC)*, 1996.

[105] S. A. Gurvitz. Measurements with a noninvasive detector and dephasing mechanism. *Physical Review B*, 56(23):15215, 1997.

[106] F. Haake, M. I. Kolobov, C. Fabre, E. Giacobino, and S. Reynaud. Superradiant laser. *Physical Review Letters*, 71:995–998, Aug 1993.

[107] A. Hagfeldt, G. Boschloo, L. Sun, L. Kloo, and H. Pettersson. Dye-sensitized solar cells. *Chemical reviews*, 110(11):6595–6663, 2010.

[108] C. Hägglund, M. Zäch, and B. Kasemo. Enhanced charge carrier generation in dye sensitized solar cells by nanoparticle plasmons. *Applied Physics Letters*, 92(1):013113, 2008.

[109] H. Haken and G. Strobl. An exactly solvable model for coherent and incoherent exciton motion. *Zeitschrift fr Physik A Hadrons and Nuclei*, 262:135–148, 1973. 10.1007/BF01399723.

[110] S. Hameroff and R. Penrose. Orchestrated reduction of quantum coherence in brain microtubules: A model for consciousness. *Mathematics and Computers in Simulation*, 40(3-4):453 – 480, 1996.

[111] M. C. Hanna, M. C. Beard, and A. J. Nozik. Effect of solar concentration on the thermodynamic power conversion efficiency of quantum-dot solar cells exhibiting multiple exciton generation. *The Journal of Physical Chemistry Letters*, 3(19):2857–2862, 2012.

[112] J. Hausinger and M. Grifoni. Qubit-oscillator system: An analytical treatment of the ultrastrong coupling regime. *Physical Review A*, 82(6):062320, Dec 2010.

[113] J. Hausinger and M. Grifoni. Qubit-oscillator system under ultrastrong coupling and extreme driving. *Physical Review A*, 83(3):030301, Mar 2011.

[114] D. Hayes and G. Engel. Extracting the excitonic hamiltonian of the fenna-matthews-olson complex using three-dimensional third-order electronic spectroscopy. *Biophysical journal*, 100(8):2043–2052, 04 2011.

[115] J. R. Heath and M. E. Davis. Nanotechnology and cancer. *Annual Review of Medicine*, 59(1):251–265, 2008.

[116] O. Heaviside. On the forces, stresses, and fiuxes of energy in the electromagnetic field. *Philosophical Transactions of the Royal Society of London. A*, pages 423–480, 1892.

[117] T. P. Hettinger. Olfaction is a chemical sense, not a spectral sense. *Proceedings of the National Academy of Sciences*, 108(31):E349, 2011.

[118] K. D. B. Higgins, S. C. Benjamin, T. M. Stace, G. J. Milburn, B. W. Lovett, and E. M. Gauger. Superabsorption of light via quantum engineering. *Nat Commun*, 5, 08 2014.

[119] B. Hille. *Ion Channels of Excitable Membranes,*. Sinauer Associates, 3rd edition, 2001.

[120] C. B. Honsberg, A. M. Barnett, and D. Kirkpatrick. Nanostructured solar cells for high efficiency photovoltaics. In *Photovoltaic Energy Conversion, Conference Record of the 2006 IEEE 4th World Conference on*, volume 2, pages 2565–2568. IEEE, 2006.

[121] K. Hornberger and J. E. Sipe. Collisional decoherence reexamined. *Physical Review A*, 68:012105, Jul 2003.

[122] S. Hoyer, M. Sarovar, and K. B. Whaley. Limits of quantum speedup in photosynthetic light harvesting. *New Journal of Physics*, 12(6):065041, 2010.

[123] J. D. Hybl, A. A. Ferro, and D. M. Jonas. Two-dimensional fourier transform electronic spectroscopy. *The Journal of Chemical Physics*, 115(14):6606–6622, 2001.

[124] E. K. Irish. Generalized rotating-wave approximation for arbitrarily large coupling. *Physical Review Letters*, 99:173601, Oct 2007.

[125] E. K. Irish, J. Gea-Banacloche, I. Martin, and K. C. Schwab. Dynamics of a two-level system strongly coupled to a high-frequency quantum oscillator. *Physical Review B*, 72:195410, Nov 2005.

[126] E. K. Irish and K. Schwab. Quantum measurement of a coupled nanomechanical resonator˘cooper-pair box system. *Physical Review B*, 68:155311, Oct 2003.

[127] A. Ishizaki, T. R. Calhoun, G. S. Schlau-Cohen, and G. R. Fleming. Quantum coherence and its interplay with protein environments in photosynthetic electronic energy transfer. *Phys. Chem. Chem. Phys.*, 12:7319–7337, 2010.

[128] A. Ishizaki and G. R. Fleming. On the adequacy of the redfield equation and related approaches to the study of quantum dynamics in electronic energy transfer. *The Journal of Chemical Physics*, 130(23):234110, 2009.

[129] A. Ishizaki and G. R. Fleming. Theoretical examination of quantum coherence in a photosynthetic system at physiological temperature. *Proceedings of the National Academy of Sciences*, 106(41):17255–17260, 2009.

[130] A. Ishizaki and G. R. Fleming. Unified treatment of quantum coherent and incoherent hopping dynamics in electronic energy transfer: Reduced hierarchy equation approach. *The Journal of Chemical Physics*, 130(23):234111, 2009.

[131] A. Ishizaki and G. R. Fleming. On the interpretation of quantum coherent beats observed in two-dimensional electronic spectra of photosynthetic light harvesting complexes. *The Journal of Physical Chemistry B*, 115(19):6227–6233, 2011.

[132] S. Jang, Y.-C. Cheng, D. R. Reichman, and J. D. Eaves. Theory of coherent resonance energy transfer. *The Journal of Chemical Physics*, 129(10):101104, 2008.

[133] E. Jaynes and F. Cummings. Comparison of quantum and semiclassical radiation theories with application to the beam maser. *Proceedings of the IEEE*, 51(1):89 – 109, 1963.

[134] J. Johansson, P. Nation, and F. Nori. Qutip 2: A python framework for the dynamics of open quantum systems. *Computer Physics Communications*, 184(4):1234 – 1240, 2013.

[135] E. Joos and H. D. Zeh. The emergence of classical properties through interaction with the environment. *Zeitschrift für Physik B Condensed Matter*, 59:223–243, 1985. 10.1007/BF01725541.

[136] E. Joos, H. D. Zeh, C. Kiefer, D. J. W. Giulini, J. Kupsch, and I.-O. Stamatescu. *Decoherence and the Appearance of the Classical World in Quantum Theory.* Springer, 1996.

[137] P. Jordan and E. P. Wigner. About the Pauli exclusion principle. *Z.Phys.*, 47:631–651, 1928.

[138] S. S. K., E. Alexander, V. Stéphanie, and A.-G. Alán. Photonics meets excitonics: natural and artificial molecular aggregates. *Nanophotonics*, 2:21, 2014-02-04T12:26:03.95+01:00 2013.

[139] P. V. Kamat. Quantum dot solar cells. semiconductor nanocrystals as light harvesters. *The Journal of Physical Chemistry C*, 112(48):18737–18753, 2008.

[140] H. Katori. Optical lattice clocks and quantum metrology. *Nat Photon*, 5(4):203–210, 04 2011.

[141] T. Kobayashi. *J-Aggregates*. Number v. 2 in J-aggregates. World Scientific, 2012.

[142] P. Kok and B. Lovett. *Optical Quantum Information Processing*. Cambridge University Press, 2010.

[143] D. König, K. Casalenuovo, Y. Takeda, G. Conibeer, J. Guillemoles, R. Patterson, L. Huang, and M. Green. Hot carrier solar cells: Principles, materials and design. *Physica E: Low-dimensional Systems and Nanostructures*, 42(10):2862 – 2866, 2010. 14th International Conference on Modulated Semiconductor Structures.

[144] A. Kress, F. Hofbauer, N. Reinelt, M. Kaniber, H. Krenner, R. Meyer, G. Böhm, and J. Finley. Manipulation of the spontaneous emission dynamics of quantum dots in two-dimensional photonic crystals. *Physical Review B*, 71(24):241304, 2005.

[145] P. Krogstrup, H. I. Jorgensen, M. Heiss, O. Demichel, J. V. Holm, M. Aagesen, J. Nygard, and A. Fontcuberta i Morral. Single-nanowire solar cells beyond the shockley-queisser limit. *Nat Photon*, 7(4):306–310, 04 2013.

[146] B. Krummheuer, V. M. Axt, T. Kuhn, I. D'Amico, and F. Rossi. Pure dephasing and phonon dynamics in gaas- and gan-based quantum dot structures: Interplay between material parameters and geometry. *Physical Review B*, 71:235329, Jun 2005.

[147] M. D. LaHaye, J. Suh, P. M. Echternach, K. C. Schwab, and M. L. Roukes. Nanomechanical measurements of a superconducting qubit. *Nature*, 459(7249):960–964, 06 2009.

[148] K. Lalumière, A. Blais, B. C. Sanders, A. F. van Loo, A. Fedorov, and A. Wallraff. Tuning from coherent interaction to super-and subradiance with artificial atoms in a 1d waveguide. In *APS Meeting Abstracts*, volume 1, page 25012, 2013.

[149] W. E. Lamb and R. C. Retherford. Fine structure of the hydrogen atom by a microwave method. *Phys. Rev.*, 72:241–243, Aug 1947.

[150] H. Lee, Y.-C. Cheng, and G. R. Fleming. Coherence dynamics in photosynthesis: protein protection of excitonic coherence. *Science*, 316(5830):1462–1465, 2007.

[151] A. J. Leggett, S. Chakravarty, A. T. Dorsey, M. P. A. Fisher, A. Garg, and W. Zwerger. Dynamics of the dissipative two-state system. *Rev. Mod. Phys.*, 59(1):1–85, Jan 1987.

[152] A. J. Leggett and A. Garg. Quantum mechanics versus macroscopic realism: Is the flux there when nobody looks? *Physical Review Letters*, 54:857–860, Mar 1985.

[153] M. Leistikow, A. Mosk, E. Yeganegi, S. Huisman, A. Lagendijk, and W. Vos. Inhibited spontaneous emission of quantum dots observed in a 3d photonic band gap. *Physical Review Letters*, 107(19):193903, 2011.

[154] R. Loudon. *The quantum theory of light*. Oxford university press, 2000.

[155] B. W. Lovett, J. H. Reina, A. Nazir, and G. A. D. Briggs. Optical schemes for quantum computation in quantum dot molecules. *Physical Review B*, 68:205319, Nov 2003.

[156] S. Lu, Z. Lingley, T. Asano, D. Harris, T. Barwicz, S. Guha, and A. Madhukar. Photocurrent induced by nonradiative energy transfer from nanocrystal quantum dots to adjacent silicon nanowire conducting channels: Toward a new solar cell paradigm. *Nano Letters*, 9(12):4548–4552, 2009. PMID: 19856942.

[157] S. Lu and A. Madhukar. Nonradiative resonant excitation transfer from nanocrystal quantum dots to adjacent quantum channels. *Nano Letters*, 7(11):3443–3451, 2007.

[158] P. C. E. S. M. Dubé. Mechanisms of decoherence at low temperatures. *Journal of Chemical Physics*, 268:257–272, 2001.

[159] P. Machnikowski and L. Jacak. Damping of rabi oscillations in quantum dots due to lattice dynamics. *Semiconductor Science and Technology*, 19(4):S299–S300, 2004.

[160] D. MacKay. *Sustainable Energy-without the hot air*. UIT Cambridge, 2008.

[161] R. MacKinnon. Potassium channels. *FEBS Letters*, 555(1):62 – 65, 2003. ¡ce:title¿126th Nobel Symposium. Membrane Proteins: Structure, Function and Assembly¡/ce:title¿.

[162] G. D. Mahan. *Many Particle Physics (Physics of Solids and Liquids)*. Springer, 3rd edition, 2000.

[163] Y. Makhlin, G. Schön, and A. Shnirman. Quantum-state engineering with josephson-junction devices. *Rev. Mod. Phys.*, 73:357–400, May 2001.

[164] T. Mančal and L. Valkunas. Exciton dynamics in photosynthetic complexes: excitation by coherent and incoherent light. *New Journal of Physics*, 12(6):065044, 2010.

[165] P. Mandel. Lasing without inversion: A useful concept? *Contemporary Physics*, 34(5):235–246, 1993.

[166] F. Mandl. *Quantum Mechanics*. Wiley, 1st edition, 1992.

[167] W. Marshall, C. Simon, R. Penrose, and D. Bouwmeester. Towards quantum superpositions of a mirror. *Physical Review Letters*, 91:130401, Sep 2003.

[168] W. Martienssen and E. Spiller. Coherence and fluctuations in light beams. *American Journal of Physics*, 32(12):919–926, 1964.

[169] K. Matsuno. Cell motility as an entangled quantum coherence. *Biosystems*, 51(1):15 – 19, 1999.

[170] J. C. Maxwell. A dynamical theory of the electromagnetic field. *Phil Trans R Soc*, 155:459–512, 1865.

[171] V. May and O. Kühn. *Charge and Energy Transfer Dynamics in Molecular Systems*. Wiley-VCH, 3rd edition, 2011.

[172] L. Mazzola, S. Maniscalco, J. Piilo, K.-A. Suominen, and B. M. Garraway. Pseudomodes as an effective description of memory: Non-markovian dynamics of two-state systems in structured reservoirs. *Physical Review A*, 80:012104, Jul 2009.

[173] G. M. McCracken and P. E. Stott. *Fusion: the Energy of the Universe*. Academic Press, 2012.

[174] J. L. McHale. Hierarchal structure of light-harvesting porphyrin aggregates. *J-aggregates.*, 2:77, 2012.

[175] D. Meiser and M. J. Holland. Steady-state superradiance with alkaline-earth-metal atoms. *Physical Review A*, 81:033847, Mar 2010.

[176] Miles and Blencowe. Quantum electromechanical systems. *Physics Reports*, 395(3):159 – 222, 2004.

[177] M. Mohseni, P. Rebentrost, S. Lloyd, and A. Aspuru-Guzik. Environment-assisted quantum walks in photosynthetic energy transfer. *The Journal of Chemical Physics*, 129(17):174106, 2008.

[178] R. Monshouwer, M. Abrahamsson, F. van Mourik, and R. van Grondelle. Superradiance and exciton delocalization in bacterial photosynthetic light-harvesting systems. *The Journal of Physical Chemistry B*, 101(37):7241–7248, 1997.

[179] P. C. E. S. N. V. Prokof'ev. Theory of the spin bath. *Rep. Prog. Phys.*, 63:669–726, 2000.

[180] D. Nagy, G. Kónya, G. Szirmai, and P. Domokos. Dicke-model phase transition in the quantum motion of a bose-einstein condensate in an optical cavity. *Physical Review Letters*, 104:130401, Apr 2010.

[181] A. K. Naik, M. S. Hanay, W. K. Hiebert, X. L. Feng, and M. L. Roukes. Towards single-molecule nanomechanical mass spectrometry. *Nature Nanotechnology*, 4(7):445–450, 07 2009.

[182] S. Nakajima. On quantum theory of transport phenomena. *Progress of Theoretical Physics*, 20(6):948–959, 1958.

[183] Y. Nakamura, Y. A. Pashkin, and J. S. Tsai. Coherent control of macroscopic quantum states in a single-cooper-pair box. *Nature*, 398(6730):786–788, 04 1999.

[184] A. Nazir. Correlation-dependent coherent to incoherent transitions in resonant energy transfer dynamics. *Physical Review Letters*, 103:146404, Oct 2009.

[185] M. A. Nielsen and I. L. Chuang. *Quantum Computation and Quantum Information*. Cambridge University Press, October 2000.

[186] T. Niemczyk, F. Deppe, H. Huebl, E. P. Menzel, F. Hocke, M. J. Schwarz, J. J. Garcia-Ripoll, D. Zueco, T. Hummer, E. Solano, A. Marx, and R. Gross. Circuit quantum electrodynamics in the ultrastrong-coupling regime. *Nature Physics*, 6(10):772–776, 10 2010.

[187] S. Noda, M. Fujita, and T. Asano. Spontaneous-emission control by photonic crystals and nanocavities. *Nature Photonics*, 1(8):449–458, 2007.

[188] A. D. O'Connell, M. Hofheinz, M. Ansmann, R. C. Bialczak, M. Lenander, E. Lucero, M. Neeley, D. Sank, H. Wang, M. Weides, J. Wenner, J. M. Martinis, and A. N. Cleland. Quantum ground state and single-phonon control of a mechanical resonator. *Nature*, 464(7289):697–703, 04 2010.

[189] J. M. Olson and C. A. Romano. A new chlorophyll from green bacteria. *Biochim Biophys Acta*, 59:726–728, 1962.

[190] B. O'Regan and M. Gratzel. A low-cost, high-efficiency solar cell based on dye-sensitized colloidal tio2 films. *Nature*, 353(6346):737–740, 10 1991.

[191] M. C. O'Sullivan, J. K. Sprafke, D. V. Kondratuk, C. Rinfray, T. D. Claridge, A. Saywell, M. O. Blunt, J. N. O'Shea, P. H. Beton, M. Malfois, et al. Vernier templating and synthesis of a 12-porphyrin nano-ring. *Nature*, 469(7328):72–75, 2011.

[192] H. Paik, D. I. Schuster, L. S. Bishop, G. Kirchmair, G. Catelani, A. P. Sears, B. R. Johnson, M. J. Reagor, L. Frunzio, L. I. Glazman, S. M. Girvin, M. H. Devoret, and R. J. Schoelkopf. Observation of high coherence in josephson junction qubits measured in a three-dimensional circuit qed architecture. *Physical Review Letters*, 107:240501, 2011.

[193] G. Panitchayangkoon, D. Hayes, K. A. Fransted, J. R. Caram, E. Harel, J. Wen, R. E. Blankenship, and G. S. Engel. Long-lived quantum coherence in photosynthetic complexes at physiological temperature. *Proceedings of the National Academy of Sciences*, 107(29):12766–12770, 2010.

[194] A. Pechen. Engineering arbitrary pure and mixed quantum states. *Physical Review A*, 84:042106, Oct 2011.

[195] A. Pechen and H. Rabitz. Teaching the environment to control quantum systems. *Physical Review A*, 73(6):062102, 2006.

[196] R. Penrose. *The Emperor's New Mind*. Oxford University Press, 1st edition, 1989.

[197] J. Petta, A. Johnson, C. Marcus, M. Hanson, and A. Gossard. Manipulation of a single charge in a double quantum dot. *Physical Review Letters*, 93(18):186802, 2004.

[198] J. Piilo, S. Maniscalco, K. Härkönen, and K.-A. Suominen. Non-markovian quantum jumps. *Physical Review Letters*, 100:180402, May 2008.

[199] M. Planck. Ueber das Gesetz der Energieverteilung im Normalspectrum. *Annalen der Physik*, 309:553–563, 1901.

[200] J. Prior, A. W. Chin, S. F. Huelga, and M. B. Plenio. Efficient simulation of strong system-environment interactions. *Physical Review Letters*, 105:050404, Jul 2010.

[201] E. M. Purcell, H. C. Torrey, and R. V. Pound. Resonance absorption by nuclear magnetic moments in a solid. *Physical Review*, 69:37–38, Jan 1946.

[202] I. I. Rabi. On the process of space quantization. *Physical Review*, 49:324–328, Feb 1936.

[203] A. I. M. Rae. *Quantum Mechanics*. Taylor and Francis, 5th edition, 2007.

[204] J. M. Raimond, M. Brune, and S. Haroche. Manipulating quantum entanglement with atoms and photons in a cavity. *Rev. Mod. Phys.*, 73:565–582, Aug 2001.

[205] M. Rätsep and A. Freiberg. Electron–phonon and vibronic couplings in the fmo bacteriochlorophyll¡ i¿ a¡/i¿ antenna complex studied by difference fluorescence line narrowing. *Journal of luminescence*, 127(1):251–259, 2007.

[206] P. Rebentrost, R. Chakraborty, and A. Aspuru-Guzik. Non-markovian quantum jumps in excitonic energy transfer. *Journal of Chemical Physics*, 131(18):184102, 2009.

[207] A. Redfield. On the theory of relaxation processes. *IBM J. Res. Div.*, 1(19-31), 1957.

[208] T. Renger and V. May. Theory of multiple exciton effects in the photosynthetic antenna complex lhc-ii. *Journal of Physical Chemistry B*, 101(37):7232–7240, 1997. cited By (since 1996) 26.

[209] T. Renger, V. May, and O. Khn. Ultrafast excitation energy transfer dynamics in photosynthetic pigmentäìprotein complexes. *Physics Reports*, 343(3):137 – 254, 2001.

[210] K. Riehemann, S. Schneider, T. Luger, B. Godin, M. Ferrari, and H. Fuchs. Nanomedicine—challenge and perspectives. *Angewandte Chemie International Edition*, 48(5):872–897, 2009.

[211] T. Ritz, P. Thalau, J. B. Phillips, R. Wiltschko, and W. Wiltschko. Resonance effects indicate a radical-pair mechanism for avian magnetic compass. *Nature*, 429(6988):177–180, 05 2004.

[212] O. Romero-Isart, A. C. Pflanzer, F. Blaser, R. Kaltenbaek, N. Kiesel, M. Aspelmeyer, and J. I. Cirac. Large quantum superpositions and interference of massive nanometer-sized objects. *Physical Review Letters*, 107:020405, Jul 2011.

[213] R. T. Ross and A. J. Nozik. Efficiency of hot-carrier solar energy converters. *Journal of Applied Physics*, 53(5):3813–3818, 1982.

[214] A. Royer. Combining projection superoperators and cumulant expansions in open quantum dynamics with initial correlations and fluctuating hamiltonians and environments. *Physics Letters A*, 315(5):335 – 351, 2003.

[215] M. S. *Principles of Nonlinear Optical Spectroscopy*. Oxford University Press, New York, 1st edition, 1995.

[216] V. Salari, J. Tuszynski, M. Rahnama, and G. Bernroider. Plausibility of quantum coherent states in biological systems. *Journal of Physics: Conference Series*, 306(1):012075, 2011.

[217] M. Schaffry, E. M. Gauger, J. J. L. Morton, J. Fitzsimons, S. C. Benjamin, and B. W. Lovett. Quantum metrology with molecular ensembles. *Phys. Rev. A*, 82:042114, Oct 2010.

[218] M. Scheibner, T. Schmidt, L. Worschech, A. Forchel, G. Bacher, T. Passow, and D. Hommel. Superradiance of quantum dots. *Nature Physics*, 3(2):106–110, 02 2007.

[219] G. S. Schlau-Cohen, A. Ishizaki, and G. R. Fleming. Two-dimensional electronic spectroscopy and photosynthesis: Fundamentals and applications to photosynthetic light-harvesting. *Chemical Physics*, 386(1-3):1 – 22, 2011.

[220] M. Schlosshauer. *Decoherence and the Quantum-to-Classical Transition*. Springer, 1 edition, 2007.

[221] R. Schnabel, N. Mavalvala, D. E. McClelland, and P. K. Lam. Quantum metrology for gravitational wave astronomy. *Nat Commun*, 1:121, 11 2010.

[222] E. Schrödinger. Die gegenwärtige situation in der quantenmechanik. *Naturwissenschaften*, 23:807–812, 823–828, 844–849, 1935.

[223] E. Schrödinger. *What is Life?* Cambridge University Press, 1st edition, 1944.

[224] D. I. Schuster, A. Wallraff, A. Blais, L. Frunzio, R.-S. Huang, J. Majer, S. M. Girvin, and R. J. Schoelkopf. ac stark shift and dephasing of a superconducting qubit strongly coupled to a cavity field. *Physical Review Letters*, 94:123602, Mar 2005.

[225] H. E. D. Scovil and E. O. Schulz-DuBois. Three-level masers as heat engines. *Phys. Rev. Lett.*, 2:262–263, Mar 1959.

[226] M. O. Scully. *Quantum optics*. Cambridge university press, 1997.

[227] M. O. Scully. Quantum photocell: Using quantum coherence to reduce radiative recombination and increase efficiency. *Physical Review Letters*, 104:207701, May 2010.

[228] M. O. Scully, K. R. Chapin, K. E. Dorfman, M. B. Kim, and A. Svidzinsky. Quantum heat engine power can be increased by noise-induced coherence. *Proceedings of the National Academy of Sciences*, 108(37):15097–15100, 2011.

[229] M. O. Scully, S. Zhu, and H. Fearn. Lasing without inversion. *Zeitschrift für Physik D Atoms, Molecules and Clusters*, 22(2):471–481, 1992.

[230] M. O. Scully, M. S. Zubairy, G. S. Agarwal, and H. Walther. Extracting work from a single heat bath via vanishing quantum coherence. *Science*, 299(5608):862–864, 2003.

[231] O. E. Semonin, J. M. Luther, S. Choi, H.-Y. Chen, J. Gao, A. J. Nozik, and M. C. Beard. Peak external photocurrent quantum efficiency exceeding 100in a quantum dot solar cell. *Science*, 334(6062):1530–1533, 2011.

[232] A. Shabani, M. Mohseni, H. Rabitz, and S. Lloyd. Optimal and robust energy transfer in light-harvesting complexes: (i) efficient simulation of excitonic dynamics in the non-perturbative and non-markovian regimes. *Physical Review E*, 03 2011.

[233] V. P. Shcherbakov and M. Winklhofer. The osmotic magnetometer: a new model for magnetite-based magnetoreceptors in animals. *European Biophysics Journal*, 28:380–392, 1999. 10.1007/s002490050222.

[234] W. Shockley and H. J. Queisser. Detailed balance limit of efficiency of p-n junction solar cells. *Journal of Applied Physics*, 32(3):510–519, 1961.

[235] B. W. Shore and P. L. Knight. The jaynes-cummings model. *Journal of Modern Optics*, 40(7):1195–1238, 1993.

[236] F. C. Spano. Fermion excited states in one-dimensional molecular aggregates with site disorder: Nonlinear optical response. *Physical Review Letters*, 67:3424–3427, Dec 1991.

[237] F. C. Spano and S. Mukamel. Superradiance in molecular aggregates. *The Journal of Chemical Physics*, 91:683, 1989.

[238] T. Tanabe, M. Notomi, E. Kuramochi, A. Shinya, and H. Taniyama. Trapping and delaying photons for one nanosecond in an ultrasmall high-q photonic-crystal nanocavity. *Nature Photonics*, 1(1):49–52, 01 2007.

[239] Y. Tanimura. Stochastic liouville, langevin, fokker–planck, and master equation approaches to quantum dissipative systems. *Journal of the Physical Society of Japan*, 75(8):082001, 2006.

[240] Y. Tanimura and R. Kubo. Time-dependent spectrum of a two-level system coupled to a heat bath driven by pulsed laser. *Journal of the Physical Society of Japan*, 58(8):3001–3012, 1989.

[241] M. Tegmark. Importance of quantum decoherence in brain processes. *Physical Review E*, 61:4194–4206, Apr 2000.

[242] M. Thorwart, J. Eckel, J. Reina, P. Nalbach, and S. Weiss. Enhanced quantum entanglement in the non-markovian dynamics of biomolecular excitons. *Chemical Physics Letters*, 478(4-6):234 – 237, 2009.

[243] T. Tokihiro, Y. Manabe, and E. Hanamura. Superradiance of frenkel excitons in linear systems. *Physical Review B*, 47:2019–2030, Jan 1993.

[244] C. D. Treiber, M. C. Salzer, J. Riegler, N. Edelman, C. Sugar, M. Breuss, P. Pichler, H. Cadiou, M. Saunders, M. Lythgoe, et al. Clusters of iron-rich cells in the upper beak of pigeons are macrophages not magnetosensitive neurons. *Nature*, 484(7394):367–370, 2012.

[245] D. Tronrud, J. Wen, L. Gay, and R. Blankenship. The structural basis for the difference in absorbance spectra for the fmo antenna protein from various green sulfur bacteria. *Photosynthesis Research*, 100:79–87, 2009. 10.1007/s11120-009-9430-6.

[246] L. Turin. A spectroscopic mechanism for primary olfactory reception. *Chemical Senses*, 21(6):773–791, 1996.

[247] T. Unold, K. Mueller, C. Lienau, T. Elsaesser, and A. D. Wieck. Optical control of excitons in a pair of quantum dots coupled by the dipole-dipole interaction. *Physical Review Letters*, 94:137404, Apr 2005.

[248] W. G. Unruh and W. H. Zurek. Reduction of a wave packet in quantum brownian motion. *Physical Review D*, 40:1071–1094, Aug 1989.

[249] K. J. Vahala. Optical microcavities. *Nature*, 424(6950):839–846, 08 2003.

[250] H. van Amerongen, L. Valkunas, and R. van Grondelle. *Photosynthetic Excitons*. World Scientific, Singapore, 2000.

[251] A. M. van Oijen, M. Ketelaars, J. Köhler, T. J. Aartsma, and J. Schmidt. Unraveling the electronic structure of individual photosynthetic pigment-protein complexes. *Science*, 285(5426):400–402, 07 1999.

[252] M. H. P. M. van Putten. Superradiance in a torus magnetosphere around a black hole. *Science*, 284(5411):115–118, 04 1999.

[253] J. H. Van Vleck. On sigma z-type doubling and electron spin in the spectra of diatomic molecules. *Physical Review*, 33:467–506, Apr 1929.

[254] A. Vaziri and M. B. Plenio. Quantum coherence in ion channels: resonances, transport and verification. *New Journal of Physics*, 12(8):085001, 2010.

[255] D. Vion, A. Aassime, A. Cottet, P. Joyez, H. Pothier, C. Urbina, D. Esteve, and M. H. Devoret. Manipulating the quantum state of an electrical circuit. *Science*, 296(5569):886–889, 2002.

[256] J. von Neumann. Wahrscheinlichkeitstheoretischer aufbau der quantenmechanik. *Göttinger Nachrichten*, 1:245–272, 1927.

[257] M. Wagner. *Unitary Transforms in Solid State Physics*. North-Holland, 1st edition, 1986.

[258] D. F. Walls and G. J. Milburn. *Quantum Optics*. Springer, 1st edition, 2008.

[259] Z. B. Walters. Quantum coherent dynamics at ambient temperature in photosynthetic molecules. *arXiv preprint arXiv:1108.5297*, 08 2011.

[260] H. Wang, X. Zheng, F. Zhao, Z. Gao, and Z. Yu. Superradiance of high density Frenkel excitons at room temperature. *Physical Review Letters*, 74(20):4079–4082, 1995.

[261] Q. Wang, S. Stobbe, and P. Lodahl. Mapping the local density of optical states of a photonic crystal with single quantum dots. *Physical Review Letters*, 107(16):167404, 2011.

[262] J. Ward, K. Ramanathan, F. Hasoon, T. J. Coutts, J. Keane, M. Contreras, T. Moriarty, and R. Noufi. A 21.5 *Progress in Photovoltaics: Research and Applications*, 10(1):41–46, 2002.

[263] U. Weiss. *Quantum Disspative Systems*. World Scientific, 2nd edition, 1999.

[264] V. V. Weisskopf and E. Wigner. Berechnung der natürlichen linienbreite auf grund der diracschen lichttheorie. *Zeitschrift für Physik*, 63(1-2):54–73, 1930.

[265] M. Wendling, T. Pullerits, M. A. Przyjalgowski, S. I. Vulto, T. J. Aartsma, R. van Grondelle, and H. van Amerongen. Electron-vibrational coupling in the fenna-matthews-olson complex of prosthecochloris a estuarii determined by temperature-dependent absorption and fluorescence line-narrowing measurements. *The Journal of Physical Chemistry B*, 104(24):5825–5831, 2000.

[266] R. Wiltschko and W. Wiltschko. *Magnetic Orientation in Animals*. Springer, 1995.

[267] H. M. Wiseman and G. J. Milburn. *Quantum Measurement and Control*. Cambridge University Press, 1st edition, 2010.

[268] P. Würfel and U. Würfel. *Physics of solar cells: from basic principles to advanced concepts*. John Wiley & Sons, 2009.

[269] H. Zhong, Q. Xie, M. T. Batchelor, and C. Lee. Analytical eigenstates for the quantum rabi model. *Journal of Physics A: Mathematical and Theoretical*, 46(41):415302, 2013.

[270] S. J. Zinkle and J. T. Busby. Structural materials for fission & fusion energy. *Materials Today*, 12(11):12–19, 2009.

[271] W. H. Zurek. Environment-induced superselection rules. *Physical Review D*, 26:1862–1880, Oct 1982.

[272] R. Zwanzig. *Statistical mechanics of irreversibility, Boulder Lecture Notes in Theoretical Physics*, volume 3. Interscience, 1960.